



POLITECNICO DI TORINO

Master degree course in Nanotechnologies for ICTs

Master Degree Thesis

Photoresponsive material for opto-acoustical applications

Towards the opto-tunability of metamaterials

Supervisors

prof. Emiliano Descrovi
prof. Antonio Gliozzi

Candidate

Niccolò MARCUCCI
matricola: 251616

A. A. 2018-2019

This work is subject to the Creative Commons Licence

Summary

The control on wave propagation phenomena has always been of great interest. This extends as much in the scientific community as for engineering, where such control could be exploited for creating a great variety of new technologies. From telecommunication, where optical fibres brought unprecedented speed in data transfer, to seismology, where deflecting seismic wave is becoming a realistic opportunity, controlling waves has now become of fundamental interest for the development of our modern day society and the introduction of metamaterials allowed great advancements in this field. First discovered in electromagnetism, the concept of metamaterial soon reached other fields where this control is one of the main goals. By introducing artificial, well determined, structures inside the natural composition of a material, it was possible to give it additional properties that would not be present in nature.

Elasto-dynamics is the branch of acoustics that focuses on the study of deformations inside solids and thus on the mechanical wave propagation in this kind of materials. In the last two decades, an increasing interest has acquired the possibility of guiding and manipulating elastic waves by means of metamaterials. Indeed, by introducing artificial, well determined, structures inside standard materials, it was demonstrated that it is possible to give additional properties that would not be present in nature. In elastic materials the introduction of new properties can be achieved exploiting at least two different physical mechanisms, i.e. by means of periodic structures and/or locally resonant structures. These lead to different types of behaviour and thus are referred with different names: phononic crystals and acoustic metamaterials (respectively). Additionally, they can either involve a physical structure (e.g. pillars, holes) or a structurization in the material properties (i.e. materials with different elastic properties arranged in the same structure).

Among all the properties that can be induced in this way, the possibility of creating acoustic band gaps in the material frequency response stands out

with respect to the others. This is because the deterministic introduction of a band gap can be exploited in a variety of ways, ranging from simple acoustic insulators to more complex devices that make use of non linear effects. For instance it is possible to obtain waveguiding effects that are selective with respect to the wave frequency, which can then be used for demultiplexing frequency components of an elastic wave. Similarly, it is possible to achieve selective focusing of specific wavelengths that can be used for detecting higher order harmonics generated by the presence of non linear effects, (which are typically associated to defects in a structure). Another very interesting application involves the field of seismology, where acoustic metamaterials are currently being studied for deflecting surface seismic waves.

The main limit that these fascinating new materials encounter is the intrinsic static nature of their structure. This is to say that when the periodic or the resonant structures have been introduced into the material, there are little things that can be done in order to change their properties. Nonetheless there have been numerous attempts for controlling and tuning the properties of these structures even after their creation. Among the techniques that have been proposed we can mention the exploitation of piezoelectric effects, temperature variations, mechanical stressing or even radio waves.

This thesis work, instead, aims at creating a tunable metamaterial controlled by photonic radiation, hence light, by exploiting a photo-induced variation of the elastic properties of a material. Among the stimuli responsive materials, photo-responsive materials have shown a great number of advantages, especially in terms of remote control (allowing to be governed from distance they reduce the influence of the control system on the active part of a device) and time of the response of the material to the external stimuli. For the purpose of this work it was chosen to deal with photo-responsive polymers because, recently, they have shown themselves capable of changing both optical properties and even topography as a response to the proper illumination. Therefore a responsivity in terms of elastic properties variation is also plausible. Moreover polymers offer many advantages in terms of production simplicity, hence costs, and also allow the control of the level of responsivity during the fabrication process. In particular it was chosen to use polydimethylsiloxane as a base material.

The goal of this thesis is therefore to design, fabricate and validate a tunable phononic crystal realized with photo-responsive polydimethylsiloxane

(PDMS). With this intention, photo-responsivity will have the role of inducing the structurization of the metamaterial, by changing the elastic properties only where the material is illuminated by the projection of a determined pattern.

Outline

The thesis is divided into three main chapter that describe three different types of studies that were carried out in order to approach the problem. The first study was meant at dealing with the theoretical background required for understanding the interaction between elastic waves and the structures the materials is composed of. The second study instead had the aim to produce a numerical model able to support the creation of acoustic band gaps into the proposed structures. While the third part consisted in the experimental characterisation of some photo-responsive polymeric samples reacting to the presence of illumination.

The theoretical description of chapter 1 covers three fundamental aspects of the analysis. First, in order to give an explanation for the existence of shear and compressive stress waves, a mathematical derivation of the wave equation valid for elastic deformations in solid is provided. Such derivation is useful to understand why the two types of waves can behave independently one from the other, when present in bulky infinite media. Then a brief description of the problem of waveguides in elastic media is presented, allowing to handle the concepts of guided modes and dispersion relations. And finally the problem of metamaterials is analysed from multiple standpoints and using different intuitive approaches. Here the difference between phononic crystals and acoustic metamaterials is carefully described together with the methods that have been used in literature to produce tunable metamaterials.

In chapter 2 two methods for dealing with the numerical analysis of metamaterials using the software COMSOL are presented. One is based on full sample analysis, where the geometry of the model is meant at solving the equations for the displacement field distribution for the entire structure of interest in stationary conditions (here the model represent a closed system, i.e. no boundary condition), while the other one focuses on the elementary cell that composes the phononic crystal structure (where proper boundary conditions need to be applied). In order to reduce computational cost, the full sample analysis was performed in two dimensions, which then forced

the periodicity of the phononic crystal to be one dimensional. During these analysis the necessity of including attenuation inside the numerical model is pointed out.

Chapter 3 follows with a detailed description of the experimental setup and the measurement performed in order to acquire information from some PDMS samples. For the projection of patterned light, a one dimensional (in terms of periodicity) mask was used. Moreover a subsection of the chapter is entirely dedicated to polydimethylsiloxane in order to investigate its elastic properties, the method for the preparation of the samples and the technique used for inducing its photo-responsivity.

Contents

List of Tables	9
List of Figures	10
1 Theoretical background	15
1.1 From an elastic deformation to a propagating wave	16
1.1.1 Strain and Stress	16
1.1.2 Elasto-dynamics	22
1.2 Guiding waves	26
1.2.1 Wave in finite systems	26
1.2.2 Dispersion relations	29
1.3 Metamaterials	32
1.3.1 Phononic crystals	33
1.3.2 Acoustic metamaterials	42
1.3.3 Tunable metamaterials	44
2 Numerical models	47
2.1 Simplest usable model	49
2.1.1 Lateral input	52
2.1.2 Top input	56
2.2 Elementary cell analysis: Band diagram and band gaps	59
2.2.1 Literature comparison	59
2.2.2 PDMS structures	62
2.3 Including attenuation	65
2.3.1 Cut-on frequency	66
2.3.2 Recovering the band gap	67
3 Experimental study	69
3.1 Experimental setup	69

3.1.1	Acoustic setup	70
3.1.2	Optical setup	72
3.2	Polydimethylsiloxane	74
3.2.1	Inducing light responsivity	75
3.2.2	The elastic properties	78
3.3	The acoustic response	86
3.3.1	Unstructured illumination	87
3.3.2	Pattern projection	90
A	Mathematical Demonstrations	97
A.1	Gibbs free energy	97
A.2	The wave equation	98
A.3	Extracting p- and s-wave equations	99
A.4	Diatomeric chain	99
Bibliography		101

List of Tables

2.1	Parameters of the first studied model. The problem is solved for different values of the contrast ε	53
2.2	Expected centre of the bang gap for various values of contrast according to eq. (2.3). To be compared to figure 2.3.	54
2.3	Parameters of the first studied model. The problem is solved for different values of the periodicity Λ	54
2.4	Parameters of the model without PBC.	57
3.1	parameters for the samples presented in figure 3.8.	79
3.2	Measured data for the three rod-like samples.	82
3.3	Measured cut-on frequency for the three rod-like samples (plus two samples with smaller height) extracted from their spectra. Values are qualitative because the cut-on is not always sharp.	84
3.4	Results from the time of flight analysis.	90

List of Figures

1.1	Scheme of an incident longitudinal wave reflecting on a surface and producing both longitudinal and transverse waves.	26
1.2	Distribution of the displacement vector for (a) Rayleigh waves and (b) Love waves. Images are taken from [3].	28
1.3	Distribution of the displacement vector for Lamb waves (a) fundamental symmetric mode and (b) fundamental antisymmetric mode. Images are taken from [3].	28
1.4	Schematic representation of the string with foundation problem. .	30
1.5	Dispersion relation for a (transverse) wave propagating in a string with a foundation.	31
1.6	(a) One dimensional multilayer structure. (b) Single unit of the multilayer structure.	34
1.7	Graphical representation of the monoatomic chain problem. . .	38
1.8	Graphical representation of the diatomic chain problem. . .	40
1.9	Band diagram resulting from the dispersion relation for the monoatomic and diatomic chains.	41
1.10	Graphical representation of the mass-in-mass chain problem. .	43
1.11	(a) Band diagram for the mass-in-mass chain problem ($\omega_i = \sqrt{K_i/M_i}$). (b) Frequency response of a typical resonator: (top) amplitude vs. frequency and (bottom) phase vs. frequency. .	44
1.12	Simple graphical representation of a resonator absorbing and re-emitting energy both in transmission and in reflection. . .	44
2.1	(a) Actual 2D simulated geometry. (b) Equivalent 3D (infinite) geometry.	50
2.2	(a) Example of spectral response il log-log scale for the parameters: $E = 2 \text{ MPa}$, $\nu = 0.49$, $h = 1 \text{ cm}$, $\Lambda = 5 \text{ mm}$, $FF = 0.5, \varepsilon = 0.5$. (b) Distribution of the displacement vector at $f = 10 \text{ kHz}$	52

2.3	Transmission spectra for various values of the contrast, with parameters in table 2.1. Notice that both x - and y -axis are plotted in log scale. (a) The input displacement is headed toward the x -direction, i.e. longitudinal wave excitation. (b) The input displacement is headed toward the y -direction, i.e. transverse wave excitation.	55
2.4	Transmission spectra for various values of the periodicity with parameters in table 2.3. Notice that both x - and y -axis are plotted in log scale. (a) The input displacement is headed toward the x -direction, i.e. longitudinal wave excitation. (b) The input displacement is headed toward the y -direction, i.e. transverse wave excitation.	55
2.5	(a) Figure 2.3a, reported here for comparison. (b) Transmission spectra for various values of the contrast, when the PBC are removed from the model in figure 2.1a. All other parameter are the same as for (a).	56
2.6	(a) New geometry. (b) Transmission spectra for various values of the contrast for the new geometry; parameters in table 2.4. Notice that both x - and y -axis are plotted in log scale.	58
2.7	(a) Structure of a 3D phononic crystal, periodic only in one direction. (b) 2D primitive cell.	60
2.8	(a) Results from [39] (the blue line is the one to be reproduced) and (b) reproduced results. Notice that on the x -axis there is the reduced wavevector $k_x^* = \frac{k_x}{\pi}a$	61
2.9	Primitive cell of a 3D phononic crystal analysed, periodic along the x - and y -directions.	61
2.10	(a) Results from [40] and (b) reproduced results. Notice that on the x -axis there is the reduced wavevector where $\Gamma \rightarrow (k_x^* = 0, k_y^* = 0)$, $X \rightarrow (k_x^* = 1, k_y^* = 0)$ and $M \rightarrow (k_x^* = 1, k_y^* = 1)$	62
2.11	Band diagram for the structure in figure 2.7, where aluminium has been replaced with PDMS.	63
2.12	(a) Band diagram for the structure in figure 2.9 where PVC was replaced with PDMS. (b) Same structure, but the internal hole has been filled with PDMS having modified elastic properties.	63
2.13	(a) Band diagram for the structure in figure 2.9 where PVC was replaced with PDMS and the size reduced by ten times. (b) Same structure, band diagram centred at higher frequencies.	64

2.14 (a) Obtained transmission spectrum for different values of the thickness. (b) Cut-on frequency value as a function of the thickness h	66
2.15 Transmission spectrum for the geometry in figure 2.6a and parameters in table 2.4, plus $\eta_s = 0.5 \text{ Pa s}$. Result for multiple values of (a) the contrast and (b) the fill factor (the latter fixing $\varepsilon = 0.5$).	67
3.1 (a) Acoustic setup. (b) Optical setup.	70
3.2 (a) Sample holder. (b) Probes.	71
3.3 (a) Oscilloscope. (b) Waveform generator and amplifier.	72
3.4 (a) Whole setup. (b) Zoom on the focusing lens and pin-hole.	73
3.5 Molecular structure of polydimethylsiloxane [41].	74
3.6 Geometrical representation of the photo-isomerization of azobenzene, from <i>trans</i> (E) to <i>cis</i> (Z). Image taken from [51].	76
3.7 Schematic representation of (a) simple guest-host system and (b) chromophore functionalized side-chain polymers. Image taken from [52].	77
3.8 (a) Azo-doped samples used in the experimental study. (b) Absorbing spectrum of copolymers based on Dispersed Red 1 Methacrylate, taken from [53].	78
3.9 Graphic representation of the dependence of E as a function of (a) the cross linker to base ratio and (b) the base to curing agent ratio. Image taken from [55].	79
3.10 Relations between ν , E and c_l for (a) constant $E = 2 \text{ MPa}$ and (b) constant $c_l = 1070 \text{ m s}^{-1}$	80
3.11 (a) Scheme of the probes location when measuring the time of flight. (b) Example of burst signal with the output response.	81
3.12 (a) Picture of the three rod-like samples. (b) Their frequency response.	82
3.13 Viscosity vs. shear rate with fitting model. Image taken from [59].	85
3.14 Example of variation in time of the transmission spectrum for one of the samples, without presence of illumination and when ecographic gel is used for improving the contact between sample and probes. Measured on sample # 3.	87

3.15 Comparisons between the effect of light onto three different samples. (a) Spectrum without illumination in blue and after 5 min of illumination in red. (b) Time evolution of the spectrum; the black line represent the moment when the LASER is turned off.	88
3.16 (a) Effect of illumination on the burst signal. (b) Zoom in the region where the output signal starts. Measured on sample # 2.	90
3.17 Mask used for the projection of the pattern.	91
3.18 Time evolution of the spectral variations. Comparison of the spectral variation upon illumination for the sample # 3. The black dashed line corresponds to the moment the LASER is turned off.	92
3.19 Picture of the tilted mask together with the pattern it generates	93
3.20 Comparison of the spectral variation upon illumination for the sample # 3 when using the mask at different tilt angle (same acquisition series as figure 3.18). (a) Spectra after five minutes of illumination compared with their rest value. (b) Time evolution of the spectral variations; black dashed line corresponds to the moment the LASER is turned off.	93
3.21 Time evolution of the spectral variations. Comparison of the spectral variation upon illumination for the sample # 4. The black dashed line corresponds to the moment the LASER is turned off.	95

Chapter 1

Theoretical background

In order to understand how to control elastic waves propagating in solid media, it is important to understand how they work and which are the microscopic mechanisms that influence their behaviour. It is thus necessary to have a look on the theoretical aspects capable of describing such mechanisms, even if with a far-from-exhaustive presentation. Although elastic waves can be studied both referring to liquid and solid media, this presentation is focused on the latter in order to avoid confusion and ambiguity.

It is necessary to first understand the underlying formalism that describes deformations inside solid media, then it will be possible to derive the equation of motion and extract important information from it. With such background it is easier to understand the basic principles of wave-guiding, and thus to understand the phenomenon of modal dispersion. Finally it will be possible describe the underlying principles behind metamaterial and phononic crystals.

Notice that all the information contained in section 1.1 have been retrieved from [1, Ch. I and III]

1.1 From an elastic deformation to a propagating wave

1.1.1 Strain and Stress

Strain

Consider a body of a given solid material. In rest conditions, imagine to associate to each constituting atom a point in space of given coordinate $\mathbf{r} = (x_1, x_2, x_3)$. When a deformation is applied to the body, its atoms will change arrangement, therefore the vector \mathbf{r} will be changed as well $\mathbf{r}' = (x'_1, x'_2, x'_3)$.

Instead of speaking about atoms and in order to allow differential analysis to take place, it is better to consider the body as a continuum. Thus replace the concept of atoms, tiny elements that build up the body, with infinitesimal volumes, tiny portion of spaces that can be localised with. It is easier to directly refer to them as points of the body.

If we consider the position of any point of the solid body before (\mathbf{r}) and after (\mathbf{r}') a deformation, we can define a *displacement vector*

$$\mathbf{u} = \mathbf{r}' - \mathbf{r}. \quad (1.1)$$

Consider now what happens at the distance between two close points A and B . The difference of their position vectors will be referred as $d\mathbf{r}$. Therefore distance dl before the deformation is simply $dl^2 = |d\mathbf{r}|^2$.

After the deformation instead it is possible to write it as a function of the displacement vector $d\mathbf{r}' = d\mathbf{r} + d\mathbf{u}$, where $d\mathbf{u}$ is just the difference between the displacements of the two points. Therefore the distance after deformation can be written:

$$dl'^2 = \sum_i (dx_i + du_i)^2 = \sum_i (dx_i^2 + du_i^2 + 2dx_i du_i) \quad (1.2)$$

where dx_i are the components of the vector $d\mathbf{r}$.

It is useful to decompose the differential of the displacement vector ($d\mathbf{u}$) into its derivatives with respect to the coordinate system:

$$d\mathbf{u} = \sum_k \frac{\partial \mathbf{u}}{\partial x_k} dx_k,$$

where the partial derivative is applied to all the components of $d\mathbf{u}$.

Thus we can rewrite eq. (1.2) as:

$$dl'^2 = dl^2 + \sum_i \left(\left(\sum_k \frac{\partial u_i}{\partial x_k} dx_k \right)^2 + 2dx_i \sum_k \frac{\partial u_i}{\partial x_k} dx_k \right) \quad (1.3)$$

The squared term can be written in the form

$$\left(\sum_k \frac{\partial u_i}{\partial x_k} dx_k \right)^2 = \sum_k \sum_l \frac{\partial u_i}{\partial x_k} dx_k \frac{\partial u_i}{\partial x_l} dx_l$$

In order to simplify the notation, from now on it will be used the *index notation* in which the presence of an index (i, k, l, etc.) implies the presence of a summation over all the components of the vector (i.e. $dl^2 = \sum_i dx_i^2$ and $dl^2 = dx_i^2$ are equivalent).

Eq. (1.3) thus takes the form

$$dl'^2 = dl^2 + \frac{\partial u_i}{\partial x_k} dx_k \frac{\partial u_i}{\partial x_l} dx_l + 2 \frac{\partial u_i}{\partial x_k} dx_k dx_i. \quad (1.4)$$

By rearranging the indexes¹ it is possible to rewrite eq. (1.4) in the form

$$dl'^2 = dl^2 + 2u_{ik} dx_i dx_k, \quad (1.5)$$

where u_{ik} is called the ***strain tensor***, written in the symmetrical form

$$u_{ik} = \frac{1}{2} \left(\frac{\partial u_i}{\partial x_k} + \frac{\partial u_k}{\partial x_i} + \frac{\partial u_l}{\partial x_i} \frac{\partial u_l}{\partial x_k} \right) \quad (1.6)$$

Since in most of the cases the deformation of the body is small, the second order term is usually neglected, thus writing the strain tensor in the simpler form

$$u_{ik} = \frac{1}{2} \left(\frac{\partial u_i}{\partial x_k} + \frac{\partial u_k}{\partial x_i} \right). \quad (1.7)$$

And what is the effect on the infinitesimal volume dV ?

By definition the volume will be the product of its infinitesimal elements $dV = dx_1 dx_2 dx_3$ and $dV' = dx'_1 dx'_2 dx'_3$. Since

$$dx'_1 = dx_1 + du_1 = dx_1 (1 + \partial u_1 / \partial x_1),$$

¹In the middle term of the right had side of the equation invert the index i with the index l , and then rewrite the rightmost term as $\partial u_i / \partial x_k dx_k dx_i + \partial u_i / \partial x_k dx_k dx_i$. Finally swap index i with k on one of the latter terms only.

which in terms of strain tensor is simply $dx'_1 = dx_1(1 + u_{11})$, the infinitesimal volume after deformation will be

$$dV' = dV(1 + u_{11})(1 + u_{22})(1 + u_{33}).$$

By expanding and neglecting the high order terms, the previous expression can be written in the form

$$dV' = dV(1 + u_{ii}),^2 \quad (1.8)$$

i.e. the diagonal element of the strain tensor represent the relative variation of the infinitesimal volume. If they are null, it means that the volume is remaining constant even after the deformation.

Stress

Consider now the forces acting inside the body. Since the forces will be distributed inside the entire volume, the total force acting on a given volume will be given by the integral over the volume of the force per unit of volume. i.e.

$$\mathbf{F} = \int \mathbf{f} dV.$$

Where the integral can be applied to each component of \mathbf{f} separately. If, for each component of the force per unit of volume (f_i), we can write such force as the divergence of a given vector field $\boldsymbol{\sigma}_i$, then following the Gauss theorem for the divergence we can write

$$F_i = \int f_i dV = \oint \boldsymbol{\sigma}_i \cdot \mathbf{n} d\Sigma = \oint \sigma_{ik} n_k d\Sigma, \quad (1.9)$$

where \mathbf{n} is the vector normal to the infinitesimal portion of surface $d\Sigma$. In such form, the tensor σ_{ik} is called **stress tensor** which is such that

$$f_i = \operatorname{div}(\boldsymbol{\sigma}_i) = \frac{\partial \sigma_{ik}}{\partial x_k}.$$

It is interesting to understand the meaning of the elements of the stress tensor. From eq. (1.9) it is possible to say that the quantity $\sigma_{ik} n_k d\Sigma$ is the i -th component of the force acting on the surface $n_k d\Sigma$, where the latter represent the projection of the surface $\mathbf{n} d\Sigma$ on the plane perpendicular to

²Notice the index notation.

the k -axis. Imagine, for instance, to take as $d\Sigma$ a small area parallel to the xy -plane. In such case σ_{iz} would be the i -th component of the force per unit area perpendicular to the xy -plane. Therefore, in general, σ_{zz} will be parallel to the z -axis, while σ_{xz} and σ_{yz} will be perpendicular to it.

A good example is when the body is going through a situation of hydrostatic compression (uniform compression from all sides). In this situation there would be a pressure p acting uniformly on every element of the surface of the body. Thus on the surface there will be an opposite force which components can be written as $-p\mathbf{n}_k d\Sigma$. This is equivalent to what comes from eq. (1.9) if the stress tensor is expressed in the form

$$p = \sigma_{ik}\delta_{ik}, \quad (1.10)$$

where δ_{ik} is a Kronecker delta, i.e. the diagonal elements of the stress tensor correspond to a compressive stress, while the off diagonal elements correspond to shear stress.

It is possible to demonstrate that the stress tensor is symmetric by performing an analysis over the total momentum [1, p. 6].

Stress vs. Strain

In order to understand the relations that interconnect stress and strain, it is important to have a look at the thermodynamics of the deformation.

The first question do be asked is the amount of work W performed by the internal forces during deformation.

$$W = \int \delta W dV = \int \delta f \cdot d\mathbf{u} dV,$$

which is the force spent on the deformation, integrated over the volume. Thanks to the definition of the density per unit volume, and integrating by part, it is possible to write

$$W = \int \delta W dV = \oint \sigma_{ik}\delta u_i n_k d\Sigma - \int \sigma_{ik} \frac{\partial \delta u_i}{\partial x_k}. \quad (1.11)$$

If the body is considered to be of infinite size, and not deformed toward infinity, it is possible to neglect the first integral³. By rewriting the second

³The surface is *located* at infinite where there is no deformation.

term

$$\frac{\partial \delta u_i}{\partial x_k} = \frac{1}{2} \delta \left(\frac{\partial u_i}{\partial x_k} + \frac{\partial u_k}{\partial x_i} \right),$$

it is possible to recognize the strain tensor, thus allowing to write

$$\delta W = -\sigma_{ik} \delta u_{ik}, \quad (1.12)$$

which is valid only for small deformations.

It is then possible to demonstrate, starting from equation (1.12) and following standard thermodynamics (see [1, p. 9]), that the stress tensor can be written as a function of the Gibbs free energy G at fixed temperature

$$\sigma_{ik} = \left. \frac{\partial G}{\partial u_{ik}} \right|_T. \quad (1.13)$$

Since in absence of a deformation the body is not subjected to stress (i.e. $u_{ik} = 0 \Rightarrow \sigma_{ik} = 0$), from eq. (1.13) follows that the expression of G must not contain any linear term in u_{ik} .⁴ Therefore the expression of the Gibbs free energy must contain only second degree terms⁵ in the displacement.

There are two ways of obtaining a scalar from a tensor: summing all the squares of the diagonal elements (u_{ii}^2) or summing the squares of all elements (u_{ik}^2). In such case G takes the form

$$G = G_0 + \frac{1}{2} \lambda u_{ii}^2 + \mu u_{ik}^2, \quad (1.14)$$

where the quantities λ and μ are constants called *Lamé coefficients*.

If the sum of the diagonal elements of the strain tensor is null, it means that the relative variation of volume is null as well (see equation (1.8)). Therefore if, during a deformation, the term in λ is null, the volume is not changing upon deformation and it takes the name of *pure shear* deformation. The opposite case is the already seen *hydrostatic compression* in which the strain tensor takes the form $u_{ik} = \text{const} \times \delta_{ik}$.

Since any deformation can be seen as a combination of *pure shear* and *hydrostatic compression* it is useful to rewrite the strain tensor in the form

$$u_{ik} = \left(u_{ik} - \frac{1}{3} u_{ll} \delta_{ik} \right) + \frac{1}{3} u_{ll} \delta_{ik}. \quad (1.15)$$

⁴Otherwise the partial derivative could become non-null even for $u_{ik} = 0$.

⁵In first approximation, neglecting higher order terms.

In this way the term inside the parenthesis represents pure shear deformation, since its diagonal elements are all null, while the term outside on the right has the form of an hydrostatic compression. By substituting these expressions in equation (1.14), the Gibbs free energy takes the form

$$G = \frac{1}{2}Ku_{ll}^2 + \mu \left(u_{ik} - \frac{1}{3}u_{ll}\delta_{ik} \right)^2, \quad (1.16)$$

where $K = (\lambda + \frac{2}{3}\mu)$.⁶

From eq. (1.16) it turns out that even the free energy can be written as a combination of hydrostatic compression and pure shear elements. Indeed the constant K takes the name of ***bulk modulus*** (or modulus of hydrostatic compression) while μ is called ***shear modulus*** (or modulus of rigidity).

In order to go further in the derivation and computing the relation between the stress tensor and the strain tensor, it is necessary to compute the differential of the Gibbs free energy. In general the differential is written in the form $dG = \partial G / \partial x_1 dx_1 + \partial G / \partial x_2 dx_2$, where $x_{1,2}$ are two generic variables from which G depends. In the present case, the two variables can be taken as the compressive strain and the shear strain (eq. (1.15)), thus rewriting the differential of G for constant temperature as

$$dG = \left[Ku_{ll}\delta_{ik} + 2\mu \left(u_{ik} - \frac{1}{3}u_{ll}\delta_{ik} \right) \right] du_{ik}. \quad (1.17)$$

From equation (1.13) then the relation between stress and strain tensors at constant temperature follows as:

$$\sigma_{ik} = \frac{\partial G}{\partial u_{ik}} \Big|_T = Ku_{ll}\delta_{ik} + 2\mu \left(u_{ik} - \frac{1}{3}u_{ll}\delta_{ik} \right). \quad (1.18)$$

It is rather interesting to compute the inverse of this relation and obtain the strain tensor as a function of the stress tensor

$$u_{ik} = \delta_{ik}\sigma_{ll}/9K + \left(\sigma_{ik} - \frac{1}{3}\delta_{ik}\sigma_{ll}/2\mu \right), \quad (1.19)$$

from which it is evident the linear dependence of the strain tensor with respect to the stress tensor. This is nothing but the ***Hook's law*** applied to an elastic deformation, which hold for small deformations only.

⁶See appendix (A.1) for all the detailed passages.

1.1.2 Elasto-dynamics

Before moving forward and computing the equations for motion and wave propagation, it is useful to introduce two new constants, which are widely used in elasto-dynamics: the Young's modulus E and the Poisson's ratio ν .

In order to introduce them, it is first necessary to analyse a simple example: the homogeneous deformation (in terms of extension or compression) of a rod. Let the rod extend along the z -axis. Let a force applied to its end be uniformly distributed on the surface generating a pressure p . Since the pressure is applied along the z -axis only, all the components of the stress tensor will be null, except for $\sigma_{zz} = p$ which equals the pressure. From eq. (1.19) it is straight forward that all components $u_{ik} : i \neq k$ will be null as well. What is left are the diagonal terms

$$u_{xx} = u_{yy} = -\frac{1}{3} \left(\frac{1}{2\mu} - \frac{1}{3K} \right) p, \quad u_{zz} = \frac{1}{3} \left(\frac{1}{\mu} + \frac{1}{3K} \right) p \quad (1.20)$$

The Young's modulus is defined such that $u_{zz} = p/E$, where u_{zz} gives the relative lengthening of the rod. Therefore

$$E = \frac{9K\mu}{(3K + \mu)} \quad (1.21)$$

The other two components instead give a measure of the transverse compression (or expansion) of the rod. The Poisson's ratio is defined such that $u_{xx} = -\nu\sigma_{zz}$. Therefore

$$\nu = \frac{1}{2} \frac{(3K - 2\mu)}{(3K + \mu)} \quad (1.22)$$

Notice that ν varies between $-1 < \nu < 1/2$.

Since they are both just constants, it is now useful to rewrite the stress strain relation in terms of Young's modulus and Poisson's ratio:

$$\sigma_{ik} = \frac{E}{1 + \nu} \left(u_{ik} + \frac{\nu}{1 - 2\nu} u_{ll} \delta_{ik} \right) \quad (1.23)$$

$$u_{ik} = [(1 + \nu)\sigma_{ik} - \nu\sigma_{ll}\delta_{ik}] / E \quad (1.24)$$

The Wave Equation

With all these information at hands, computing the equation describing the dynamics of an elastic deformation should be easy. The equation of motion comes by equating the internal stresses to the inertial term, as long as no external force is acting on the body,

$$\rho \ddot{u}_i = \frac{\partial \sigma_{ik}}{\partial x_k}.$$

Substituting in the latter the result from (1.23) and the definition of the strain tensor in (1.7), one obtains⁷

$$\rho \ddot{u}_i = \frac{E}{2(1+\nu)} \frac{\partial^2 u_i}{\partial x_k^2} + \frac{\nu E}{2(1+\nu)(1-2\nu)} \frac{\partial^2 u_l}{\partial x_i \partial x_l}, \quad (1.25)$$

which can be finally written in vectorial form

$$\rho \ddot{\mathbf{u}} = \frac{E}{2(1+\nu)} \Delta \mathbf{u} + \frac{\nu E}{2(1+\nu)(1-2\nu)} \nabla (\nabla \cdot \mathbf{u}). \quad (1.26)$$

Even if it is more complicated than the simple D'Alambert equation, this is exactly the wave equation for elastic waves propagating in a solid isotropic medium. In order to understand it properly it is useful to start from the simplest example of propagating wave.

Consider a plane wave propagating into an infinite isotropic medium. Imagine this wave to be propagating on the x -axis. Performing all the derivatives in eq. (1.26), many terms disappear upon derivation, and what remains are three distinct equations for the components of the displacement vector \mathbf{u}

$$\frac{\partial^2 u_x}{\partial x^2} - \frac{1}{c_l^2} \frac{\partial^2 u_x}{\partial t^2} = 0, \quad \frac{\partial^2 u_\perp}{\partial x^2} - \frac{1}{c_t^2} \frac{\partial^2 u_\perp}{\partial t^2} = 0 \quad (1.27)$$

where u_\perp can be either u_y or u_z .

In this form the traditional wave equation can be easily recognized. These two equations basically suggest that there can exist two completely independent waves, both propagating along the x -direction, but different in the sense that one produces a displacement parallel to the propagation direction with speed c_l (compressive wave or **p-wave**) while the other one produces a

⁷For the detailed mathematical steps see appendix A.2

displacement perpendicular to it and propagating with speed c_l (shear wave or **s-wave**). The two propagation velocities can be written in the form

$$c_l = \sqrt{\frac{E(1-\nu)}{\rho(1+\nu)(1-2\nu)}}, \quad c_t = \sqrt{\frac{E}{2\rho(1+\nu)}}. \quad (1.28)$$

It is interesting to compare the two velocities. It is straight forward that $c_l = \sqrt{2\frac{1-\nu}{1-2\nu}}c_t$. By considering the range of values that ν can assume, it is always true that $c_l > \sqrt{4/3} c_t$ and diverges for ν very close to 1/2 (as well as for ν approaching -1).

It is actually possible to write the wave equation in terms of p- and s-waves even for the case of generic waves (not planar). Rewriting (1.26) in terms of transverse and longitudinal velocities one gets

$$c_t^2 \Delta \mathbf{u} + (c_l^2 - c_t^2) \nabla (\nabla \cdot \mathbf{u}) = \ddot{\mathbf{u}}. \quad (1.29)$$

It is always possible to decompose the displacement vector into a transverse component and a longitudinal component, in such a way that the following relations are satisfied

$$\nabla \cdot \mathbf{u}_t = 0 \text{ and } \nabla \wedge \mathbf{u}_l = 0, \quad (1.30)$$

where the operation $\nabla \wedge$ is a *curl* operation and $\nabla \cdot$ is a divergence operation. In order to obtain a more compact form of the equation, it is necessary to perform some manipulations. First substitute \mathbf{u} with $\mathbf{u}_l + \mathbf{u}_t$

$$c_t^2 \Delta(\mathbf{u}_l + \mathbf{u}_t) + (c_l^2 - c_t^2) \nabla (\nabla \cdot \mathbf{u}_l) = \ddot{\mathbf{u}}_l + \ddot{\mathbf{u}}_t. \quad (1.31)$$

By performing the divergence operation on both sides, it is possible to extract the longitudinal part only. After some mathematical arrangements, following few identities for vectorial calculus (see appendix A.3 for the details), one finally gets

$$\nabla \cdot (\ddot{\mathbf{u}}_l - c_l^2 \Delta \mathbf{u}_l) = 0 \quad (1.32)$$

Since from the definition (1.30) also the $\nabla \wedge (\ddot{\mathbf{u}}_l - c_l^2 \Delta \mathbf{u}_l) = 0$, it means that the argument of (1.32) is identically null, thus leading to a wave equation for p-waves

$$\frac{\partial^2 \mathbf{u}_l}{\partial t^2} - c_l^2 \Delta \mathbf{u}_l = 0. \quad (1.33)$$

In a very similar manner, by performing the **curl** on the wave equation (1.31), after similar manipulations and using the identity (1.30), a similar equation for shear waves can be obtained

$$\frac{\partial^2 \mathbf{u}_t}{\partial t^2} - c_t^2 \Delta \mathbf{u}_t = 0. \quad (1.34)$$

1.2 Guiding waves

If one was dealing solely with bulk waves in infinite media, the only peculiar aspect present with respect to a normal wave propagation problem would be the simultaneous presence of transverse and longitudinal waves propagating at different speeds. From any other standpoint equations (1.33) and (1.34) are trivial wave equations. Instead, when it come to finite systems, thus in presence of many interfaces, things becomes more complicated.

To understand this it is useful to have a look at the known analytical solutions, whose derivation will not be presented here.

1.2.1 Wave in finite systems

What it is not obvious at first sight is that since s- and p- waves can coexist, a pure wave of one type hitting an interface can be partially transformed into the other type, i.e. a reflected p-wave will generate also a shear stress that will propagate as an s-wave and vice versa. Indeed at an interface the stresses and the displacement must satisfy four condition of continuity and therefore for each incident wave one may expect to have two reflected waves and two refracted waves [2, Ch. 5.4].

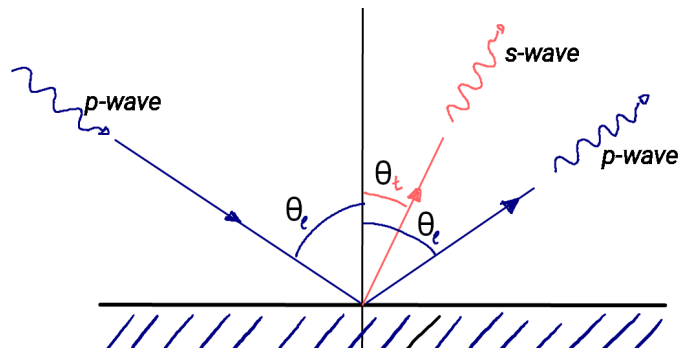


Figure 1.1: Scheme of an incident longitudinal wave reflecting on a surface and producing both longitudinal and transverse waves.

For the sake of understanding which are the consequences, consider a semi infinite bulk material which surface is not in contact with an elastic material. Such interface is called *free boundary* and interfaces between solids an air are typically considered as such. By imposing the tangential component of the \mathbf{k} -vector (spatial frequency) of the incident and refracted waves to be equal,

one obtains the Snell law

$$\frac{\sin \theta}{\sin \theta'} = \frac{c}{c'} \quad (1.35)$$

where θ and c are the incident angle and wave speed, while θ' and c' are the reflected ones.

As it was pointed out, an incident wave of one type will produce two reflected waves. Imagine therefore the incident wave to be purely longitudinal (i.e. $c = c_l$). It is rather obvious that the reflected longitudinal wave will be propagating at the same speed, which means

$$c' = c_l \quad \rightarrow \quad \theta'_l = \theta. \quad (1.36)$$

For the reflected transverse wave it is not the case, therefore it is possible to manipulate the Snell's law and extract the reflected angle

$$c' = c_t l \quad \rightarrow \quad \theta'_t = \arcsin \left(\frac{c_t}{c_l} \sin \theta \right) \quad (1.37)$$

Known solutions

As it is well known in electromagnetism, the presence of an interface or multiple interfaces can lead to the generation of waves which field is confined in a specific region of space, usually referred as *guided modes*. They are generated by the interference of multiple reflections of the wave, that usually creates a stationary field on the plane perpendicular to the propagation direction.

As it has been shown, elastic waves colliding an interface go through this phenomenon of mode conversion, therefore the interference among multiple reflections can be very hard to analyse. Nonetheless there are a few particular cases which solution is well known and are worth noticing since they are responsible for the propagation in many real case scenarios.

In case there is a single interface with a purely elastic material (e.g. air or vacuum), there can exist two types of surface waves.

The firsts are called *Rayleigh* waves. They are characterized by out of plane elliptical displacement along the yz -plane (where z is the propagation direction). The wave height has to be much smaller than the thickness of the material. Waves on the surface of a liquid (sea waves) are a familiar example of those.

The second type of surface waves are called *Love* waves. They are distinguished by transverse oscillation on the xz -plane, i.e. parallel to the surface.

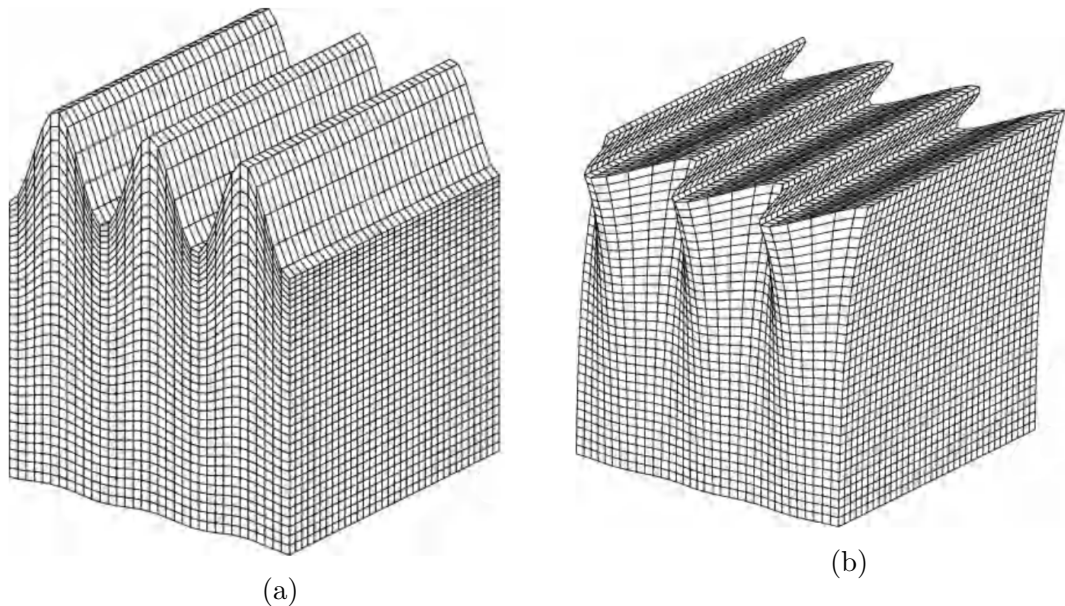


Figure 1.2: Distribution of the displacement vector for (a) Rayleigh waves and (b) Love waves. Images are taken from [3].

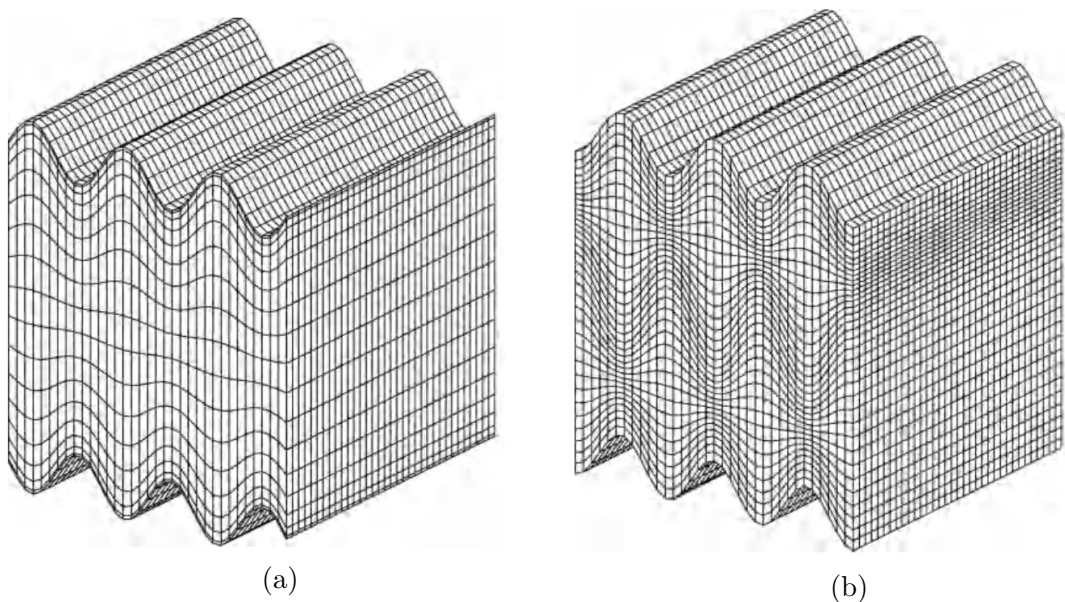


Figure 1.3: Distribution of the displacement vector for Lamb waves (a) fundamental symmetric mode and (b) fundamental antisymmetric mode. Images are taken from [3].

In case instead the material is confined in an infinite plate between two (free) interfaces a particular type of guided waves can occur called *Lamb* waves. For these waves the motion of the displacement vector is quite complex, but they subdivide into two main categories: symmetric and antisymmetric. To understand them better, see figure 1.3.

1.2.2 Dispersion relations

Whenever a boundary condition has to be satisfied, that is to say, whenever a wave is not anymore free to propagate in the bulk of a material, plane waves may not represent a solution for the wave equation. The main characteristic of a plane wave is that it posses a linear relation that connects the wave vector with the angular frequency

$$k = \frac{\omega}{c},$$

that is to say their propagation velocity is constant in frequency.

When boundaries are imposed, the wave equation usually takes a form that finds solutions only if the wave vector satisfies a specific relation with respect to the angular frequency. Such relation takes the name of *dispersion relation* and contains many important information about the propagation of a wave inside the given structure. Moreover there can exist different eigenmodes able to propagate in the structure and each of them can have a different dispersion relation. In such case the dispersion relation could be written in the form

$$k_i = k_i(\omega), \quad \text{or} \quad \omega = \omega(k_i) \quad (1.38)$$

where the propagation velocity depends on the angular frequency and the index i refers to a given eigenmode.

It is interesting to notice that it is called *dispersion relation* because when a wave packet is injected in this kind of system, components of the packet having different frequencies will propagate at different speeds, resulting in a physical spatial dispersion of the wave packet.

Finding the dispersion relation for a given problem is thus a critical step in the analysis of wave propagation behaviour, but it is not always possible to find analytical solutions for it. In such cases finite element analysis is usually able to find good approximations both for the field distributions and the dispersion relation.

String with foundation

A useful example from which to extract the dispersion relation is the analysis of flexural modes into a string that has been anchored to the ground by means of springs [4, Ch. 2], here referred as *foundation*.

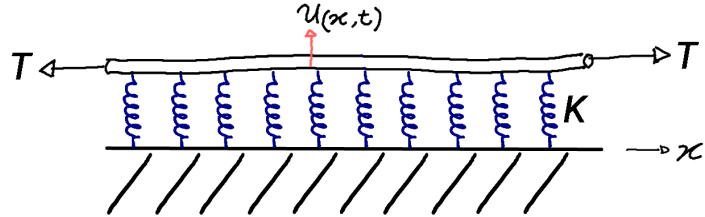


Figure 1.4: Schematic representation of the string with foundation problem.

For vertical deformation inside string it is possible to demonstrate that the governing equation takes the form

$$T \frac{\partial^2 u_{(x,t)}}{\partial x^2} + q_{(x,t)} = \rho \ddot{u}_{(x,t)}, \quad (1.39)$$

where u is the vertical displacement of the string, T is its tension, ρ its density and q is an external force (per unit of length) acting in the vertical direction on the string. In case the foundation is present (as in figure 1.4), the springs act as the external force thus

$$q_{(x,t)} = -Ku_{(x,t)}.$$

By writing the solution in the form

$$u_{(x,t)} = Ae^{i(kx-\omega t)},$$

and substituting the two in the governing equation 1.39, one easily gets

$$\left(-k^2 - \frac{K}{T} + \omega^2 \frac{\rho}{T}\right) Ae^{i(kx-\omega t)} = 0.$$

From the latter the dispersion relation can be extracted and written in the form

$$\omega = \sqrt{\frac{T}{\rho} \left(k^2 + \frac{K}{T} \right)}. \quad (1.40)$$

It is easy to find that when the foundation is not present ($q_{(x,t)} = 0$), the dispersion relation takes a linear form $\omega = \sqrt{\frac{T}{\rho}} k$.

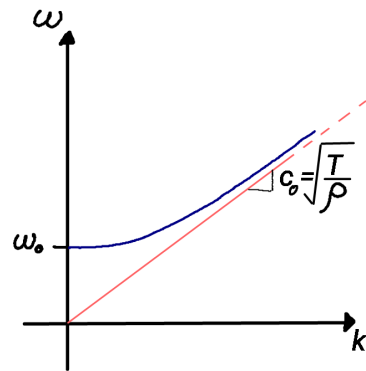


Figure 1.5: Dispersion relation for a (transverse) wave propagating in a string with a foundation.

By observing at figure 1.5 it becomes clear what was the effect of the foundation on the propagation of a wave, even showing the formation of a band gap at low frequencies.

This example was analysed not only due to its simplicity, but also because it is a peculiar case where propagation at low frequency is forbidden by the constraints imposed on the system and not by the presence of attenuation.

1.3 Metamaterials

It is now well known from other disciplines that the introduction of periodic structures into wave conducting materials can produce new unexpected effects. First among them there is crystallography and solid state physics, where the study of periodic atomic structures has allowed an incredibly deep understanding of the behaviour of electrons inside atomic crystals, opening the doors to microelectronics. Then researchers noticed that the same mathematical methods could be applied also to electromagnetism and Maxwell equations because Bloch theory was possible due to the intrinsic wave nature of elementary particles, thus building the basement for the new field of photonic crystals. The passage towards other fields involving wave propagation was only natural.

In electromagnetism these periodically structured materials took the name of *metamaterials* where the prefix *meta* comes from the Greek and means above, beyond. The name wanted to underline that by means of such artificial structures it was possible to introduce new properties that go beyond the normal properties of the material alone [5].

In acoustics there is usually a distinction between acoustic waves in fluids and elastic waves in solids, since the constitutive equations are different [6]. Nonetheless these waves are very similar in nature and these structured materials are usually referred with the common name of *acoustic metamaterials* or *phononic materials* (PM, sometimes distinguished in acoustic PMs and elastic PM).

Actually, due to its peculiar properties, in the case of elastic structured materials, the word *metamaterial* has not the same meaning as in electromagnetism. This is because in elasto-dynamics there are two ways of introducing new properties in a material by means of the structures, and the two have distinct physical driving mechanisms:

- introducing periodic crystal-like structures, exploiting Bragg's effect;
- introducing resonant structures that act as absorber at specific frequencies, producing local resonant effect.

Due to this distinction in the origin of the two phenomena, they also take different names. The firsts are typically referred as *phononic crystals* or elastic *phononic materials*, and are the latter that maintain the name of *acoustic metamaterials*. Nonetheless the boundary between the two is not commonly

agreed and often the name metamaterial tends to include both categories, also because sometimes both mechanism are included in the same structure. In other fields, such as fluid acoustics and electromagnetism, this distinction does not exist.

But which are the “new” properties that characterise these materials?

The first and most noticeable one is the introduction of acoustic band gaps in the frequency response of the material. This is to say by introducing such structures there will be certain ranges of acoustic frequencies able to propagate freely inside the materials and others that will be completely attenuated. The reason of this attenuation is better explained in the following subsections.

Additionally to this, among those frequencies which are able to pass, there are some bands that exhibit unique refractive characteristics. Negative mass or negative bulk modulus can also occur, and, when they occur together, it is possible to obtain negative refraction [7–10] very similarly to what is observed in electromagnetism when both permittivity and permeability are negative [11, 12]. There, negative refraction is very attractive phenomenon that could be used for the creation of the so called *perfect* lens [13], which allows to overcome the diffraction limit, ideally increasing the resolution at will.

An interesting possibility of usage of those properties is in selective focusing [14], where the structure could allow for passing only those frequencies which (equivalent) refractive index allows for focusing in a given region of space. This is a technique that can be very useful in the field of non-linear acoustics and also for structural health monitoring [15, 16].

Another option is to use phononic crystal for waveguiding. The fascinating use of this option is obtained by inserting in the lattice a sort of ‘line of defects’ (i.e. removing the structurization inside a given path), and this allow to introduce new additional propagating modes that have been shown to be confined inside the defect line [17].

1.3.1 Phononic crystals

The theoretical analysis of phononic crystals⁸ ought almost everything to the field of Block wave analysis in Solid State Physics. The key concept is that

⁸Remember that in this context phononic crystal is a synonym for elastic Phononic Materials (PM).

waves propagating in periodic structures tend to scatter more when their wavelength is close to the periodicity of the structure. Then these scattered waves are able to interfere with each others in Bragg-like fashion, and for certain frequencies interfere destructively, thus producing forbidden acoustic bands.

The main problem with elastic wave scattering in these structures is the presence of multiple types of waves (see section 1.2.1) that propagate at different speeds. When considering the same temporal frequency, different propagation velocities imply different wavelengths and therefore the interaction with the periodic structure might have effect for one type of wave and not for the others. Here is where Bloch theory comes handy, being able to treat the problem as a whole, allowing to find band gaps valid for all the types of waves which take the name of global band gaps [18].

The Bragg reflector

Before getting through the key passages of Bloch wave theory it is useful to have a look at a simple case of Bragg scattering where it is evident how the interference of scattered waves produces a band gap: the *Distributed Bragg Reflector* (DBR).

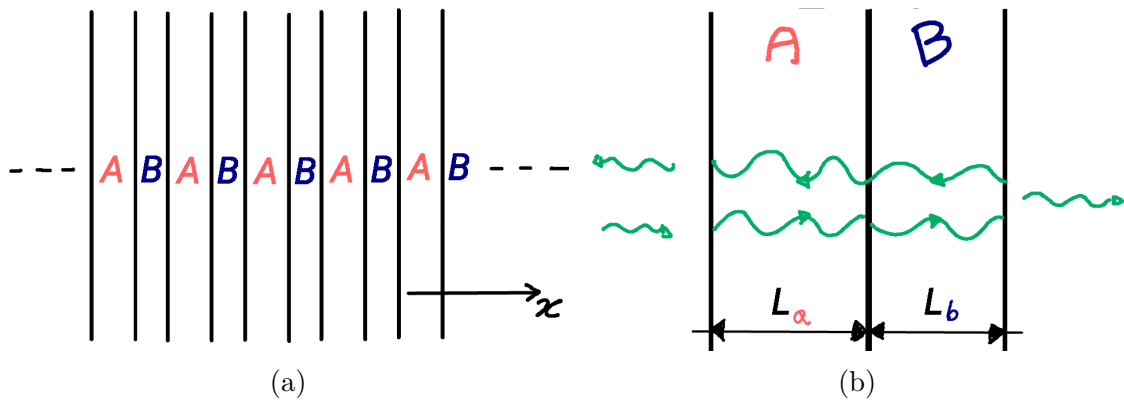


Figure 1.6: (a) One dimensional multilayer structure. (b) Single unit of the multilayer structure.

Consider a one dimensional sequence of two materials having different elastic properties as shown in figure 1.6a (one dimensional in the sense that it has periodicity only in one direction). Imagine for instance that a longitudinal wave is propagating along the direction perpendicular to the interface

between the materials. Such configuration, from the wave perspective, can be seen as a sequence of two types of interfaces: interface between material *A* and *B* and vice versa.

When encountering each interface part of the wave will be transmitted and part will be reflected. The propagation of the wave will be determined by the interference of all the waves reflecting and transmitting at the various interfaces which, for such simple geometry, will be propagating along the *x*-direction.

The simplest approach to this problem is to consider only the elementary unit of the sequence in fig. 1.6b, and study the problem only from a phase perspective while neglecting for a moment the exact value of transmission or reflection. Consider the wave starting from the beginning of material *A*, crossing the interface where it is partially transmitted in material *B*, reach the second interface where it is partially reflected and then come back to the beginning of *A*.

Given that the two materials extend for length l_a and l_b , the phase shift occurring in each material, for the wave that crossed it, can be easily written as

$$\phi_x = k_x l_x = \frac{2\pi}{\lambda_x} l_x.$$

Destructive interference is obtained for

$$\phi = \frac{2\pi f}{c_a} l_a + \frac{2\pi f}{c_b} l_b = m\pi,$$

where c_x is the propagation velocity in material X. By rearranging the terms and extracting the frequency, the *Bragg condition* is finally obtained.

$$f_m = \frac{m\pi}{2} \left(\frac{l_a}{c_a} + \frac{l_b}{c_b} \right) \quad (1.41)$$

This simple relation tells when in the single unit the best condition for destructive interference occurs. Of course this is an oversimplification, because other than neglecting the actual value of the amplitudes of the waves, also the effect of multiple reflections is ignored. Nonetheless, when it comes to consider a sequence of those single units, the effect of such destructive interference is amplified and results in the creation of a band gap centred at the frequency given by 1.41.

The spectral width of the band gap is associated with the contrast between the propagation velocities in the two different media. For electromagnetism,

in photonic crystals it is possible to obtain a simple expression for the spectral width in the case in which $l_a = l_b$ [19]:

$$\frac{\Delta f}{f_0} = \frac{4}{\pi} \arcsin \frac{n_b - n_a}{n_b + n_a}.$$

Since the optical refractive index can be expressed in terms of the wave propagation velocity $n_x = c_0/c_x$ ⁹, such expression can be generalised to the generic wave problem in the form

$$\frac{\Delta f}{f_0} = \frac{4}{\pi} \arcsin \frac{c_a - c_b}{c_a + c_b}, \quad (1.42)$$

which is valid as long as the wave satisfies D'Alambert equation. In section 1.1.2 it was shown that transverse and longitudinal waves in elastic media do respect such equation.

If one is interested to compute the total transmissivity and reflectivity of a sequence of N single units, it is necessary to consider also reflectivity and transmissivity of the two interfaces. Then it would be possible to find and analytical approximation for it [20] or otherwise treat the problem with a transfer matrix approach and use it to compute frequency response of an arbitrary sequence.

But this is beyond the scope of this work and is no further treated.

Bloch theory

Whenever dealing with waves propagating in periodic structures Bloch theory is surely one of the strongest technique to gather information on their behaviour. It was first developed for the study of atoms arranged in a crystal structure and for the electrons that move in the periodic potential the nuclei generate, but it is more general and can be applied wherever a periodic function is introduced in the constituting equation of wave propagation. Periodicity that could be for instance the presence of a periodic potential in a crystal, the periodic variation of the optical refractive index in a photonic crystal, or the periodic variation of the elastic properties (e.g. the Young's modulus) inside a solid material. Indeed Bloch theory is actually a particular case of the so called *Floquet theory*, used to analyse ordinary differential equations with periodic coefficients.

⁹ c_0 is the speed of light and it cancels out when substituting in the expression.

The presence of the infinite periodic lattice, also called *Bravais lattice*, allows to reduce the analysis on the elementary cell composing the lattice. The elementary cell, usually called *primitive cell*, is the smallest portion of the lattice that, when repeated in space, can fill the entire lattice without overlapping. The most powerful tool of the lattice analysis is the possibility to consider a *reciprocal lattice*.

Despite its rigorous definition, in order to understand the reciprocal lattice imagine first to consider a plane wave propagating inside a three dimensional Bravais lattice in the form

$$\Psi = e^{i\mathbf{k}\cdot\mathbf{r}}.$$

Such wave will have a spatial periodicity along a given direction determined by the wavevector \mathbf{k} . Such periodicity is generally different from the periodicity of the lattice, but there is a certain set of wavevectors that match the periodicity of the lattice. Therefore the reciprocal lattice is defined by the set of wavevectors \mathbf{G} which spatial periodicity matches the periodicity of the lattice [21].

By defining $\mathbf{R} = na_1, ma_2, la_3$ (with a_i period in direction x_i and $n, m, l \in \mathbb{Z}$) as the vector that fully describes the lattice, then it is straight forward that

$$e^{\mathbf{G}(r+\mathbf{R})} = e^{\mathbf{G}\cdot\mathbf{r}}, \quad (1.43)$$

from which the definition of the reciprocal lattice vector follows

$$e^{\mathbf{G}\cdot\mathbf{R}} = 1 \quad \longrightarrow \quad \mathbf{G} \cdot \mathbf{R} = 2\pi m. \quad (1.44)$$

Bloch theorem than states that the eigenstates of an electron propagating in a periodic potential can be written as the product of a periodic function $\tilde{f}(\mathbf{r})$ and an exponential term [21];

$$\Psi_n(\mathbf{r}) = e^{i\mathbf{k}\mathbf{r}} \tilde{f}_n(\mathbf{r}), \quad (1.45)$$

which implies that $\Psi_n(\mathbf{r} + \mathbf{R}) = e^{i\mathbf{k}\mathbf{R}} \Psi_n(\mathbf{r})$. And $\tilde{f}(\mathbf{r})$ can be decomposed in its Fourier series in the reciprocal space, because it is periodic

$$\tilde{f}_n(\mathbf{r}) = \sum_G c_{n,G} e^{i\mathbf{G}\cdot\mathbf{r}}.$$

Since the electron wavefunction is a combination of its eigenstates, it is also true that

$$\Psi(\mathbf{r} + \mathbf{R}) = e^{i\mathbf{k}\mathbf{R}} \Psi(\mathbf{r}). \quad (1.46)$$

It can be demonstrated that the latter result (often referred as an alternative expression for the Bloch theorem) is valid for any wave propagating in periodic structures.

The importance of the reciprocal lattice lies on the fact that, in practical terms, it is nothing but the Fourier transform of the real space and allows to solve the wave equation by decomposing the solution into its Fourier series, which then brings to the solution of an eigenvalue problem. Moreover, as the direct lattice can be entirely described by observing the primitive cell, also called *Wigner-Seitz cell*, the very same is valid for the reciprocal lattice, where the primitive cell takes the name of *First Brillouin Zone* (FBZ).

The so called band diagram is nothing but the collection of the eigenfrequencies (for the eigenvalue problem) determined for every point in the first Brillouin zone. Thus it brings a dispersion relation that connects the wavevector \mathbf{k} to the temporal (angular) frequency ω . Since it would be graphically troublesome to actually represent it for every point in the FBZ, usually it is represented along some segments inside it.

From the monoatomic chain to FEM analysis

In order to understand the mechanism underlying phononic crystal, it is very useful to have a look at the simple example of 1D atomic crystal, i.e. the monoatomic and diatomic chains [6].

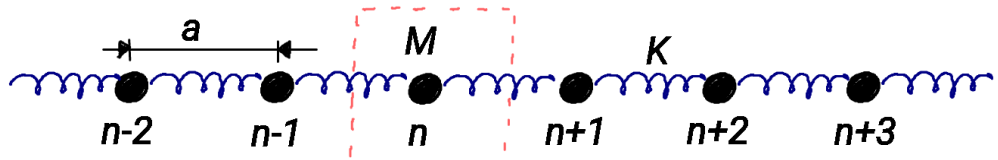


Figure 1.7: Graphical representation of the monoatomic chain problem.

Imagine first a one dimensional chain composed by an infinite number of identical masses M connected via a spring having elastic constant K at a distance a . For this type of 1D lattice the primitive cell is composed by a single mass. Each mass can be located in space with any multiple of a . The displacement of the n -th mass is referred as u_n .

Upon displacement of one of the masses the springs will generate forces in the system and the equation of motion will be given by the balancing of the

forces acting on/from the neighbouring masses. Therefore for the n -th mass, the total force acting on it will be given by the effect of the the springs on the right and on the left.

$$M\ddot{u}_n = -K[\underbrace{(u_n - u_{n-1})}_{\text{left spring}} - \underbrace{(u_{n+1} - u_n)}_{\text{right spring}}]. \quad (1.47)$$

Assuming that Bloch theorem (1.46) is valid, it is possible to seek for a solution in the form¹⁰

$$u_n = e^{i(kr - \omega t)} \tilde{u}(r),$$

where the n dependence is hidden in $r = na$ and \tilde{u}_n can be decomposed in its Fourier series

$$\tilde{u}_n = \sum_G c_G e^{iG \cdot na}.$$

It is possible to substitute it in the previous expression and obtain

$$-M\omega^2 e^{-i\omega t} \sum_G c_G e^{i(k+G)n} = -Ke^{-i\omega t} \sum_G c_G e^{i(k+G)n} [2 - e^{i(k+G)a} - e^{-i(k+G)a}],$$

from which one can remove redundant terms and extract the angular frequency

$$\omega = \sqrt{2 \frac{K}{M} [1 - \cos((k + G)a)]} = 2\sqrt{\frac{K}{M}} \left| \sin \left(\frac{(k + 2\pi m/a)}{2} a \right) \right|, \quad (1.48)$$

since for this problem $G = 2\pi m/a$.

Equation 1.48 brings a dispersion relation that connects the angular frequency with the wavevector of a wave propagating in the lattice.

Despite the intrinsic meanings hidden in such relation, the interesting part for the purpose of this thesis is how to obtain, it because this approach can be extended to give an intuitive derivation of the Finite Element Method approach. From the diatomic chain problem this will be more evidenced.

For this new problem the primitive cell contains two atoms with different masses, therefore, for balancing the forces, it will be necessary to consider also the internal interactions. For simplicity let the spring constant be the same everywhere and the distance between atom equal to $a/2$. The first mass

¹⁰It is equivalent to say that the assumption is that the displacement is caused by a wave propagating inside the chain.

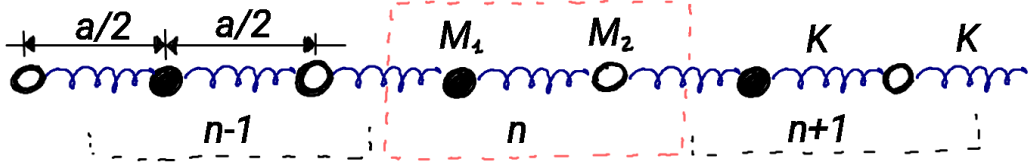


Figure 1.8: Graphical representation of the diatomic chain problem.

n -th primitive cell is referred as $u_{n,1}$ and the other as $u_{n,2}$. For each of the two mass there will be a different equation of motion:

$$\begin{aligned} M_1 \ddot{u}_{n,1} &= -K[(u_{n,1} - u_{n-1,2}) - (u_{n,2} - u_{n,1})], \\ M_2 \ddot{u}_{n,2} &= -K[(u_{n,2} - u_{n,1}) - (u_{n+1,1} - u_{n,2})]. \end{aligned}$$

Writing the solution directly in the form

$$\begin{aligned} u_{n,1} &= A_1 e^{i(kna - \omega t)}, \\ u_{n,2} &= A_2 e^{i(k(n+1/2)a - \omega t)}, \end{aligned}$$

where the A_i term takes into account for amplitude and phase difference between the two masses. Substituting and cancelling redundant terms (see appendix A.4) one gets a pair of coupled equations that have to be true simultaneously

$$\begin{bmatrix} (2K - M_1\omega^2) & -(2K \cos ka/2) \\ -(2K \cos ka/2) & (2K - M_2\omega^2) \end{bmatrix} \begin{bmatrix} A_1 \\ A_2 \end{bmatrix} = 0. \quad (1.49)$$

Since the two equations are coupled, in order to have non trivial solutions for A_1 and A_2 , it is necessary for the determinant of the matrix to be zero, which is nothing but an **eigenvalue problem**. Performing such operation allows to find a relation that links the angular frequency ω to the wavevector k , thus obtaining the band diagram. The peculiar part of such band diagram is that the presence of the second mass has introduced a band gap in the dispersion relation, as shown in figure 1.9.

Again, despite the hidden meanings of such band diagrams, here the interesting part is the presence of the eigenvalue problem, because it places the basement for finite element method analysis.

Summarising, the matrix that defines the eigenvalue problem in 1.49 was obtained by considering three types of contribution: the inertia of the masses,

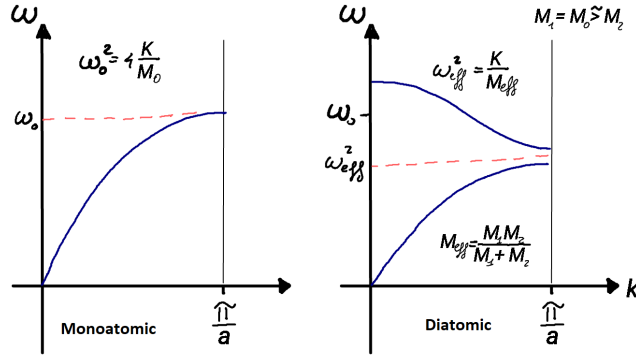


Figure 1.9: Band diagram resulting from the dispersion relation for the monoatomic and diatomic chains.

the interaction between the two masses inside the elementary unit and the interaction of the latter with those outside the elementary units. Therefore it is possible to see that the matrix defining it can be expressed with three different matrices:

- one containing an inertial term involving the two masses, referred as *mass matrix* [M];
- one containing information about the internal interactions by means of the springs, referred as *stiffness matrix* [K];
- one containing information with the interaction between the atoms inside the elementary cell and the boundaries, called *boundary matrix* [B].

In formulas this translates in

$$[M] = [I] \begin{bmatrix} -M_1 \\ -M_2 \end{bmatrix}, \quad [K] = [I] \begin{bmatrix} 2K \\ 2K \end{bmatrix}, \quad [B] = \begin{bmatrix} 0 & -(2K \cos ka/2) \\ -(2K \cos ka/2) & 0 \end{bmatrix}; \quad (1.50)$$

where $[I]$ is the identity matrix. In this way the matrix defining the problem can be written as the sum o the three matrices $[M]\omega^2 + [K] + [B]$.

Imagine to have now a primitive cell containing N different masses. Analysing the problem in the same way will produce the same three matrices containing separate information about the inertia, the internal forces and the boundaries, which can then be combined in order to create an eigenvalue problem.

A **finite element** approach is able to extract these three matrices even from more complicated problems where each mass is substituted with information about a point in a mesh, and the spring constants about the interactions between neighbouring points. In any case the stiffness matrix will always contain information about the interactions internal to the primitive cell, while the mass matrix will contain information about the inertia of the problem and the boundary matrix about the interaction with other primitive cells.

In such, more complicated problems, extracting an analytical expression for the dispersion relations, and thus the band diagram, is practically impossible. As shown for the two mass problem (eq. (1.50)), the wavevector appears only in the boundary matrix. By numerically imposing a value for the wavevector k in the boundary matrix, it is possible to solve the eigenvalue problem, thus finding a numerical solution both for the eigenfrequency and also the coefficients A_i . By solving the eigenvalue problem for all the wanted k of the first Brillouin zone, it is possible to build the infamous band diagram.

1.3.2 Acoustic metamaterials

Phononic crystals were the first type of structured material studied for the manipulation of elastic waves, since they were following the same “line” as photonic crystals in electromagnetism. Then in the year 2000 Liu et al. [22] were able to create an acoustic metamaterial in which the acoustic band gap occurred at frequencies for which the wavelength was two orders of magnitude greater than the dimension of the structure. In normal phononic crystal the interaction with the structure happens in the form of scattering, therefore the wavelength has to be comparable to the size of the structure. This is why metamaterials are considered a completely different class with respect to phononic crystals.

At first the resonant structures were introduced inside the primitive cell of a periodic structure, but soon researchers realised that the periodicity is not actually necessary [23, 24]. This fact, together with the ability of using structures orders of magnitude smaller than the wavelength they interact with, makes them extremely attractive for seismic applications [25, 26], but also to allow the creation of low frequency band gaps. Moreover the possibility to free from the constraint of periodicity allows to create the so called *rainbow traps*, where resonators having different resonant frequencies are combined together to form larger band gaps (again in [23, 24]).

For this type of structured materials, the equivalent 1D chain example would be the mass-in-mass problem, where for each mass in the chain there is a secondary mass attached to it and to it only (fig. 1.10). For such

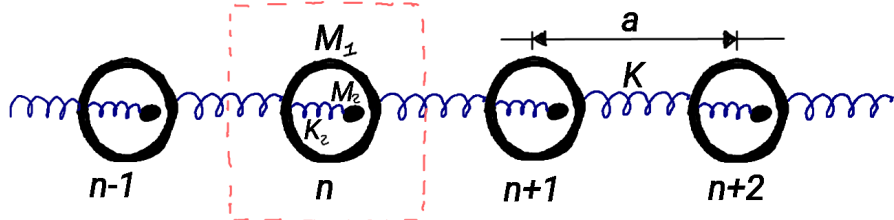


Figure 1.10: Graphical representation of the mass-in-mass chain problem.

example it is possible to show that, if $M_2 \ll M_1$, the gap starts exactly at the resonant frequency of the inner spring-mass system, and that it possesses a negative equivalent mass¹¹ in those frequencies in between the gap [27].

But for a better understanding of the gap formation it is easier to have a look at how a single resonator acts at the passage of a wave. It is easy to imagine that the resonator acts as an absorber at those frequencies for which it resonates. Obviously it cannot absorb indefinitely, therefore it either dissipate the stored energy or re-irradiated it as a reflected and/or transmitted wave. The frequency response of a typical resonator shown in figures 1.11b and 1.12 gives an intuitive understanding of the phenomenon. It is well known that the amplitude plot of the frequency response will have an asymptote at the resonant frequency (or a Lorentzian shape if attenuation is taken into account), while the phase diagram goes through a reverse of phase when going from frequencies before the resonance an those above. Ideally the transition is abrupt at the resonant frequency, but in practise will be a smooth transition due to damping.

It is thus clear that when the resonator will re-irradiate at a frequency greater than the resonant frequency, it will have a phase shifted by $\pi \cdot \text{rad}$ which therefore interferes destructively with the propagating wave. Obviously the frequency cannot be much greater than the resonance because, otherwise the stored (and re-irradiated) energy will not be sufficient to interfere destructively.

¹¹The mass that an equivalent monoatomic chain should have in order to display the same properties.

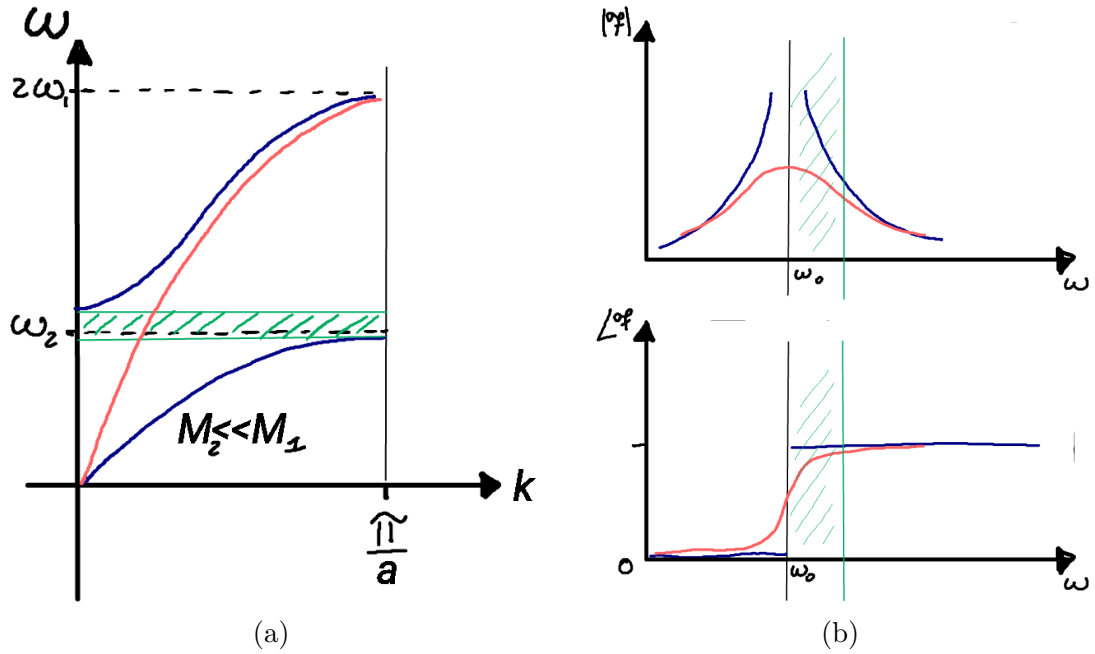


Figure 1.11: (a) Band diagram for the mass-in-mass chain problem ($\omega_i = \sqrt{K_i/M_i}$).
 (b) Frequency response of a typical resonator: (top) amplitude vs. frequency and (bottom) phase vs. frequency.

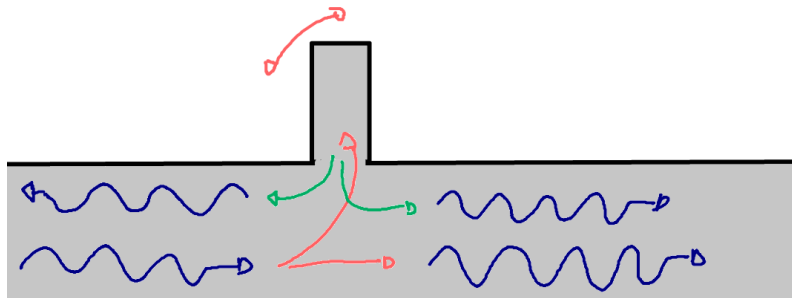


Figure 1.12: Simple graphical representation of a resonator absorbing and re-emitting energy both in transmission and in reflection.

1.3.3 Tunable metamaterials

Phononic crystal and acoustic metamaterial have demonstrated to be able to control elastic waves in a variety of ways. The main limit that they encounter is the static nature of their structure. That is to say that once the periodic structure is created, there are little things that can be done in order to change a phononic crystals properties; once the resonant structures in

acoustic metamaterials are created it is not easy to change their resonance frequency.

In order to have control on the metamaterial properties it is necessary to either possess live control on the structure size and shape or on the material elastic properties. Unfortunately exerting such control in a reversible manner is not trivial and its achievement can be a deal breaker for the field of metamaterials.

There have been numerous attempts in creating tunable metamaterials and phononic crystals. Changing the structure means to physically change the shape or the size of the features in the material, therefore it is something that can affect only partially the behaviour of the system. Even though there are some cases in which this is possible to some extent, surely it is impossible to let the periodic structure or a resonator appear and disappear at will. For instance it is possible to create a fixed matrix consisting of hollow cavities that can be filled with different fluids. Thus the acoustic band gap will be located according to the fluid properties [28].

When it comes to control the elastic properties of a material, there is instead a variety of phenomenon that can be exploited. Researchers were able to exploit magneto elastic materials in order to induce changes in the acoustic response of phononic crystals [29, 30]. Multiple studies have shown the possibility of using temperature variations as source for the elastic properties variation, both in the case of phononic crystals [31] and acoustic metamaterials [32]. Even the possibility of making use of electric fields [33, 34] and also radio waves [35] was shown. The most interesting results were probably obtained for acoustic metamaterials, because changing the resonant frequency of a structure is typically not troublesome. For instance it was possible to even exploit the resonance frequency of a piezoelectric resonator connected to a shunt system [36]. The shunt system is able to change the resonance of the piezoelectric component and thus shifting the location of the band gap.

Another option that has yet to be investigated, which is actually the reason why this thesis work was conducted, is the possibility of using light as a mean to change the elastic properties of a material. For this purpose it is thus necessary to use a photo-responsive material which responsivity would imply a change in Young's modulus, density or even Poisson's ratio.

Here is where polymers become particularly handy, since they come in a wide variety of properties and tend to be easy and cheap to produce.

Moreover it is often possible to introduce in the polymer matrix a photo-responsive molecule which is then able to affect the properties of the matrix itself. A better explanation on how this could be happening is better given in section 3.2. For now is only important to know that a change in the steric hindrance of the doping molecule when absorbing energy from a photon may affect also the polymer chains in which it is surrounded, thus vary locally the elastic properties of the polymer.

A photo-responsive material could then be used as the base material for creating either a metamaterial (MM), with resonant structures on it, or a phononic crystal (PC), which periodic structure may or may not be already present. Then a photon beam can be used to affect the resonant structures of the MM, which will lead to a deformation of the acoustic band gaps, or to affect the periodic structure of the PC, or even to directly induce a PC structure by means of the projection of a pattern. This latter option is the one that seems more appealing and innovative and that is investigated in this thesis work, because it offers the possibility of inducing a structurization (of the elastic properties only) in a material that is completely unstructured.

The main problem with polymers is that they tend to be very sensitive to temperature variations, due to the (often) low *glass transition temperature*. Therefore one of the hardest challenges of this approach will be the distinction between the effect of the photo-responsivity on the elastic properties and the effect of the temperature increase caused by the thermal relaxation of the excited molecules.

Chapter 2

Numerical models

Before performing any experiment it is always a good practice to add support to one's arguments with numerical information, by means of numerical models and/or computer support. This becomes particularly necessary when it comes too hard (or even impossible) to obtain analytical solutions. Elastic wave propagation in solid media is often one of these problems.

Indeed when one has to consider also interfaces, i.e. any finite size problem, the analytical solution becomes so hard to obtain that the problem is treated only numerically more often than not. Especially when it comes to control elastic waves by means of metamaterials or phononic crystals, computer aided design is fundamental.

In order to numerically analyse the behaviour of elastic waves in solids, there are four main options that comes into play:

1. Finite Element Modeling (FEM)
2. Finite Difference Time Domain (FDTD)
3. Plane Wave Expansion (PWE)
4. Transfer Matrix (TM)

The first consists in solving the stationary problem of the differential equations governing elastic waves using approximations by means of finite elements, thus finding the stationary behaviour of the displacement vector for each given frequency. The second one consists in solving the time dependent wave equation in order to find the time evolution of the displacement vector, evolving from a given initial condition. The third one consists in transforming the constituting equations into an eigenvalue problem and finally the last

one consists in computing the transmission matrix for the elementary components constituting the structure, and combining them by simply multiplying one with the other.

For the purpose of this work, it was chosen to deal only with FEM analysis. The main reason lays in the fact that the extraction of the band diagram, thus the frequency response, of metamaterials and phononic crystals is more easily computed by means of FEM analysis, while with the FDTD technique is harder because it requires to know a priori the distribution of the displacement (the shape) of the eigenmodes in order to properly excite them. Moreover the implemented method is very similar to PWE, since it requires to find the eigenmodes of the elementary cell. Instead the transfer matrix approach, even if it is probably the (conceptually) simplest, was discarded because it can be applied only to very simple geometries. Nonetheless it should be noted that all these methods are typically used in parallel, in order to integrate the information acquired by each of them.

In the present work, in order to perform FEM analysis, it was chosen to use the software toolkit *COMSOL Multiphysics*[®][37], by means of the acoustics module. The following chapter contains a description of all the tests and geometries which numerical solution has been computed with such tool, together with comments and analysis of the results.

Before performing the elementary cell analysis, it was decided to begin with a full sample analysis in order to gather some basic information on the properties of the material involved (PDMS) [37]. The basic idea is to compute the stationary solution of the elastic wave equation, for a geometry similar to the one of the samples that will be used in the experimental setup. The geometry for the numerical problem is going to include some regions in which the material properties are left unchanged, while others (the structure) will possess different values (to which extent is the case of study).

In order to study the stationary frequency response of a model, it is necessary to include in the problem something that acts as an input source. In FEM analysis the way of introducing an input is by means of the boundary condition. In particular a prescribed deformation is forced on the input boundary .

Then, during the stationary analysis, the solver will find a solution for the given set of frequencies, where for each frequency the input boundary is forced to vary sinusoidally at such frequency, with amplitude equal to the prescribed value. This is to say that by prescribing a boundary to be displaced along

the x -direction of a given amount X , the solver finds the stationary solution for the problem in which such boundary varies position in time according to the function $y = X \sin(\omega t)$.

It is good practice to prescribe an acceleration instead of a direct deformation, in order to keep the energy entering in the system constant while varying the frequency.

The elastic properties used in the computation have been chosen to resemble those of *polydimethylsiloxane*, since it was chosen to deal with this material for this whole thesis work. During the preliminary study the values suggested by the material library of [37] were be used (since the exact values of the results are not important there), and then those values were adjusted according to the literature and some measurement performed in parallel.

2.1 Simplest usable model

In order to understand the limits and the possibilities of this method it is useful to start with a simple geometry. The best way to simplify a problem is to reduce its dimensions. Since during the whole duration of this work the intention is to work with a slab material, it was chosen to use as basic geometry a two-dimensional slab. It is well known that performing a 2D simulation is like simulating a 3D problem in which the missing dimension extend indefinitely. This is to say that the simulated 2D rectangle is like a section of a slab that is infinite along one direction only (as it is better shown in figure 2.1).

The metamaterial-like structure is the simplest one could get: the periodic repetition of two materials with different elastic properties. Obviously in the real experiment these two materials will not be different, but the intention is to induce such variation of the elastic properties (into specific regions of the sample) by means of light and the material photo-responsivity. Indeed the actual purpose of these computations is to understand to what extent light has to modify the elastic properties of the material in order to obtain a detectable result in the acoustic response of the material.

The first problem to be faced is to choose how to compute the output, i.e. from where to extract a frequency response, since the response is spacial dependent. As shown in fig. 2.1, the structure is basically divided in three parts:

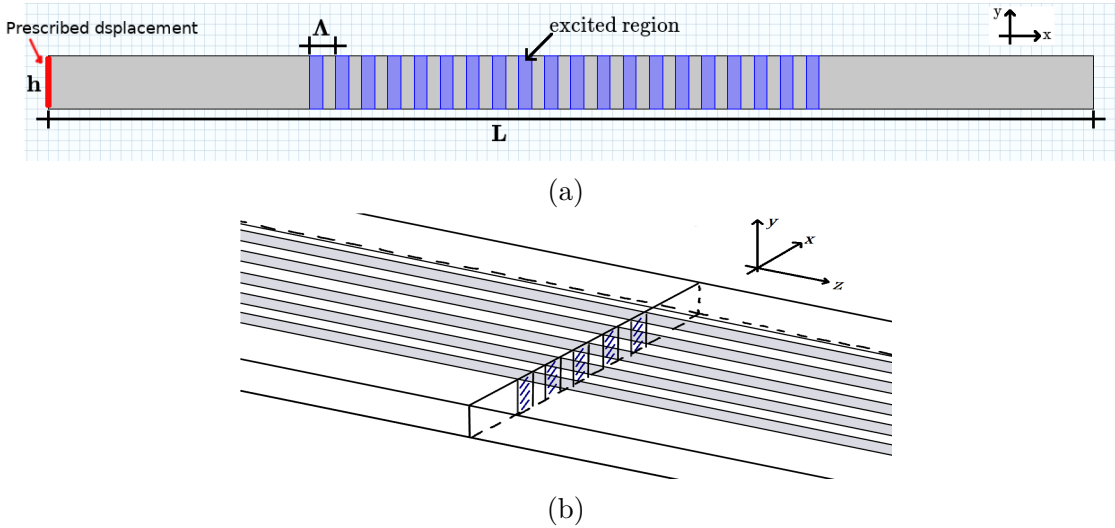


Figure 2.1: (a) Actual 2D simulated geometry. (b) Equivalent 3D (infinite) geometry.

- the left side where the input boundary lays;
- the central part where the periodic structure is located;
- and a right part which represent the output region.

Since computing the output at one of the right boundary would be too limiting, it was chosen to consider as the output the modulus of the displacement averaged over the entire output region. In order to allow for a fair comparison, also the input was considered to be the average of the modulus of the displacement, computed in the entire input region.

In a nutshell

$$I = \frac{1}{A_{in}} \int_{A_{in}} |\mathbf{u}|^2 dx dy, \quad O = \frac{1}{A_{out}} \int_{A_{out}} |\mathbf{u}|^2 dx dy \quad (2.1)$$

And the transmission spectrum is obtained taking the ratio between output and input

$$T(\omega) = \frac{O(\omega)}{I(\omega)}. \quad (2.2)$$

Sometimes it will be shown the logarithm of the transmission spectrum in order to show high attenuation details.

The second problem to be faced is to choose which parameters to vary in the central part in order to observe relevant information in the frequency

response. The central region will be therefore a repetition of two material one with the elastic parameters set to be the default value, and another one which parameters are varied in order to simulate the photo-responsivity of the material. The latter region will be referred as *excited*. The sequence of these two material, which is called a cell, will be repeated N times.

The length of the sample was arbitrarily chosen to keep the computational cost reasonable, while allowing for the repetition of a sufficient number of elements in the central region. The remaining parameters can be changed in such a way that different behaviours of the structure can be observed (e.g. to vary the location and or the width of the band gab).

The elastic properties that can be controlled are the Young's modulus E , the Poisson's ratio ν and the density ρ . Instead for changing the location and shape of the acoustic band gap, it is possible to change either the periodicity Λ of the structure or the fill factor FF .¹ By observing at the wave equation (1.26), it is possible to see that a variation in the Young's modulus has a similar effect to a variation of density, even if in the opposite direction. Therefore, for the purpose of this study, varying the first will be sufficient to gather information on the problem.

Changing the Poisson's ration could be instead troublesome. The reason for this it not trivial. For PDMS its value is very close to 0.5, therefore one of the terms in the wave equation tend to diverge (in particular the p-wave velocity c_l (1.33)) which is obviously unphysical. Anyway despite the choice of its exact value, it has to be noted that slight variations of its value may produce huge variation on the propagation velocities, which is very unlikely to occur in a real life situation. For this reason it was chosen not to study the effect of a variation of the Poisson's ratio.

The central part will be characterised by a contrast between the Young's modulus of the excited part and its default value. Such contrast will be referred with the Greek letter $\varepsilon = E_x/E_0$, where x suffix refers to the excited material (i.e. the part of the central structure which Young's modulus has been changed).

2.1.1 Lateral input

For the first set of models, the input boundary is set to be the leftmost side of the rectangle in figure 2.1. The prescribed displacement on such boundary

¹In the present case the FF is defined as the ratio between the area of the material of one type over the total area of the elementary cell.

is imposed to be either longitudinal or transverse only (with respect to the main axis of the geometry).

Then, even if it might seem unphysical, to the top and bottom boundaries there have been imposed *periodic boundary conditions* (PBC) of the *continuity* type, i.e it is as if the top and bottom boundary are joint together. This was done in order to emulate a sort of infinite domain along the y -direction, which is fair enough for the type of input it is inserted in the system (since the latter is perpendicular to the boundary at which PBC are applied), and should allow to excite pure p- and pure s-waves. Basically in this way the central region should act as a Bragg reflector. Finally, to the right side a free boundary condition (FBC) is imposed.

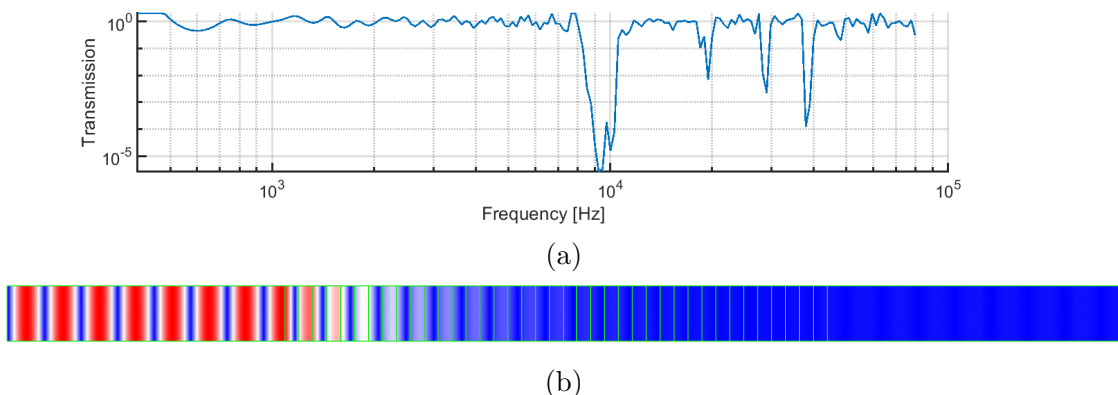


Figure 2.2: (a) Example of spectral response il log-log scale for the parameters: $E = 2 \text{ MPa}$, $\nu = 0.49$, $h = 1 \text{ cm}$, $\Lambda = 5 \text{ mm}$, $FF = 0.5$, $\varepsilon = 0.5$. (b) Distribution of the displacement vector at $f = 10 \text{ kHz}$.

Just to have a look at how the result looks like, on figure 2.2 an example of result is presented. The parameter for which the problem was solved are written in the caption. It is possible to see the presence of a band gap roughly centred at $\approx 9 \text{ kHz}$ and also observe the higher order gaps.

Notice that if it really was an infinite domain along the y -direction, such type of input would correspond to a simple plane wave. Therefore it is possible to compare the location of the band gap with the one that comes from an analysis of the phononic crystal as if it was of Bragg type. As it was already shown in section 1.3.1, for a p-wave the Bragg condition is satisfied for:

$$f = \frac{m}{2\Lambda} \left(\frac{FF}{c_{lx}} + \frac{1 - FF}{c_{l0}} \right)^{-1}, \quad (2.3)$$

where x suffix refers to the excited material (i.e. the part of the central structure which Young's modulus has been changed) and m is any positive integer. Since the contrast is defined on the Young's modulus it's better to rewrite it

$$f = \frac{mc_{l0}}{2\Lambda} \left(\frac{FF}{\sqrt{\varepsilon}} + (1 - FF) \right)^{-1}, \quad (2.4)$$

Substituting the values

Changing the Young's modulus

The first analysis was performed by studying the effect of reducing the Young's modulus in the *excited* part of the central region. The reason for this is actually because when considering the real situation of azo-doped PDMS illuminated by a laser, one actually expect a softening of the material, thus a reduction of E .

The Young's modulus is thus varied in a range $0.75 \text{ kPa} < E < 750 \text{ kPa}$, while the other parameters are collected in table 2.1.

Parameter	Value	Unit	Parameter	Value	Unit
ν	0.49	/	h	1	cm
E_0	750	kPa	L	20	cm
ε	$0.1 \div 0.9$	/	N	20	/
Λ	5	mm	FF	0.5	/

Table 2.1: Parameters of the first studied model. The problem is solved for different values of the contrast ε .

In figure 2.3 the transmission spectrum is shown for multiple values of the Young's modulus. A new problem has been solved for each of those values. First of all it has to be noted that these are not proper transmission spectra because they can reach values greater than the unity. This obviously comes from the fact that they are computed as the ratio of two averages (2.2). At high frequency instead the spectrum seems to become noisy, which is the result of the numerical error inevitably occurring when the wavelength of the propagating wave reaches a value close to the mesh size. In such conditions the FEM approach loses its efficacy.

Nonetheless it is possible to observe the presence of multiple gaps forming inside the spectrum. As expected from the Bragg condition (2.4) the gap

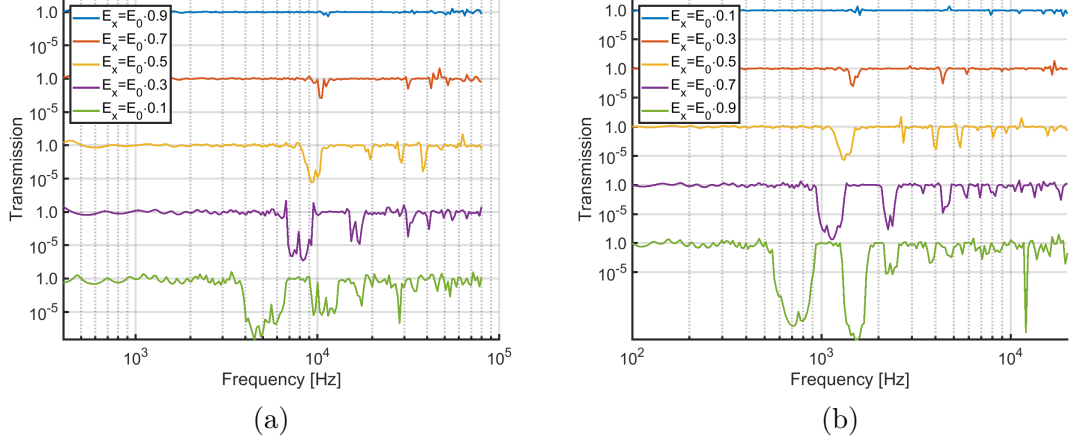


Figure 2.3: Transmission spectra for various values of the contrast, with parameters in table 2.1. Notice that both x - and y -axis are plotted in log scale. (a) The input displacement is headed toward the x -direction, i.e. longitudinal wave excitation. (b) The input displacement is headed toward the y -direction, i.e. transverse wave excitation.

shifts toward low frequency when E is reduced in magnitude. This happens because a reduction of E implies also a reduction of the propagation velocity inside the *excited region*. By testing the Bragg condition for each value of the contrast the table 2.2 is obtained and there is perfect agreement with location of the centre of the band gap even for the second order band gaps.

ε	$f_{l,gap}$	$f_{t,gap}$
0.1	5.5 kHz	0.8 kHz
0.3	8.1 kHz	1.1 kHz
0.5	9.5 kHz	1.3 kHz
0.7	10.5 kHz	1.5 kHz
0.9	11.2 kHz	1.6 kHz

Table 2.2: Expected centre of the bang gap for various values of contrast according to eq. (2.3). To be compared to figure 2.3.

Another thing worth noticing is the increase of bandwidth with the increase of contrast, which again is expected for a Bragg reflector.

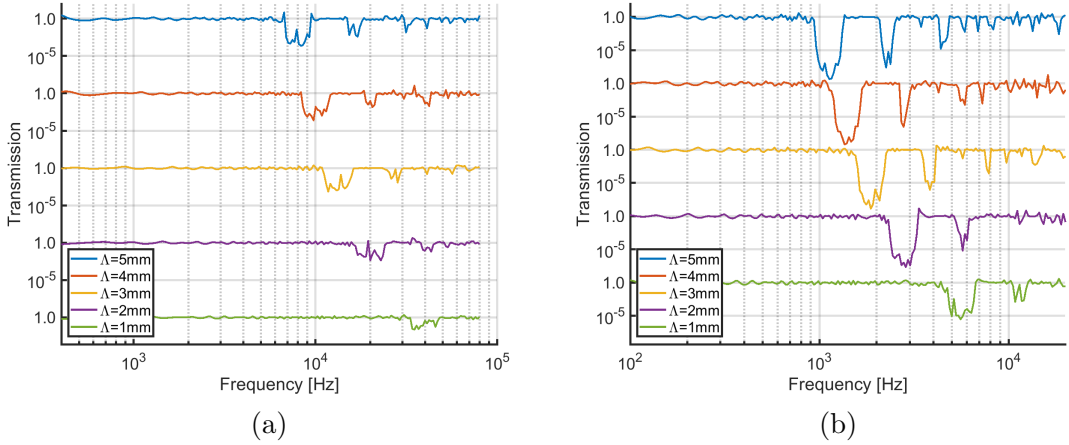


Figure 2.4: Transmission spectra for various values of the periodicity with parameters in table 2.3. Notice that both x - and y -axis are plotted in log scale.
 (a) The input displacement is headed toward the x -direction, i.e. longitudinal wave excitation. (b) The input displacement is headed toward the y -direction, i.e. transverse wave excitation.

Changing the spacing

A new test was performed to observe the evolution of the band gap when changing the periodicity of the central structure, while keeping fixed the value of the contrast. The parameters used for these test are summarised on table 2.3.

Parameter	Value	Unit	Parameter	Value	Unit
ν	0.49	/	h	1	cm
E_0	750	kPa	L	20	cm
ε	0.3	/	N	20	/
Λ	1÷5	mm	FF	0.5	/

Table 2.3: Parameters of the first studied model. The problem is solved for different values of the periodicity Λ .

The results in fig 2.4 show clearly a shift of the band gap while changing the periodicity.

2.1.2 Top input

The previous tests were performed in order to directly observe if elastic waves developing in a material produced ‘Bragg’ interference patterns when analysed with the tools provided by COMSOL [37]. But in order to have more realistic result it is necessary to make a few changes. First and foremost the periodic boundary conditions have to be removed.

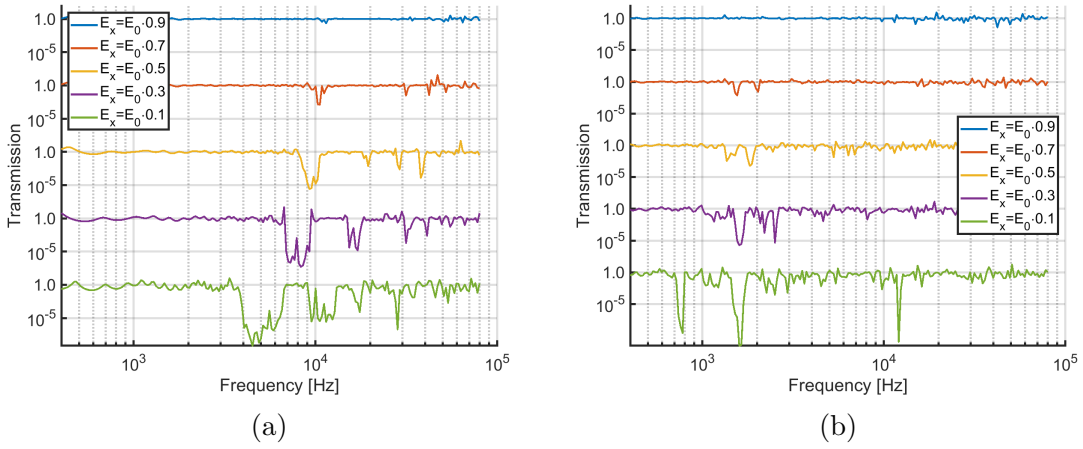


Figure 2.5: (a) Figure 2.3a, reported here for comparison. (b) Transmission spectra for various values of the contrast, when the PBC are removed from the model in figure 2.1a. All other parameter are the same as for (a).

In figure 2.5 a comparison between the case with and without PCB is performed. As it is shown in fig. 2.5b, without PBC small band gaps are still forming, but their location is not as predictable as before. Interestingly enough, if one were to compare the location of the band gap for this new case with the one were the input displacement was set perpendicular (figure 2.3b), one would find better agreement. As if the longitudinal input, that was supposed to excite mainly longitudinal waves, had more effect in producing shear waves. This happens because the analysed geometry can no longer be considered a bulk material, but it behaves as a waveguide.

Since without PBC the geometry represent a real section of a slab, it might be useful to use a more realistic input source. Therefore a prescribed displacement was imposed onto a portion of the top boundary, that can be better understood by observing figure 2.6a. Notice that in this case the displacement is imposed only in the direction perpendicular to the boundary.

Also the height has to be set such that the model in fig. 2.6a becomes

a realistic representation of the section of a slab, thus should be set for a thinner value. Moreover, the reduction of the height allows for creating a finer mesh which improves the resolution at high frequency.

Parameter	Value	Unit	Parameter	Value	Unit
E_0	2	MPa	h	2.5	mm
ν	0.4997	/	L	7	cm
ε	0.1÷0.9	/	N	20	/
Λ	2	mm	FF	0.5	/

Table 2.4: Parameters of the model without PBC.

Performing some studies on PDMS, as it will be described in the next chapter, it appears that the Young's modulus can be modified during the preparation of the samples. Therefore for this model it was chosen to use a value that better fits better the real samples Young's moduli.

Moreover this elastomer has a peculiarity: even though E can be adjusted at will, the propagation velocity does not change much [38]. In order to take into account for this fact even in the computations, the value of the Poisson's ratio was changed in order to obtain a propagation velocity for the longitudinal waves comparable with the one proposed in [38], where the author measured the longitudinal velocity of a polydimethylsiloxane sample with different hardnesses. More details on the topic are presented in section 3.2.

The parameters for the new model are all summarised in table 2.4.

With these new, more realistic, conditions the results are not satisfying, if not worst. It is hard to uniquely identify band gaps, which suggest that the confinement along the y -direction forbids to treat the problem as simple Bragg reflector. At this point the geometry has to be considered a waveguide, where the effect of the dispersion of modes cannot be ignored. Nonetheless the introduction of a global band gap should still be possible, even if not with a predictable location (which is the whole point of these numerical computations).

It will be shown in the next sections and in the next chapter, that the main problem for these results comes from the nature of PDMS of being an almost perfect rubber. The fact that the value of the Poisson's ratio is so close to 0.5 makes the difference between longitudinal and transverse waves velocities diverge (see the relation (1.28)). Therefore the various modes that can propagate inside the waveguide can have very different velocities (orders

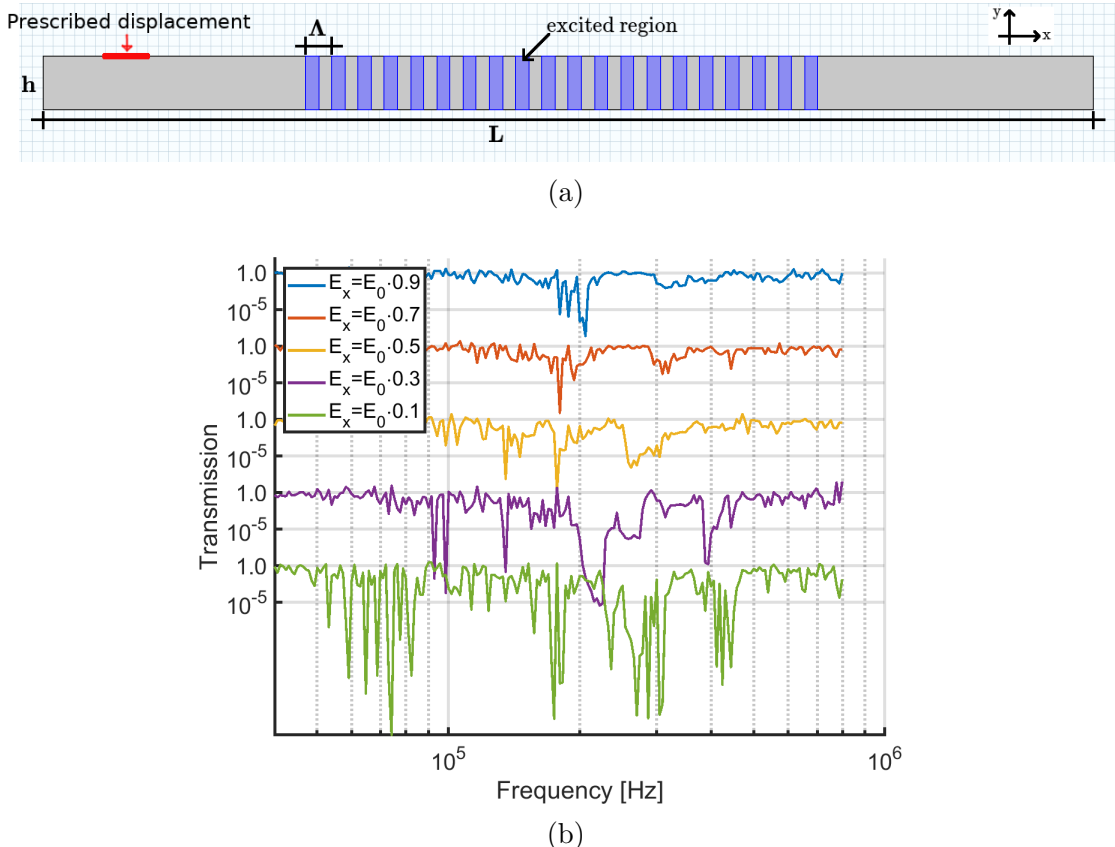


Figure 2.6: (a) New geometry. (b) Transmission spectra for various values of the contrast for the new geometry; parameters in table 2.4. Notice that both x - and y -axis are plotted in log scale.

of magnitude), which makes creating a band gap valid for all these modes very difficult as well. By taking into account for the attenuation of the material, this problem will partially be solved.

2.2 Elementary cell analysis: Band diagram and band gaps

The best way to study and analyse the behaviour of metamaterials and/or phononic crystals, is to study the elementary cell or the elementary resonator that composes them.

In the case of phononic crystals, the analysis of the primitive cell is performed in order to extract the band diagram. For metamaterials which resonant structure is embedded in the primitive cell of a lattice, the band diagram can be computed using the very same technique.

A description of the extraction of the band diagram has already been given in section 1.3.1. It basically consists in solving an eigenvalue problem by looking for the eigenmodes of the primitive cell, after the assignment of proper boundary conditions at the borders.

In the particular case of COMSOL, once the primitive cell is created, the study has to be set as *eigenfrequency*. At those boundaries for which the periodicity exists, PCB of *Floquet* type are imposed. These allow to force a value for k -vector at the boundaries, and then find a set of corresponding eigenfrequencies.

In order to show the validity of this technique, first some results presented in the literature are reproduced. Then an analysis of the same structures is performed using the properties of the material and of the samples used in the experimental part of this thesis work.

2.2.1 Literature comparison

The first structure that was analysed is an example that was proposed in a PhD thesis work [39] where a two dimensional periodic structure² is analysed by means of FEM and COMSOL.

The proposed structure is presented in figure 2.7. The material used for the structure was aluminium having properties $\rho = 2699 \text{ kg m}^{-3}$, $E = 70.3 \text{ GPa}$ and $\nu = 0.3436$. Unfortunately the author forgot to mention the exact values used for the periodicity a and the internal square side m , therefore three

²As in previous subsection this is equivalent to a three dimensional structure, infinite in the direction of the missing dimension.

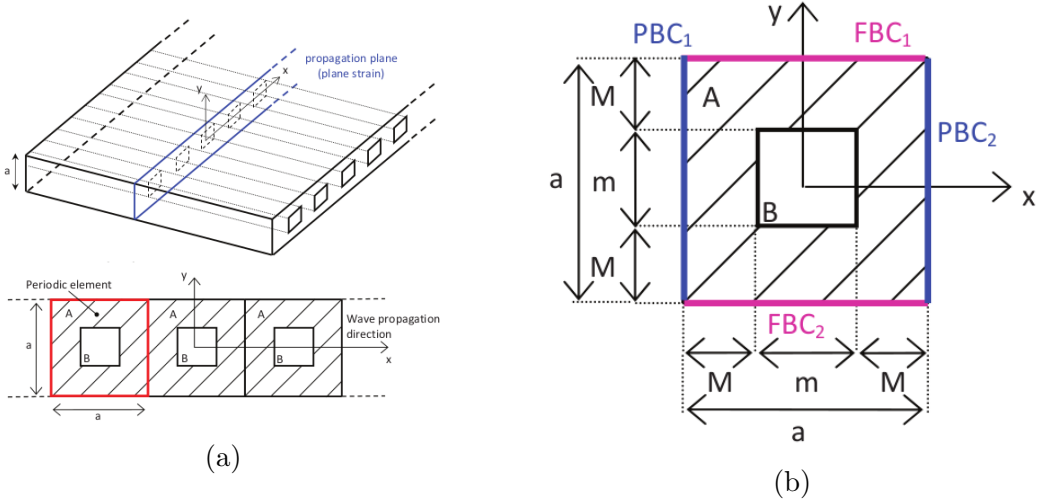


Figure 2.7: (a) Structure of a 3D phononic crystal, periodic only in one direction.
 (b) 2D primitive cell.

values for the first where used in this work, while the second was extracted from the figure ($m \approx \frac{2}{5}a$).

Since the structure is periodic only along the x -direction, periodic boundary condition are only applied at the boundaries perpendicular to this direction, while for all the others Free Boundary Conditions are imposed. A wave propagating in the structure can therefore propagate only along the x -direction, which means that the FBZ will be limited to the k_x vector.

The results proposed in figure 2.8 show the formation of a band gap. Depending on the primitive cell square side, the whole band diagram is scaled accordingly. As one may expect the greater a is (i.e. the thicker the slab in figure 2.7a is), the lower are the frequencies in the band diagram and, for $a \approx= 1$ mm the band gap is found to be very similar to what proposed in [39]. The remaining non matching features of the band diagram can be accounted for the improper value of the $\frac{m}{a}$ ratio, and further testing would be pointless since perfect matching for the next structure will be shown (which size is perfectly known).

The second comparison is made with the results proposed on [40] where the structure in figure 2.9 is analysed. This consist of a infinite slab of thickness h covered with cross like holes with periodicity a both in x - and y -directions. In this case the PBC have to be applied (separately) to the side facing the x -direction and the side facing the y -direction, while on the others FBC are

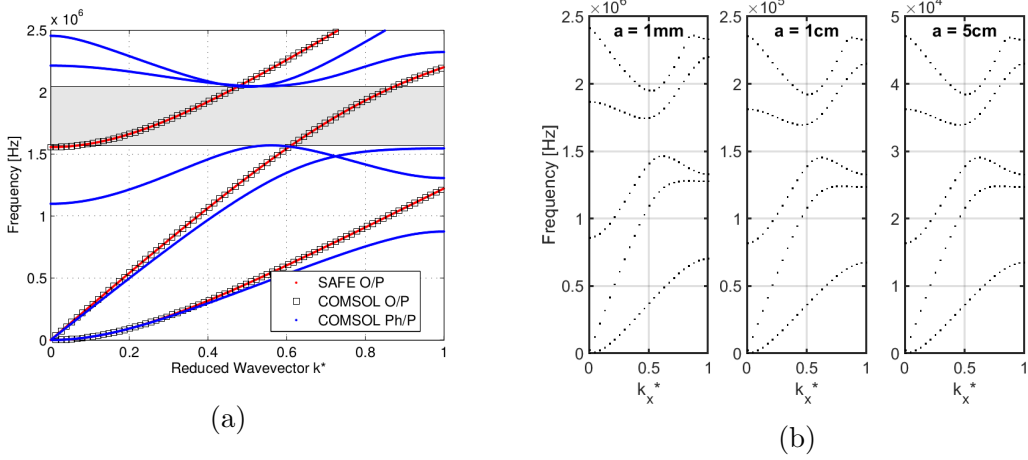


Figure 2.8: (a) Results from [39] (the blue line is the one to be reproduced) and (b) reproduced results. Notice that on the x -axis there is the reduced wavevector $k_x^* = \frac{k_x}{\pi}a$.

imposed.

The structure parameters are $a = 20\text{ mm}$, $h = \frac{3}{5}a$, $b = 18\text{ mm}$ and $c = 3\text{ mm}$, and the material is considered to be made out of PVC with $\rho = 1430\text{ kg m}^{-3}$, $E = 3\text{ GPa}$ and $\nu = 0.4$.

This time, the periodicity develops in two dimensions, the FBZ will extend for both k_x and k_y . Due to symmetrical reasons the band diagram is usually represented in the so called *irreducible* Brillouin zone and the result is shown in figure 2.10.

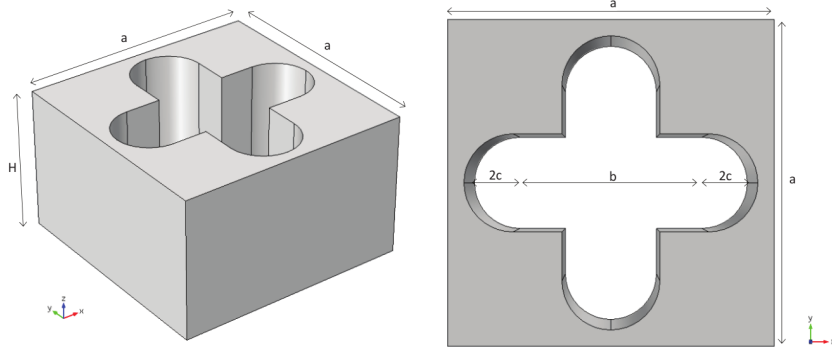


Figure 2.9: Primitive cell of a 3D phononic crystal analysed, periodic along the x - and y -directions.

The band diagram shows the presence of two global band gaps and perfect matching is found with respect to literature.

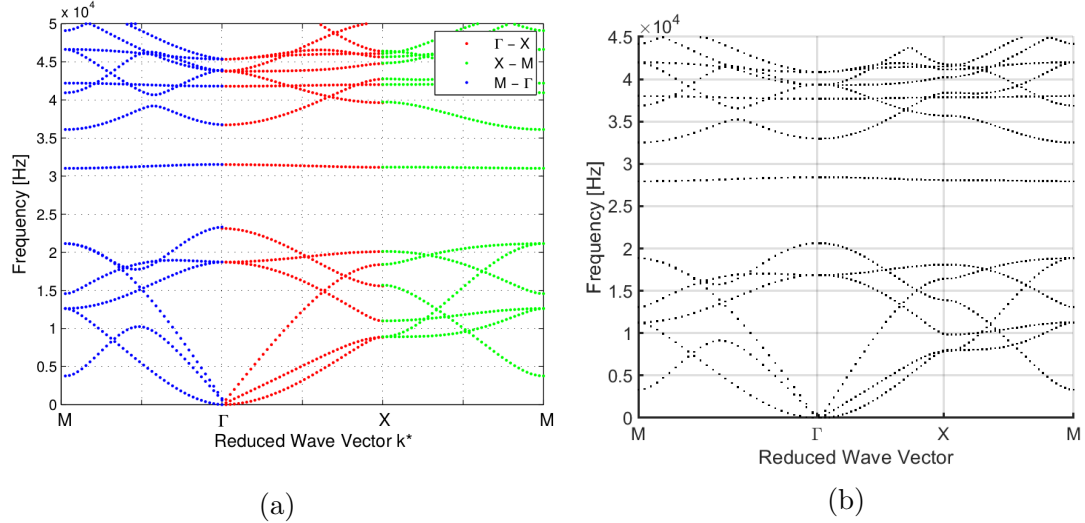


Figure 2.10: (a) Results from [40] and (b) reproduced results. Notice that on the x -axis there is the reduced wavevector where $\Gamma \rightarrow (k_x^* = 0, k_y^* = 0)$, $X \rightarrow (k_x^* = 1, k_y^* = 0)$ and $M \rightarrow (k_x^* = 1, k_y^* = 1)$.

2.2.2 PDMS structures

Since the previous structures were able to show the formation of a band gap, it seems natural to use them, changing the intrinsic material with the one proposed for this thesis work, i.e. substitute aluminium with polydimethylsiloxane.

For the first structure (fig. 2.7) the formation of a band gap is shown, but the frequency at which it forms is much lower than what happened for the aluminium case. This obviously is addressed to the material properties since PDMS has a Young's modulus at least three orders of magnitude smaller than aluminium. Moreover section 3.2 will show that the presence of attenuation makes impossible dealing with such low frequencies.

This structure revealed to be not usable for the application this thesis is aiming to produce. As shown in the next chapter, in practice the pattern will be created by means of light projected on top of a slab-like sample. It is necessary, even in the numerical model, for any section along the thickness of the slab to be identical. For this reason the second pattern suits the best.

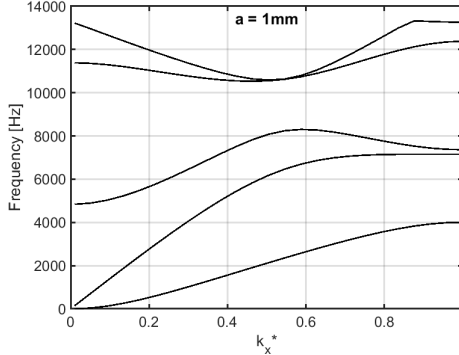


Figure 2.11: Band diagram for the structure in figure 2.7, where aluminium has been replaced with PDMS.

The structure in figure 2.9 was analysed changing the intrinsic material from PVC to PDMS and the presence of a band gap (fig. 2.12a) can be seen even for this case. However, this kind of primitive cell does not contain

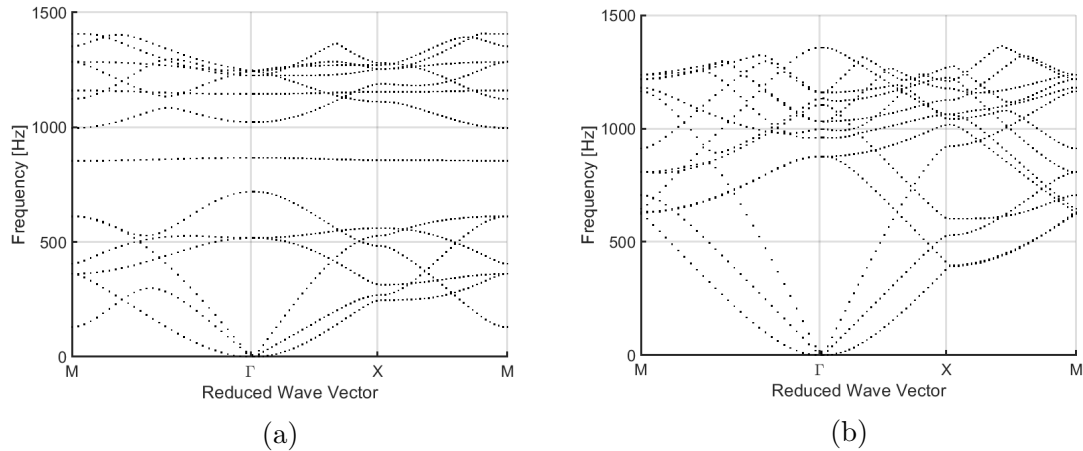


Figure 2.12: (a) Band diagram for the structure in figure 2.9 where PVC was replaced with PDMS. (b) Same structure, but the internal hole has been filled with PDMS having modified elastic properties.

any part with different elastic properties, therefore it is does not resemble the configuration where an external illumination has changed the material elastic properties. Following the same meaning as in the previous section, the contrast between the inner and outer Young's moduli was set to $\varepsilon = 0.5$. Unlike the result in figure 2.12b clearly shows the absence of any gap. Even reducing the thickness (and all other features) by ten times produces

no different result.

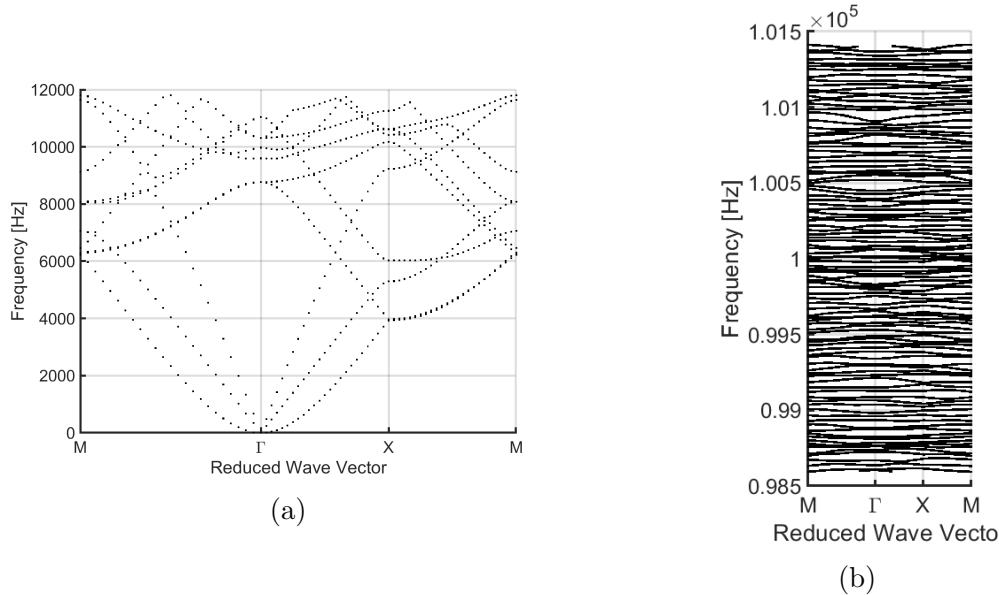


Figure 2.13: (a) Band diagram for the structure in figure 2.9 where PVC was replaced with PDMS and the size reduced by ten times. (b) Same structure, band diagram centred at higher frequencies.

From the study of the various band diagrams one thing seems to be inevitable: this kind of study performed on PDMS focuses only on low frequency modes. But this is not compatible with the result from section 3.2.2 that clearly shows the impossibility of working at low frequencies using slab-like PDMS samples. Performing instead a study of the same kind but forcing the creation of the band diagram for high frequencies is completely useless, and the reason is evident in figure 2.13b. At high frequencies the FEM model detects too many modes that can hardly be distinguished one from the other.

The only option left do be done is to include in the numerical models also the effect of attenuation.

2.3 Including attenuation

When it comes to interference phenomena, and particularly in metamaterials and phononic crystals, attenuation and damping are hardly welcome. Attenuation tends to reduce the formation of band gaps by reducing the formation of interference and therefore it may change the behaviour of the material even in unpredictable ways.

The reason is simple: if attenuation is present it means that the more a wave travels the more its amplitude is reduced, and therefore it is more unlikely for it to interfere (constructively or destructively) with another wave. For metamaterials and phononic crystals this is extremely deleterious.

Another way of seeing the problem is by thinking of the effect of attenuation on the spectrum of a wave. It is well known that even for a pure single frequency excitation, damping will induce in the generated wave a broadening of its spectral line, thus introducing new spectral components. The wider is the spectrum of a wave, the harder it is for it to interfere with other waves.

Nonetheless sometimes it is impossible to avoid attenuation effects and therefore it is necessary to include it also in numerical models, by including the intrinsic viscosity of the material involved.

In the previous section it was shown how FEM could be used to extract the band diagram from the primitive cell of a phononic crystal. In few words the technique consists in finding the eigenmodes of the primitive cell structure when at this is applied particular (periodic) boundary conditions.

The effect of viscosity of PDMS has to be introduced in this study also to allow to numerically reproduce zero transmission at low frequencies, as the laboratory measurement are showing [3.2.2](#). For an eigenvalue problem, including attenuation doesn't mean to exclude low frequency modes, instead it means that the found solutions will have complex eigenvalues. With this kind of analysis it is practically impossible to distinguish between propagating and non propagating modes. This means that the standard method used for the analysis of the primitive cell cannot be used any more.

One option is to proceed with the same model (fig. [2.6a](#) and tab. [2.4](#)) used in the first section of this chapter and include the effect of viscosity. For this purpose a value for the shear viscosity of $\eta_s = 0.5 \text{ Pa s}$ was used. In order to simplify the problem the full model proposed in figure [3.13](#) was not implemented and also the bulk viscosity was neglected since its value can be even one order of magnitude smaller than the shear one.

Another option could be to give up on FEM analysis and shift to FDTD

method, but this will not be performed in this work.

It should be noted that in the following many information presented in the next chapter (more precisely in section 3.2) will be used, therefore some information will be presented here without additional explanations.

2.3.1 Cut-on frequency

Before analysing the model and look for the formation of a band gap in the frequency response, it is necessary to verify if the model is able to reproduce the behaviour of the samples presented in section 3.2.2. Basically rod-like and slab-like PDMS samples show the presence of a cut-on frequency which value seems to be related to smallest feature (thus the thickness) of the structure. This cut-on frequency was not present in any of the numerical models analysed so far.

For this kind of analysis the presence of the pattern (the regions having different Young's modulus) is not necessary. Therefore the pattern was removed by simply imposing the contrast to be $\varepsilon = 1$. Then the numerical problem was solved using different values of the thickness h in order to observe the consequent behaviour of the transmission spectrum.

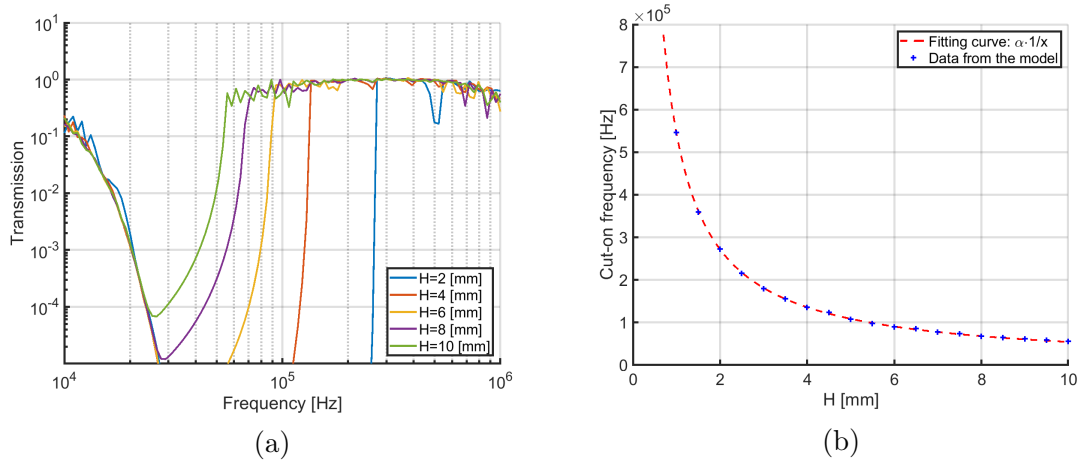


Figure 2.14: (a) Obtained transmission spectrum for different values of the thickness.
 (b) Cut-on frequency value as a function of the thickness h .

The result of the computation shows no transmission in a wide range of frequencies as a consequence of taking into account for the viscosity. Since the full model of figure 3.13 was not implemented, at low frequencies there

still is transmission, but it is not important as long as it is possible to extract the value of the cut-off frequency.

In figure 2.14 this operation was performed for many values of thickness and then the value of the cut-on frequency is extracted for each of them. Figure 2.14b shows also that between the two there is a relation of the type $f_{cut} \propto 1/x$.

2.3.2 Recovering the band gap

Even though the obtained cut-on frequencies were not perfectly matching the ones from the samples of sec. 3.2.2, it is reasonable to say that there is a very good agreement. It is now necessary to study how the system behaves when the periodic structure is reinserted in the model.

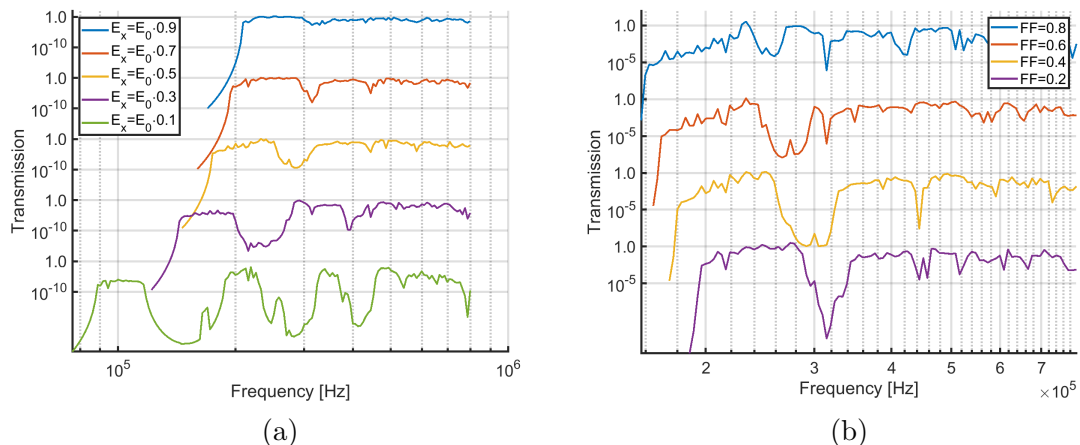


Figure 2.15: Transmission spectrum for the geometry in figure 2.6a and parameters in table 2.4, plus $\eta_s = 0.5$ Pa s. Result for multiple values of (a) the contrast and (b) the fill factor (the latter fixing $\varepsilon = 0.5$).

Therefore the structure proposed in fig. 2.6a was analysed, using again the parameters in tab. 2.4. The results are reported in figure 2.15 and they clearly show the formation of a wide band gap. Unexpectedly the value of the cut-on frequency strongly varies when the contrast is changed. For low values of contrast the transmission spectrum seems to never reach the unity value, therefore the formation of the band gaps becomes of minor relevance (everything is attenuated).

For this numerical analysis the expected centre of the gap (according to the Bragg condition) is always lower than the one resulting from the figure.

For instance for $\varepsilon = 0.5$ the Bragg condition is satisfied for $f_g = 222\text{ kHz}$, while in the computation the centre of the gap is close to 280 kHz and at 222 kHz the gap is not even present.

Another study that might be of interest for the experimental work is on the effect of the fill factor FF on the band gap. Thus the numerical model was solved again, fixing the value of the contrast to $\varepsilon = 0.5$ while changing FF in the range $0.2 \div 0.8$.

The result in figure 2.15b shows a slight variation of the central frequency of the gap when the FF varies and also an effect on the cut-on frequency is observed.

Conclusions

In this chapter it was possible to demonstrate that taking into account the material attenuation is fundamental to properly model the acoustic response of polydimethylsiloxane. Therefore it was shown that the analysis of the elementary cell is practically impossible, while it becomes necessary to rely on full sample analysis.

Nonetheless it was also shown, in the full sample model, that it is still possible to introduce an acoustic band gap in the frequency response of the material, as long as the Young's modulus in the illuminated regions changes at least by $20\% \div 30\%$ with respect to the rest value.

Chapter 3

Experimental study

The numerical model were able to provide some useful results. They were able to support the possibility of introducing a band gap by means of changing the elastic properties of the sample in local regions. However, the unavailability of the standard methods used for the analysis of the primitive cell forbids to make predictions when dealing with complex patterns, and therefore it forces the experimental research to proceed following less reliable assumptions.

This chapter aims to present the experimental work that allowed to gather information about the acoustic behaviour of some photo-responsive polymeric samples when they are illuminated with a simple pattern. Due to time limitation, this has to be considered a preliminary analysis because only the pattern studied in the numerical analysis (section 2) was tested in the lab and, unfortunately, more complex and two dimensional patterns were not tested.

3.1 Experimental setup

Combining optics when working with acoustic instruments is not a standard procedure (except when dealing with Doppler Vibrometers), therefore for the purpose of this work it was necessary to create an ad-hoc setup.

The setup basically consist of a sample holder which can handle two ultrasound piezoelectric probes and one sample beneath them. An amplifier is used to bring the signal from a signal generator to the injecting probes and an oscilloscope is used to read the output coming from the other probe. Then a LASER is used to illuminate the sample in a region between the two probes and a mask is placed in the middle of the optical path in order to create the pattern. Both the acquisition from the oscilloscope and the control of the

LASER where performed by means of MATLAB.

A scheme of the setup is shown in figure 3.1.

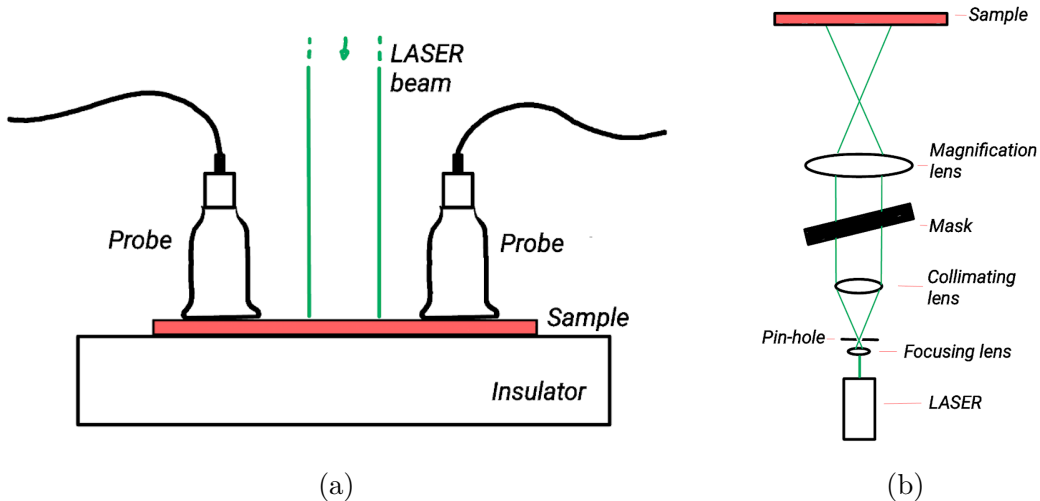


Figure 3.1: (a) Acoustic setup. (b) Optical setup.

3.1.1 Acoustic setup

The probes used for the injection and sensing of ultrasound waves are two piezoelectric probes from DAKEL¹. Their frequency response is centred at 250 kHz and they are typically used in structural health monitoring, for listening the ultrasound waves produced by the micro-movements of a structure caused by wearing and ageing (acoustic emission experiments).

The sample holder consist of a polyurethane basement fixed onto a rigid metallic structure. Such basement has to be able to isolate the sample from the environment and it is necessary because the flexibility of the samples forbids to use any configuration where the latter is suspended in air.

The probes are then fixed to the metallic structure to which the basement is attached. In this way the sample can be placed in between the basement and the probes, which can then be tightly fixed, forming a stable firm configuration. The stability of this configuration is fundamental because, due to the soft nature of the polymer composing the sample, any little change in position of the probe may produce changes in the shape of the acquired

¹Diagnostics department of ZD Rpety, CZ; visit www.dakel.cz

3.1 – Experimental setup

spectrum. If happening during the acquisition of the spectral time evolution in an experiment, it would nullify the entire acquisition series.

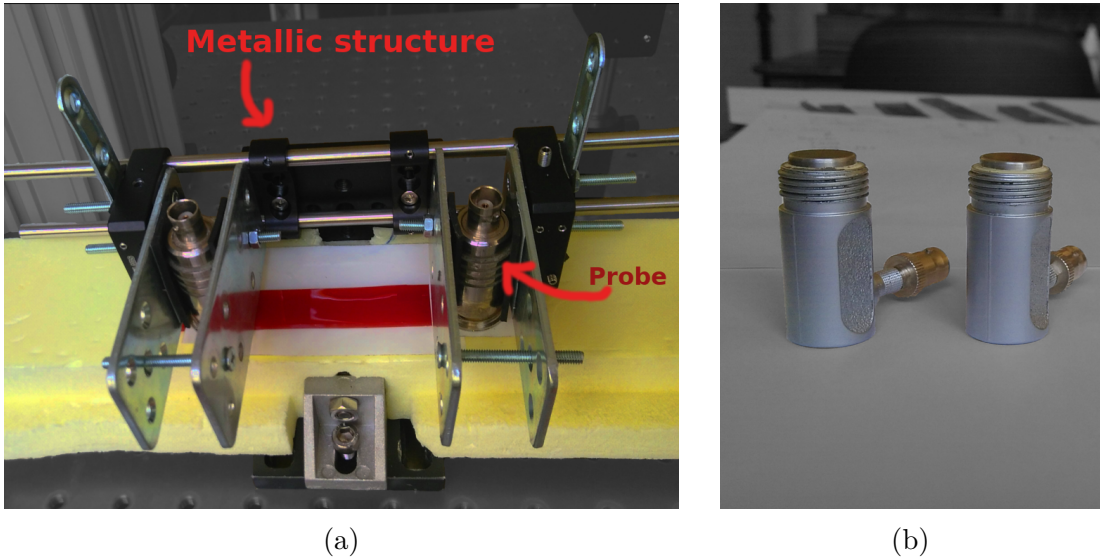


Figure 3.2: (a) Sample holder. (b) Probes.

The contact between the probes was at first enhanced by means of eco-graphic gel and then substituted with simple bi-adhesive tape.²

The signal was produced by an arbitrary waveform generator from *Agilent* - 33500 Series. Then it is amplified with a voltage amplifier from *FLC Electronics* (which amplifies the signal by twenty times) and it is injected in one of the two probes placed on the sample holder. The signal is collected by means of an high definition oscilloscope from *Agilent* - DSO9024H which bandwidth reaches 250 MHz.

The spectral response is obtained by injecting a signal with a wide frequency spectrum and simply comparing it with the spectrum of the output. If such signal is created by means of the *sweep* function of the waveform generator, its spectrum can be considered approximately uniformly distributed along a given range of frequency. The sweep function creates a signal in the form

$$y = A_0 \sin(\omega_{(t)} t),$$

²The reason for this change is described in the following sections.



Figure 3.3: (a) Oscilloscope. (b) Waveform generator and amplifier.

where $\omega_{(t)}$ varies linearly between a minimum and a maximum frequency, and then it is repeated in time.

The acquired signal is then analysed in a post-processing procedure by means of Fast Fourier Transform algorithm (FFT) in order to extract the output spectrum from the recorded signal. Since the input spectrum is practically "flat"³, it is possible to directly consider the spectrum of the output signal as the frequency response of the sample under test, without the need to compute the ratio of output versus input. It should be noted that, for the very same reason, in this way the actual value in terms of decibel of the frequency response is meaningless. Nonetheless all measurement were performed using a signal with the same amplitude and acquiring using the same parameters on the instruments, which makes the various spectra comparable.

3.1.2 Optical setup

The illumination is provided by a 532 nm torus LASER from *Laser Quantum*. The unit is controlled by an mpc 3000 controller, which can be driven via serial port using simple commands sent with MATLAB. The LASER can provide a power ranging between 50 mW - 750 mW.

³The Fourier transform of a sweep function is approximately flat over the range of frequencies the sweep covers.

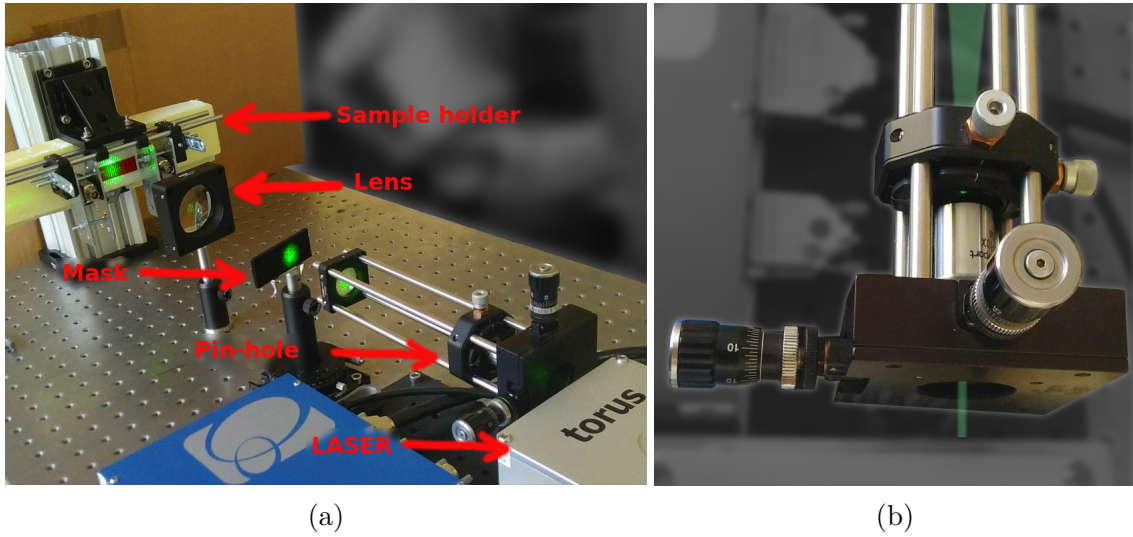


Figure 3.4: (a) Whole setup. (b) Zoom on the focusing lens and pin-hole.

The LASER beam exiting from the LASER box has a diameter of approximately 1.7 mm, therefore it is necessary to increase its size in order to illuminate a wider spot on the photo-responsive sample. For the purpose the beam is first focused onto a pin-hole, which allows to clean the spatial distribution of the beam, and then it is collimated again using a 25 mm lens with focal length of 75 mm. This creates a beam of approximately 25 mm in diameter.

The sample holder is then placed onto a vertical rail for positioning the sample perpendicularly to the LASER beam. A mask can then be placed in the middle of the beam path, in order to project a patterned illumination, and it may be combined with a lens in order to also scale the latter. The mask is placed on top of a rotating element in order to allow the deformation of the projected pattern.

3.2 Polydimethylsiloxane

It is now necessary to give some information about the polymer used for the samples.

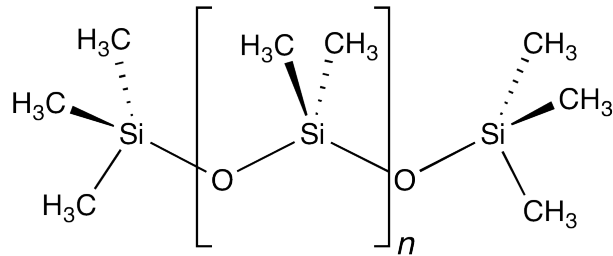


Figure 3.5: Molecular structure of polydimethylsiloxane [41].

Polydimethylsiloxane, usually known with its acronym PDMS, is an elastomer that gained a great popularity in the field of MEMS and micro-fluidics (e.g. [42, 43]). The reason for its popularity comes from its ease of use which allows the creation of very precise elastic micro-structures. It is flexible, optically transparent and it is inert to many organic/inorganic compounds. In the above mentioned fields devices and structures can be created by simply pouring the polymer onto prestructured stamps, by means of the casting technique. Moreover it has a relatively low cost.

Other than those, the main reason why this material was chosen to perform these studies comes from the possibility of inducing light responsiveness by introducing in the polymer matrix a chromophore molecule. In the following subsection the mechanism behind these photo-responsive chromophores will be presented.

Previous works have already shown the capabilities of light responsive polymers. In [44] researchers have shown how the refractive index of an azo-doped PDMS thick membrane could be illuminated with a Gaussianly distributed beam, at a wavelength at which the responsiveness is greater, and change reversibly the refractive index according the beam spatial distribution. Therefore the graded refractive index, which can be approximated with a parabolic behaviour close to the centre of the beam, could be used as a tunable lens acting on those wavelengths to which the membrane is most transparent. In [45] the authors were able to create photo-responsive polymeric substrates in which micro-pillars deformed their shape along the

direction of the polarisation of the illumination. Then use these substrates to force, or partially confine, the growth of substrate sensitive cancer cells, along and by means of the pillar direction. In [46] the authors were able to observe strong mechanical deformations onto a suspended light responsive micro-membrane.

Light responsiveness is not the only way to change the properties of a material by means of a stimulus. In fact they are part of a broader category of the stimuli-responsive materials, which introduces the concept of *smart* materials, and these results, together with many others [47], shows how such materials could be used for new promising applications.

For the purpose of this thesis work, the stimuli responsiveness of such materials has to imply a change in its elastic properties. Since many of these smart materials are able to show a mechanical response upon illumination [45, 46, 48], a variation of the elastic properties is also to be expected.

The reason why it was chosen to focus on light responsiveness is rather intuitive. First and foremost the use of light allows for remote control, which allows to decouple the control system from the actual device. Moreover, thanks to simple or, if necessary, complex optical setups it is possible to have a very high precision in such control, both spatially and temporally. For instance the use of a spatial light modulator could be used for the projection of any desired pattern, and controlling it by means of a computer could open for new possibilities by integration with AI.

3.2.1 Inducing light responsivity

In the framework of light responsive materials, it is typical to use chromophore molecules to induce the desired photo-responsivity. These molecules exhibit the ability of switching between two conformational states, upon absorption of properly energized photons. These two states have distinct spectroscopic and physical properties and, when embedded inside the atomic structure of a material, a switch between the two can induce a change also in the bulk properties of the material [49]. Properties that could include shape, phase, wettability, permeability and solubility [50].

One of the most studied photochromic molecules is the so called *azobenzene*, together with its derivatives. It is an aromatic molecule in which two phenyl rings are connected by a nitrogen double bond, which indeed is called azo-linkage. Such bond is absorbent in the UV, and partially in the visible,

part of the spectrum.

The thing that characterizes azobenzene as a photochromic molecule is the photo-isomerization between a *trans* and a *cis* state [51]. Upon absorption of a photon from the azo-linkage, the molecule passes from a thermally stable *trans*-form to a metastable *cis*-form. Basically, as shown in figure 3.6, the metastable form is characterized by a 90° twisting of the phenyl rings relative to the plane of the azo bond.

The reversible reaction toward the stable state occurs either by thermal relaxation or photon emission. The time scale at which an azobenzene can relax to the *trans*-state can range from the order of second to even hours.

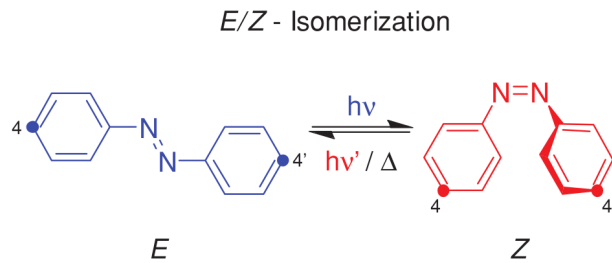


Figure 3.6: Geometrical representation of the photo-isomerization of azobenzene, from *trans* (*E*) to *cis* (*Z*). Image taken from [51].

In order to incorporate the photochromic molecule into a polymer, there are two main possibilities. The easiest way is to create a guest-host system by dissolving the molecule into the polymer matrix. Surely cost effective, because simply mixing the two constituent together is sufficient, it is not very efficient in terms of effects transferred on the polymer matrix. This is because the molecule is not bonded to the polymer chains, thus can be subjected to aggregation or even macroscopic phase separation.

To overcome these problems the molecule can be chemically attached to the polymer backbone. A simple representation of these two methods is presented in 3.7.

Azo-doped PDMS

Since in previous works [44] polydimethylsiloxane samples were successfully doped in order to obtain photo-responsive thick membranes, it was chosen to follow the same method for creating the sample, which is well described in [52, ch. 4.1].

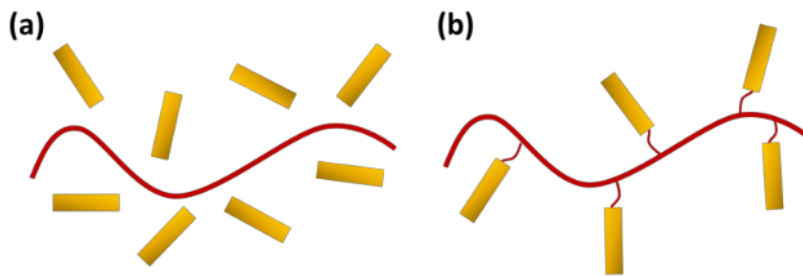


Figure 3.7: Schematic representation of (a) simple guest-host system and (b) chromophore functionalized side-chain polymers. Image taken from [52].

The developed material is a mixture of PDMS and poly(Dispersed Red 1 Methacrylate), resulting into a simple guest-host system (fig. 3.7). The former is made with a kit from Dow Corning (DOWSIL™ 184 Silicone Elastomer Kit), which consist of a base and a curing agent. Using different relative amounts of the two produces samples with different hardness and the extent of this is discussed in the following subsection. The doping is thus made with pDR1M, which is basically a colourant that offers good miscibility with PDMS (thanks to the presence of the methyl group). The powder sold by Sigma Aldrich was used.

Therefore the samples are prepared in the following way:

1. pDR1M is dissolved in toluene (anhydrous, $\geq 99.8\%$, Sigma Aldrich) with a concentration of 2wt.%, without stirring but using an ultrasound bath for 1h40min;
2. the proper amount of the solution is vigorously mixed with the PDMS base and the whole is left resting, either in low vacuum or under the fume hood, to allow for the solvent to evaporate;
3. the desired amount of curing agent is added to the mixture, stirred and kept in low vacuum for some minutes (not for too long otherwise the risk is to solidify before its casting) in order to remove all the air bubbles;
4. finally the (yet) viscous liquid is poured onto the stamp and kept into an oven at 60°C for at least 2h, for thermal curing.

The author of [52] found that the amount of pDR1M-toluene solution to be added on the PDMS base, in order to get the best results, should be $70\ \mu\text{L}$ of the solution for every 5 mL of base. For the purpose of this thesis such

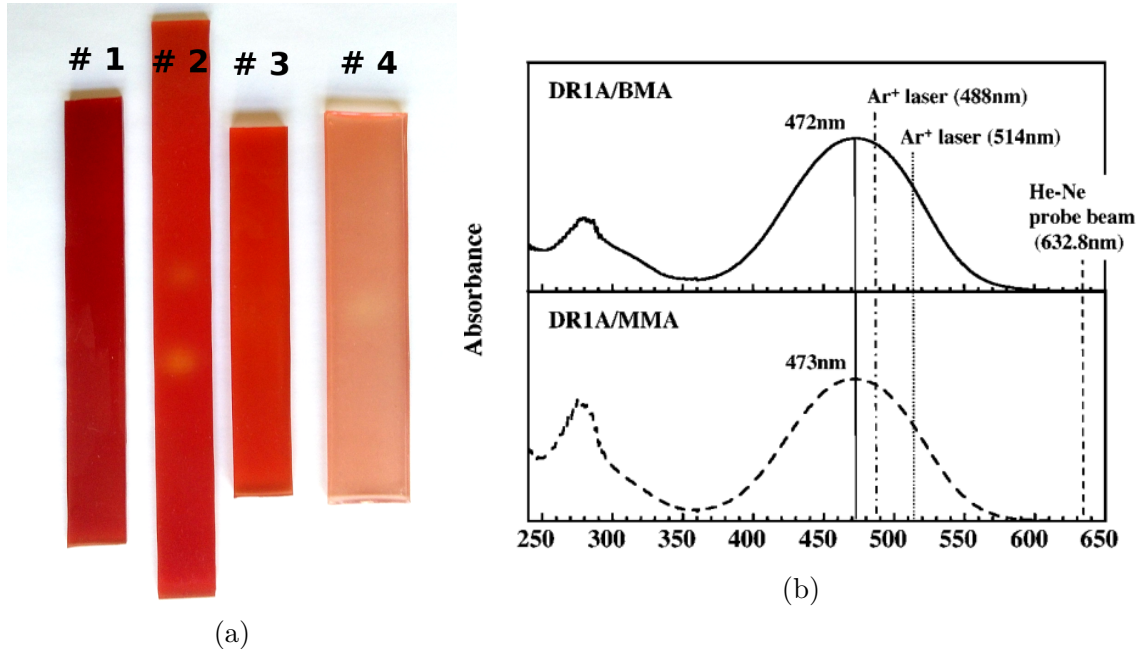


Figure 3.8: (a) Azo-doped samples used in the experimental study. (b) Absorbing spectrum of copolymers based on Dispersed Red 1 Methacrylate, taken from [53].

concentration is too low in order to obtain considerable effects in the acoustic response of the sample, therefore samples with higher concentration were produced: (70,150,250,700) μ L for every 5 mL of base used, which corresponds to a relative volumetric concentration of (1.4, 2.9, 4.8, 12.3)%. Such samples are represented in figure 3.8.

Actually the exact amount used is not to be trusted, because pDR1M wasn't able to completely dissolve into toluene and some residuals were present in grains at the bottom of the container. This might caused by the ageing of the pDR1M powder. Obviously the solution was inserted into the polymer base taking care of avoiding those grains too.

The samples characteristics are summarized in table 3.1.

3.2.2 The elastic properties

Polydimethylsiloxane is a very flexible polymer having an extensively cross linked matrix that makes it an elastomer. Being a (silicon) rubber, its Poisson's ratio is very close to 0.5. Since it is such a popular material for a variety of applications, it has also been studied in great details and its

Sample #	Thickness	Length	Width	base/curing	pDR1M sol %
1	3 mm	106 mm	22 mm	10:1	1.4 %
2	4 mm	101 mm	16 mm	10:1	2.9 %
3	2.5 mm	159 mm	16 mm	10:1	4.8 %
4	2 mm	126 mm	16 mm	3:1	12.3 %

Table 3.1: parameters for the samples presented in figure 3.8.

properties are well known.

In terms of elastic properties, the main interesting fact that one comes across is the possibility of tuning the hardness of the material just by changing the base to curing agent ratio. In multiple studies researchers have shown the variation of various elastic properties as a function of the base to cure ratio. In [54] they were able to show the trend of the Young's modulus when reducing such ratio by measuring with stress-strain technique. In [55] the authors were able to report a roughly linear relation between the amount of cross linker (curing agent) and the resulting E (one of the authors reported more results in its PhD thesis work [56]). Since their results were used as a reference for creating the PDMS samples for this thesis work, they are reported in figure 3.9.

As it was already mentioned in one of the previous chapter, there is one peculiarity about these relation. In [38] researchers found out that changing the hardness of the material does not affect the propagation velocity in the

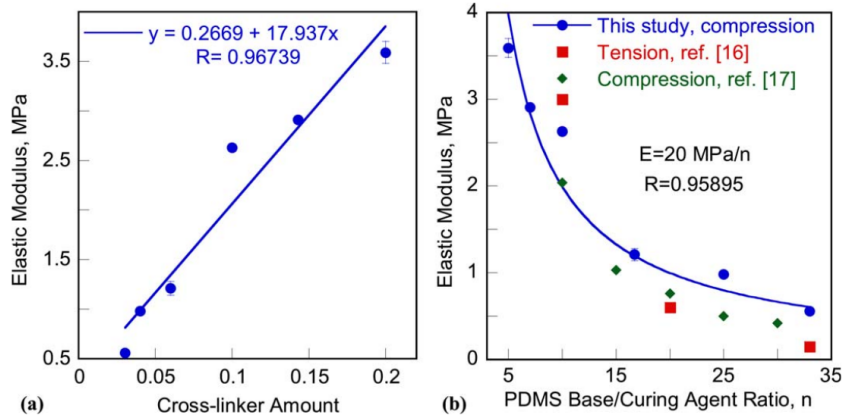


Figure 3.9: Graphic representation of the dependence of E as a function of (a) the cross linker to base ratio and (b) the base to curing agent ratio. Image taken from [55].

same way. Actually they measured the propagation velocity of p-waves and seen a very slight variation, if not null, upon variation of the base to cure ratio. For values ranging from 10:1 to 2:1 the velocity was measured of being between 1050 m s^{-1} and 1100 m s^{-1} .

Instead, if one were to consider the relation found in fig. 3.9 and insert it in equation (1.28), he would find a square root behaviour of the velocity with respect to the curing agent amount.

$$c_l = \sqrt{\frac{E(1-\nu)}{\rho(1+\nu)(1-2\nu)}}$$

For the range of values previously mentioned the Young's modulus varies $\approx 2 \text{ MPa}$ to $\gtrsim 4 \text{ MPa}$, which means that it basically doubles its value. This should translate into an increase of c_l of about $\sqrt{2}$ times which, as explained, it was not measured. This phenomenon might be explained by inserting some values in these equations.

Considering for instance a fixed propagation velocity of $c_l = 1070 \text{ m s}^{-1}$, with density $\rho = 970 \text{ kg m}^3$ and Young's modulus $E = 2 \text{ MPa}$ (which correspond to 10:1 base to cure ratio), one finds that the corresponding Poisson's ratio has to be $\nu \approx 0.4997$. If instead one considers $E = 4 \text{ MPa}$ while imagining both the velocity and the density to be constants, he finds $\nu \approx 0.4994$ which is a relative variation of only -0.06% . That is to say that an extremely

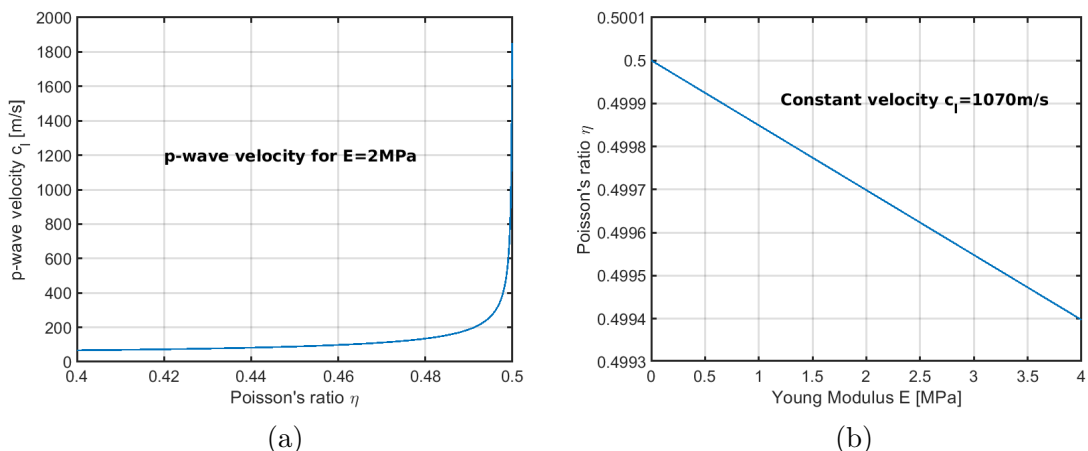


Figure 3.10: Relations between ν , E and c_l for (a) constant $E = 2 \text{ MPa}$ and (b) constant $c_l = 1070 \text{ m s}^{-1}$.

small variation of the Poisson's ratio is sufficient to keep the propagation velocity constant, because its value is too close to 0.5 that is a singularity in expression 1.28. This is well understood by observing figure 3.10 where the relations between ν , E and c_l are translated into plots.

Information from the sample testing

In order to have a quick (and rough) verification of the propagation velocity behaviour, a few samples of plain PDMS were produced and their acoustic response was measured using the apparatus described in section 3.1. The samples are rod-like with a rectangular section

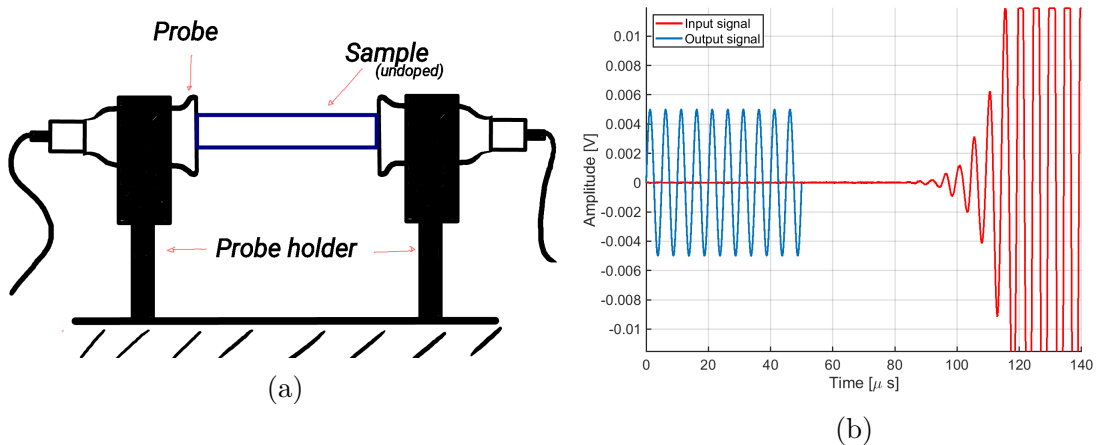


Figure 3.11: (a) Scheme of the probes location when measuring the time of flight.
 (b) Example of burst signal with the output response.

To measure the propagation velocity the best method is to measure the time of flight (*tof*) of an acoustic burst signal. In order to measure it, two ultrasound probes are located at the two extreme ends of the sample on the section perpendicular to their main axis (fig. 3.11a). This type of sample will surely presents some waveguiding properties (presence of multiple modes and their dispersion), nonetheless the one proposed should be the best configuration to excite mainly longitudinal waves. Then, by means of a signal generator and an amplifier, a burst wave packet is injected from one probe. The burst consist of a brief signal, sometimes having a pulse shape or sometimes being a short sequence of sinusoidal periods. In this case it was chosen to use ten periods of a sinusoid of frequency 200 kHz (period 5 μ s). The time of flight is then measured with an oscilloscope as the time between the first

peak recorded from the output probe and the first peak of the input burst, i.e the velocity of the fastest deformation to reach the other end of the sample.

Then the velocity is computed as the ratio between the rod length and the *tof*. As shown in table 3.2, despite the exact value (which is comparable with the results from [38]) the constancy of the propagation velocity upon variation of the Young's modulus is verified.

Base:Cure	Length	<i>tof</i>	c_0
5:1	85.0 cm \pm 0.5 mm	82.2 μ s \pm 0.1 μ s	1031 m s $^{-1}$ \pm 7 m s $^{-1}$
10:1	84.0 cm \pm 0.5 mm	81.6 μ s \pm 0.1 μ s	1029 m s $^{-1}$ \pm 7 m s $^{-1}$
20:1	83.5 cm \pm 0.5 mm	82.0 μ s \pm 0.1 μ s	1017 m s $^{-1}$ \pm 7 m s $^{-1}$

Table 3.2: Measured data for the three rod-like samples.

Another useful information that could be measured is the frequency response of the samples. For this measurements the probes are located on one of the top side and the sample is placed on top of a insulating foundation. Transmission spectrum then obtained as explained in section 3.1.1. The input spectrum (i.e. the sweep function frequency limits) was set to be limited between 30 kHz and 600 kHz.

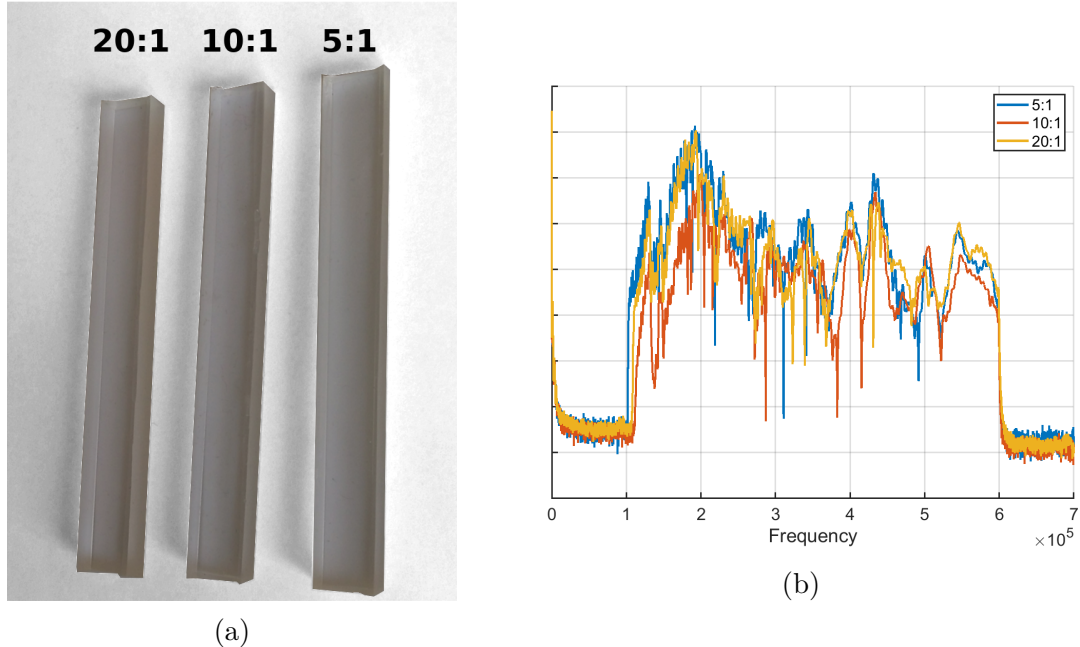


Figure 3.12: (a) Picture of the three rod-like samples. (b) Their frequency response.

The first thing that one inevitably notices is the presence of two boundary in the transmission spectrum. While the upper limit is just the limit of the input spectrum, the lower limit seems to be behaving as a *cut-on* frequency. This behaviour was not to be expected. The second thing is that the cut-on location doesn't seem to follow any trend with respect to the value of the Young's modulus.

Even though the PDMS is known to be a good acoustic insulator [57], a cut-on in its frequency response was not predicted. There are few cases in which it is possible to obtain complete attenuation at low frequency:

1. presence of a foundation as in section 1.2.2;
2. limits in the response of the probes;
3. quality of the contact between probes and sample;
4. a waveguiding effects, thus dispersion of the propagating modes;
5. a frequency dependent absorption coefficient for PDMS.

The firsts three possibilities are easily verifiable. To avoid the foundation it was simply necessary to use place the probes as in figure 3.11a. This didn't produce any result significantly different from fig. 3.12b. Then, neither changing the probe or substituting the ultrasound gel with bi-adhesive tape gave any relevant change in the cut-on frequency.

In order to verify the fourth possibility it is sufficient to modify the geometry of the samples. In particular the cut-off frequency of mode dispersion often depend on the size of the minimal feature of the structure. Therefore a change in height should be sufficient to observe a variation of the spectral position of the cut-on frequency. For this purpose another couple of sample were created with different heights and from their spectral response it is clear that there is a strong dependence on it. In table 3.3 the values of the cut-on frequencies are collected for all these samples.

These results surely confirm that the dispersion of the propagating modes is playing a significant role in introducing a cut-on frequency. Nonetheless it would be wrong to assume that it depends only on that. Indeed for such simple slab-like or rod-like geometries it is not known (at least not by the author of this work) of any configuration for which the dispersion relation for the fundamental mode propagating in the waveguide should posses a cut-on frequency. Or better, the only know configuration is in presence of a foundation, which has been demonstrated not to be the case.

Base:cure	height	f_{cut}
5:1	5.6 mm	103 kHz
10:1	5.9 mm	113 kHz
20:1	5.7 mm	109 kHz
20:1	3.3 mm	174 kHz
10:1	2.5 mm	205 kHz
10:1	0.5 mm	620 kHz

Table 3.3: Measured cut-on frequency for the three rod-like samples (plus two samples with smaller height) extracted from their spectra. Values are qualitative because the cut-on is not always sharp.

Another case where low frequency waves cannot propagate is when the wavelength of the propagating wave is smaller than the total length of the sample. In such condition indeed reflected and propagating waves inevitably interfere destructively, but with longer samples it was seen only a worsening of the signal and an increase of the cut-on frequency.

Therefore there's only one option left to consider, the presence of attenuation of elastic waves into the material.

Viscoelasticity

In elasto-dynamics the general assumption is that for small deformations Hook's law holds, but this means that only one side of the coin is taken into account. In the infamous mass-spring model it is well known that it is necessary to introduce a dissipative term in order to make the model more realistic: the dashpot.

When a deformation in a solid is no more elastic, it means that it starts to creep, i.e. the deformation becomes permanent. The creeping mechanism can be considered as a flow inside the solid, therefore it is possible to study it in the same way as in viscous fluids. The field that studies such type of dissipative flow is called *Rheology* and those solids which present both elastic and viscous properties are called viscoelastic solids [58, ch. 12, 13].

Even if in some way every solid possesses some viscoelastic properties, they can usually be neglected. For many polymers instead it is not the case and viscoelasticity plays a significant role in their mechanical behaviour, thus in their acousto-elastic properties too. This means that to fully characterise a polymeric medium, such as the PDMS samples used in these work, it is necessary to know both the bulk longitudinal and shear attenuation values

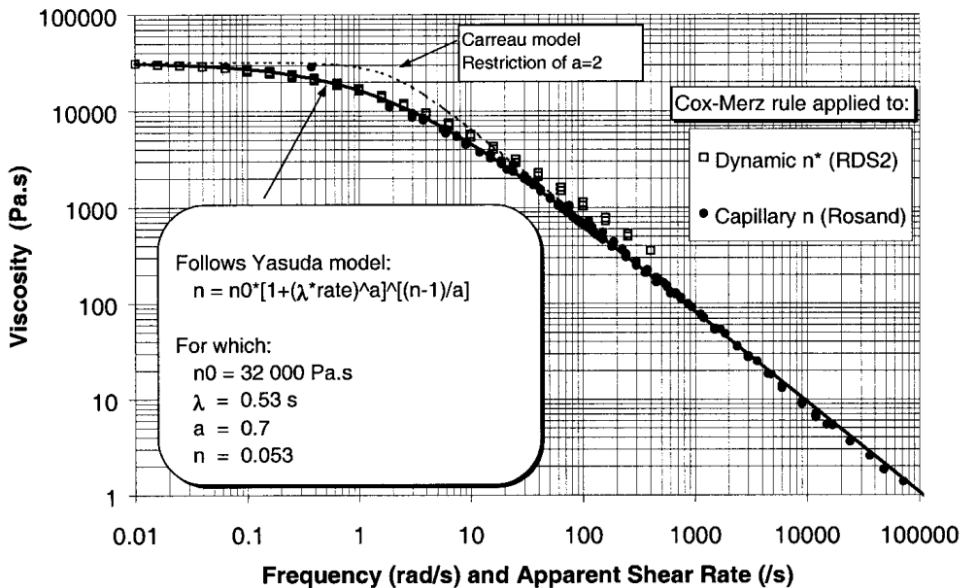


Figure 3.13: Viscosity vs. shear rate with fitting model. Image taken from [59].

[4, ch. 17]. As it was already shown in the previous chapter, the knowledge of the shear stress attenuation is fundamental for creating numerical models capable of emulating the real behaviour of the used samples.

Fortunately the shear viscosity of PDMS was fully characterised by the producer (Dow Corning) of the product used for this work and were published in [59]. Their results clearly shows a strong dependence of the viscosity of PDMS depending on the shear frequency and are reported in figure 3.13. They surely explain why attenuation at low frequencies was so strong in the samples and, by inserting this information in the numerical model, it is possible to explain also the behaviour of the cut-on frequency when changing the thickness of the samples (section 2.3).

3.3 The acoustic response

The set up described at the beginning of this chapter was finally used in order to measure the effect of illumination on the photo-responsive materials and on their frequency response. The samples used are the ones described in table 3.1. These were created in order to be neither too thin, since the cut-on frequency of the sample tend to increase the thinner the sample (as explained in the previous section), nor too thick, otherwise the projected light crossing the sample would deliver an uneven distribution of power along the thickness (since an exponential decay of the latter is expected inside an absorbing material).

In order to observe a global effect on the photo-responsivity, the samples were first illuminated with an homogeneous distribution of light, on a circular spot (with size $r \approx 25$ mm) located in a point in between the two probes. A collimated LASER beam at a wavelength of 532 nm was used for the illumination. This allowed to gather information on the variation of propagation velocity together with the effect observed on the spectrum.

Then the samples were illuminated according to the pattern used in the numerical analysis and the time variation of the spectrum was recorded.

One issue encountered during the acquisition of the spectra was their stability in time. Indeed even if let resting in place on the sample holder, the transmission spectrum of the samples was experiencing deformations and variation in time in such a way that two spectra measured in a time range of few hours may not have been reliably comparable. The main cause of this issue was the usage of ecographic gel placed in between the probes and the sample in order to improve the contact. Therefore it was substituted with bi-adhesive tape, that still wasn't effective in the long run. Other effects that could be playing an important role are temperature variations, the sample holder stiffness (and its ability to maintain the probes properly still) and probably also the fact that PDMS is an elastomer, which makes it soft and deformable.

For the single measure this is not a big issue. When the spectra are modified due to the isomerization of the azo-molecule, they return to their original condition when the excitation is removed. Nonetheless comparing spectra measured at a time distance of hours or even days becomes inappropriate. Therefore each measurement sequence will have to be considered as a stand alone measurement.

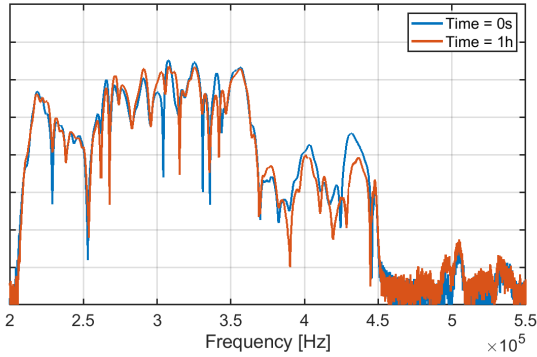


Figure 3.14: Example of variation in time of the transmission spectrum for one of the samples, without presence of illumination and when ecographic gel is used for improving the contact between sample and probes. Measured on sample #3.

It is important to remember that the lower limit of the spectra are present due to the properties of the sample, because the input sweep function start always at a frequency between 30 kHz and 100 kHz (depending on the specific measurement), while the upper limit is always present due to the upper limit of the sweep function.

3.3.1 Unstructured illumination

As shown in table 3.1 the samples where produced using different amount of azo-dopant. The effects of photo-excitation should be more evident the more the samples are doped.

In order to analyse the effect of the photo-responsivity the first things to analyse are the variations of the transmission spectrum recorded as explained in 3.1.1. The moment the recording starts, the LASER is turned on, producing a circular illumination spot on the sample. Then, it is kept on for long enough such to obtain a stable variation of the spectrum, which accounted for approximately five minutes. In the meanwhile, the spectrum shape is acquired every 10 s. After the LASER is turned off the sample starts relaxing and the spectrum is recorded until it reaches its initial shape.

From the plots in figure 3.15 it is possible to observe that the first sample, which has little doping, shows the least sensitivity, while the other samples show significant variations on the spectrum.

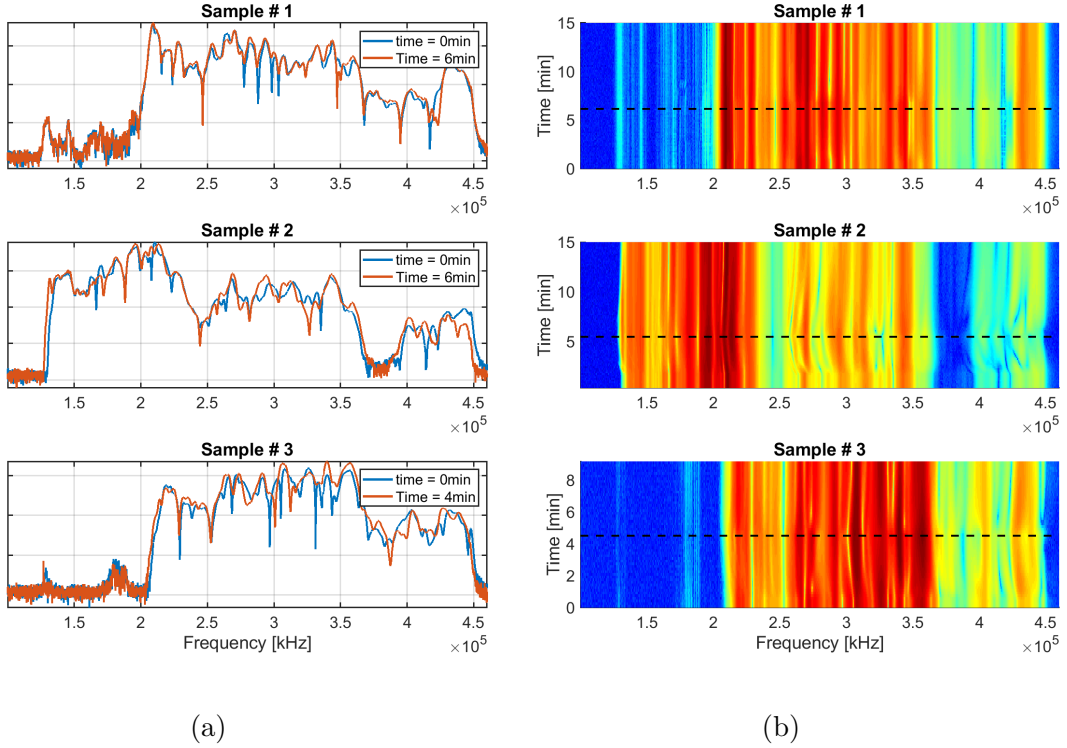


Figure 3.15: Comparisons between the effect of light onto three different samples.
 (a) Spectrum without illumination in blue and after 5 min of illumination in red. (b) Time evolution of the spectrum; the black line represent the moment when the LASER is turned off.

Elastic properties variations

When illuminating the sample without projecting any pattern, the elastic properties should be varying approximately uniformly in the illumination spot. Therefore one can imagine that the propagation velocity of a wave propagating inside the material is going to change only in the region of the spot.

In order to measure the propagation delay it is necessary to perform a time of flight (*tof*) measurement. With respect to the configuration used in section 3.2.2, this time the sample has to stay horizontally on the sample holder and the two probes cannot face each other. Therefore, when a burst signal is injected from one probe, the propagating wave will have to encounter multiple reflections and the exact distance that it travels to cannot be known a priori.

Approximating the illumination spot to a rectangle in the centre of the slab, the sample can be modelled as a one dimensional line in which there is a central region where the wave propagates at a different velocity. It is straight forward that the time to travel from one end to the other can be expressed as

$$t_1 = \frac{L - l_x}{c_0} + \frac{l_x}{c_x}, \quad (3.1)$$

where the x index refer to the central, illuminated, region and it is fixed to a value of 2.5 cm (size of the collimated LASER beam), while L is the total length of the sample.

In chapter 2 it was introduced the concept of contrast as the ratio between the Young's modulus in the illuminated region (E_x) and the value at rest, in such a way that $E_x = \varepsilon E_0$ and that the propagation velocity of a bulk wave (eq. (1.28)) could be written as

$$c_x = \sqrt{\varepsilon} c_0.$$

Even if this time it would be completely wrong to assume that the propagation velocity is the one of a bulk wave, it is still reasonable to assume that the dependence on the contrast still holds. This assumption allows to extract the value of the contrast from the expression of the propagation delay (3.1)

$$\varepsilon = \left(\frac{l_x}{t_1 c_0 - L + l_x} \right)^2. \quad (3.2)$$

Since c_0 can be measured from the propagation delay on the sample when there is no illumination, i.e. $c_0 = L/t_0$, the previous equation takes an even more compact form

$$\varepsilon = \left(\frac{1}{\left(\frac{t_1}{t_0} - 1 \right) \frac{L}{l_x} + 1} \right)^2. \quad (3.3)$$

Thanks to this simple expression, even if the exact value of the total length travelled is not known, it is possible to obtain a good estimate of the variation of the elastic properties.

In figure 3.16 it is possible to understand how to extract the *tof* from the burst signal. This operation was performed for three samples and then the contrast was computed. The options for the value of the total length were:

- to consider the minimum distance between the two probes (L_p);
- to consider the distance between the centre of the two probes (L_c);

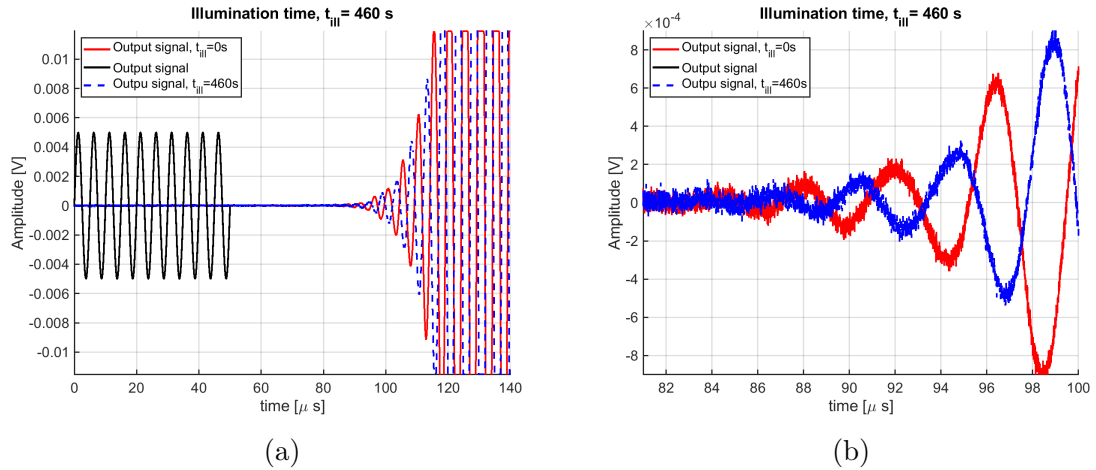


Figure 3.16: (a) Effect of illumination on the burst signal. (b) Zoom in the region where the output signal starts. Measured on sample # 2.

Sample #	Length type	Value	t_0	t_1	ε
1	L_p	63.5 mm	96 μs	98 μs	0.90
	L_c	88.0 mm			0.87
	L_t	112.5 mm			0.84
2	L_p	56 mm	87 μs	90 μs	0.86
	L_c	80.5 mm			0.81
	L_t	101 mm			0.77

Table 3.4: Results from the time of flight analysis.

- to consider the total length of the sample (L_t).

Obviously none of these options are correct, but the corresponding result will still give useful information. These are collected in table 3.4 and show that only in the best case scenario the contrast will be sufficient to generate a band gap wide enough to be significantly visible in the spectrum. At least this is what the numerical analysis performed in sections 2.1, 2.3 are suggesting (more precisely in figures 2.6, 2.15).

3.3.2 Pattern projection

The previous subsection proved that there is evidence of a variation of propagation velocity inside the material when the azo-doped samples are illuminated with the proper light source. But in order to gain control over

the propagating elastic waves, it is necessary to induce such variations in a structured manner.

The created samples do not possess any predefined structure and, in particular, they do not possess any resonant structure, therefore the effect of illumination is not going to create or alter any metamaterial-like behaviour (no resonant mechanism present). Instead light could be used to induce a phononic crystal-like alteration of the elastic properties by simply projecting a periodic pattern on the material. This surely looks an attractive opportunity and this thesis represents a first attempt in this direction.

The projection of a pattern could be done in several ways, for instance by means of a computer controlled spatial light modulator (SLM) or even a digital micromirror device (DMD). For the purpose of this work though, it was chosen to use a simpler approach in order to perform a feasibility study, i.e. a mask to be placed in front of the collimated beam.

The shape of the mask was chosen in order to recreate the pattern proposed in sections 2.1, 2.3, even though it is a one dimensional pattern which in a 3D solid might not be sufficient. The mask was 3D printed using an extrusion 3D printer and it is shown in figure 3.17.

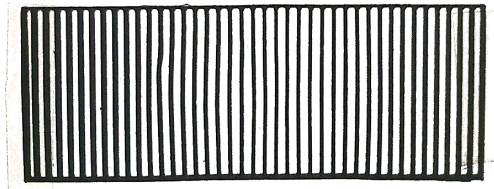


Figure 3.17: Mask used for the projection of the pattern.

The measurements were performed by controlling both the LASER and the time acquisition via MATLAB, thus activating the LASER for 5 min and recording the receiving signal every ten seconds for at least twenty minutes since the activation of the LASER. The samples were illuminated with and without masks in order to compare the effect on the spectrum in the two cases and, since using the mask reduces the total power reaching the samples, also the effect using different power were measured.

In figure 3.18 the effect of illumination (using the maximum power available from the LASER) on the spectrum when the mask is present is compared

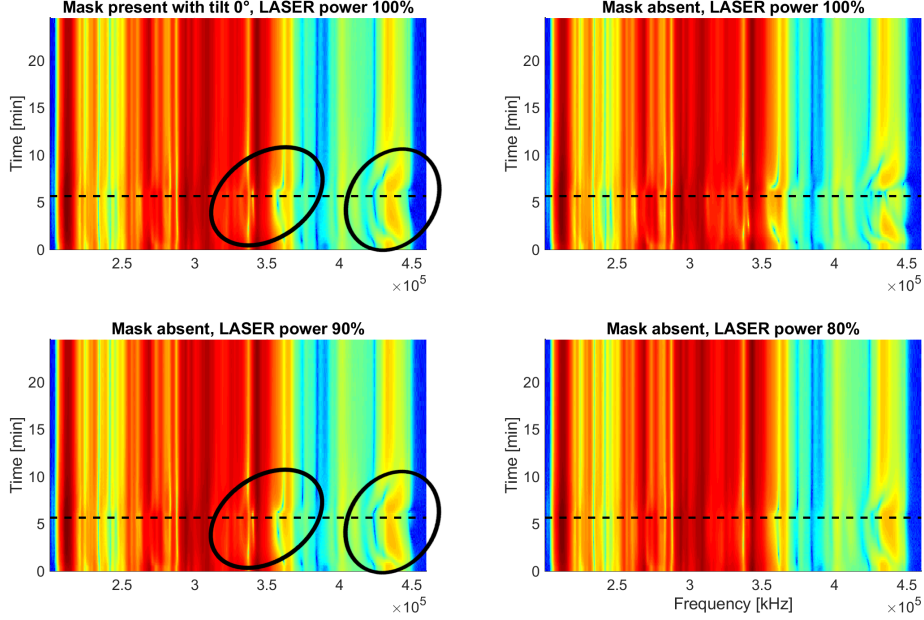


Figure 3.18: Time evolution of the spectral variations. Comparison of the spectral variation upon illumination for the sample # 3. The black dashed line corresponds to the moment the LASER is turned off.

to the effect when it is not present. The latter was acquired in three ways, the first using the maximum power available, the second using 90% of that value and the last one using 80% of it. In the figure the salient variation where highlighted and it seems that the effect of the presence of the mask is very similar to the effect without mask, but using 90% of the maximum available power.

In order to insert some variations on the projected pattern, the mask was tilted along the axis perpendicular to the LASER beam as shown in figure 3.19. Due to simple optical perspective, the generated pattern is still going be formed by alternating lines, but the spacing between them (the periodicity) and the relative width of the single line with respect to the spacing (the fill factor) will change, together with the total power reaching the sample.

Since period and fill factor of the induced structurization are changed, one would expect that the corresponding variations in the spectrum would be subjected to an increment (or reduction) in size, or possibly a shift in frequency. At least if such variations were strictly correlated to the presence

3.3 – The acoustic response

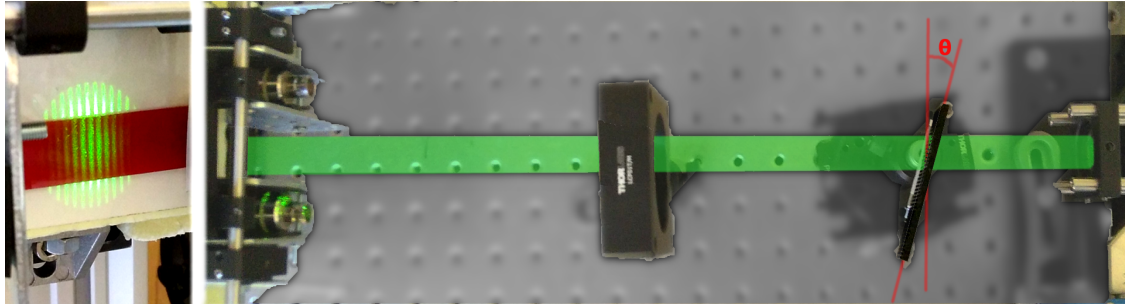


Figure 3.19: Picture of the tilted mask together with the pattern it generates

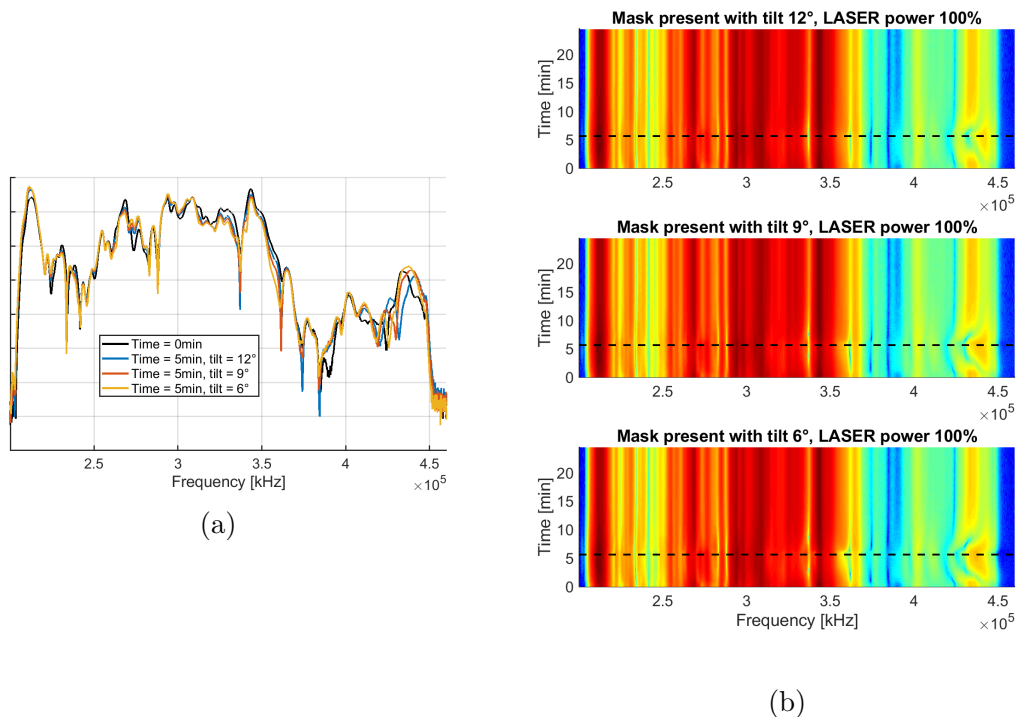


Figure 3.20: Comparison of the spectral variation upon illumination for the sample # 3 when using the mask at different tilt angle (same acquisition series as figure 3.18). (a) Spectra after five minutes of illumination compared with their rest value. (b) Time evolution of the spectral variations; black dashed line corresponds to the moment the LASER is turned off.

of the projected pattern. Unfortunately, from figure 3.20 it is difficult, or not even possible, to observe a variation of such, while they seem more correlated to the variations in the total injected power.

One final test was performed in order understand if the structure induced by the projected pattern was producing any effect. In the middle between the mask and the sample a lens was placed (from Thor Labs, specification *focal length* 100 mm, diameter 5.8 cm) in order to magnify the projected pattern. In this way the total projected power is the same, while the power density changes. The lens should then be used to create an image of the mask on the material by using the simple lens law, where both the object and its image have to change position in order to change the magnification factor. Since the light coming from the LASER is collimated, the magnification of the image forming on the sample depend only on the distance from the lens to the sample. Therefore it was chosen to simply insert the lens in the middle between the mask and the sample, and consider only the distance lens-sample. Even though, in this way, the exact value of the magnification is not known, for this preliminary analysis it is sufficient to understand if there is a consistent difference between the various pattern generated.

For this final acquisition it was chosen to illuminate the sample for only two minutes in order to reduce heating and degradation of the photosensitive molecules. The mask was kept at a tilting angle of 8° in order to obtain a fill factor of approximately 50%. The results are collected in figures 3.21, where the variations of the spectrum were recorded for three different distances of the lens, first with the mask in front of the beam and then without it.

Even in this case it not possible to claim a dependence of the variations of the spectrum from the size of the pattern .

Conclusions

In this final chapter of this thesis it was possible to record important variations in the acoustic response upon illumination, but unfortunately it was not possible to show a direct correlation between the presence of the one dimensional mask and the acoustic spectral behaviour. For the kind of sample we used, a one dimensional mask might not be sufficient in order to induce a global band gap, even if the numerical model was showing contrary. Indeed the latter, being a two dimensional model, might not represent a good simplification of the real samples. It is therefore necessary to extend the experimental, and possibly the numerical, analysis also to more complex bi-dimensional patterns.

Nonetheless there was proof of an induced variation of $-10\% \div -20\%$ for the Young's modulus inside the material after illumination with light (assuming only the Young's modulus is being affected, leaving the density

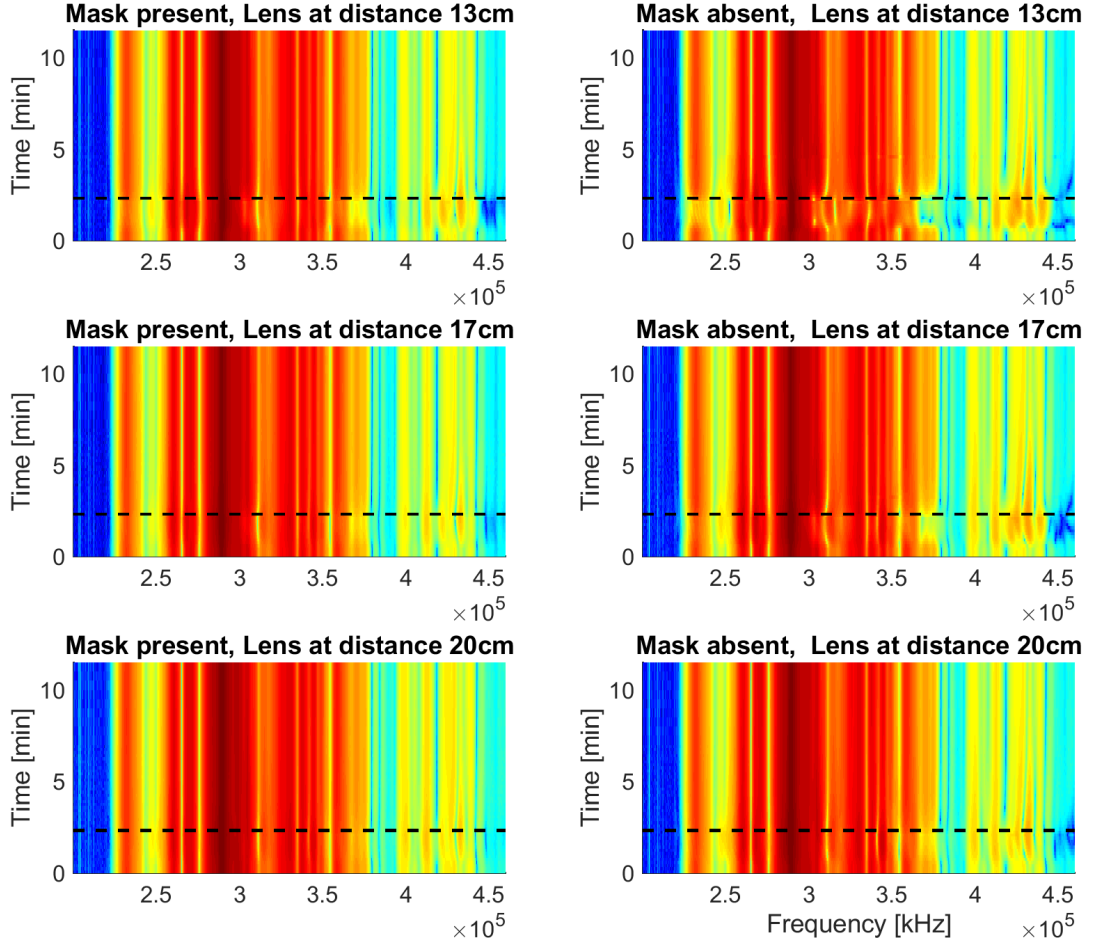


Figure 3.21: Time evolution of the spectral variations. Comparison of the spectral variation upon illumination for the sample # 4. The black dashed line corresponds to the moment the LASER is turned off.

and the Poisson's ratio invariant) which is just below the minimum value that the numerical analysis pointed out. Nonetheless with more complex two dimensional patterns it might still be possible to obtain more distinct phononic crystal effects.

Moreover it shall be noted that polydimethylsiloxane is an elastomer and its nature makes it more suited for insulating application rather than for a metamaterial. Other than attenuation, the huge difference between the shear and compressive wave propagation velocities created problems in the

numerical analysis, forbidding the primitive cell analysis and the extraction of the band diagram. For the slap-like samples that are required for this work, a more rigid, hence stiffer, material would be better suited, allowing also for measuring in configurations where the sample is suspended (better propagation of Lamb waves, that often dominate in thin media).

The study presented in this thesis work has to be therefore considered a preliminary study. More analysis have to be carried out in order to obtain more effective results. The numerical models could be created using FDTD analysis instead of FEM. Masks with more complex pattern should be tested. And finally, the polymer used for the work could be changed, maybe shifting to stiffer polymers, which attenuation coefficient can be neglected.

Appendix A

Mathematical Demonstrations

A.1 Gibbs free energy

It was said that the Gibbs free energy and the strain tensor could be expressed in the form

$$G = G_0 + \frac{1}{2} \lambda u_{ii}^2 + \mu u_{ik}^2,$$

$$u_{ik} = \left(u_{ik} - \frac{1}{3} u_{ll} \delta_{ik} \right) + \frac{1}{3} u_{ll} \delta_{ik}.$$

The term in λ has only diagonal terms, thus only the hydrostatic compression term remains

$$\frac{1}{2} \lambda u_{ii}^2 = \frac{1}{2} \lambda \left(\frac{1}{3} u_{ll} \delta_{ik} \right)^2 = \frac{1}{2} \lambda u_{ll}^2$$

since $\delta_{ik} = \sum_{i,k} \delta_{ik} = 3$.

$$\begin{aligned} & \mu \left[\left(u_{ik} - \frac{1}{3} u_{ll} \delta_{ik} \right) + \frac{1}{3} u_{ll} \delta_{ik} \right]^2 = \\ & \mu \left(u_{ik} - \frac{1}{3} u_{ll} \delta_{ik} \right)^2 + \mu \left(\frac{1}{3} u_{ll} \delta_{ik} \right)^2 + 2\mu \frac{1}{3} u_{ll} \delta_{ik} \left(u_{ik} - \frac{1}{3} u_{ll} \delta_{ik} \right) = \\ & \mu \left(u_{ik} - \frac{1}{3} u_{ll} \delta_{ik} \right)^2 + \mu u_{ll}^2 + 2\mu \frac{1}{3} u_{ll} \delta_{ik} u_{ik} - 2\mu \left(\frac{1}{3} u_{ll} \delta_{ik} \right)^2 = \\ & \mu \left(u_{ik} - \frac{1}{3} u_{ll} \delta_{ik} \right)^2 + \mu u_{ll}^2 + 2\mu \frac{1}{3} u_{ii} u_{ll} - 2\mu u_{ll}^2. \end{aligned}$$

Since $u_{ii}u_{ll} = \sum_{i,l} u_{ii}u_{ll} = (\sum_l u_{ll})^2 = u_{ll}^2$ the Gibbs free energy can be written as

$$G = G_0 + \frac{1}{2} \left(\lambda + \frac{2}{3} \mu \right) u_{ll}^2 + \mu \left(u_{ik} - \frac{1}{3} u_{ll} \delta_{ik} \right)^2.$$

A.2 The wave equation

It was said that the equation of motion for a deformation in an elastic body is

$$\rho \ddot{u}_i = \frac{\partial \sigma_{ik}}{\partial x_k}.$$

It was also said that the stress tensor has the form

$$\sigma_{ik} = \alpha(u_{ik} + \beta u_{ll} \delta_{ik}),$$

where $\alpha = \frac{E}{1+\nu}$ and $\beta = \frac{\nu}{1-2\nu}$. Performing its derivative

$$\frac{\partial \sigma_{ik}}{\partial x_k} = \alpha \frac{\partial u_{ik}}{\partial x_k} + \alpha \beta \frac{\partial (u_{ll} \delta_{ik})}{\partial x_k}.$$

Remembering the definition of the strain tensor (1.7)¹,

$$\begin{aligned} \frac{\partial \sigma_{ik}}{\partial x_k} &= \frac{\alpha}{2} \frac{\partial (\partial u_i / \partial x_k)}{\partial x_k} + \frac{\alpha}{2} \frac{\partial (\partial u_k / \partial x_i)}{\partial x_k} + \alpha \beta \frac{\partial (\delta_{ik} \partial u_l / \partial x_l)}{\partial x_k} \\ &= \frac{\alpha}{2} \frac{\partial^2 u_i}{\partial x_k^2} + \frac{\alpha}{2} \frac{\partial^2 u_i}{\partial x_k \partial x_i} + \alpha \beta \frac{\partial^2 u_l}{\partial x_i \partial x_l}. \end{aligned}$$

Since the sum over l and the sum over k are independent

$$\frac{\partial \sigma_{ik}}{\partial x_k} = \frac{\alpha}{2} \frac{\partial^2 u_i}{\partial x_k^2} + \alpha \left(\beta + \frac{1}{2} \right) \frac{\partial^2 u_i}{\partial x_k \partial x_i}.$$

Finally, substituting the values for α and β one gets equation (1.25).

¹notice that while u_{ik} refers to the strain tensor, u_i refers to the i -th component of the strain vector \mathbf{u}

A.3 Extracting p- and s-wave equations

The wave equation takes the form

$$c_t^2 \Delta(\mathbf{u}_l + \mathbf{u}_t) + (c_l^2 - c_t^2) \nabla \cdot (\nabla \cdot \mathbf{u}_l + \mathbf{u}_t) = \ddot{\mathbf{u}}_l + \ddot{\mathbf{u}}_t,$$

where $\mathbf{u}_l + \mathbf{u}_t = \mathbf{u}$ and they satisfy the following relations

$$\nabla \cdot \mathbf{u}_t = 0 \text{ and } \nabla \wedge \mathbf{u}_l = 0,$$

where the operation $\nabla \wedge$ is a *curl* operation and $\nabla \cdot$ is a divergence operation.

Performing the divergence on both sides it is possible to write

$$\begin{aligned} c_t^2 \nabla \cdot \Delta(\mathbf{u}_l + \mathbf{u}_t) + (c_l^2 - c_t^2) \nabla \cdot \nabla (\nabla \cdot \mathbf{u}_l + \nabla \cdot \mathbf{u}_t) &= \nabla \cdot (\ddot{\mathbf{u}}_l + \ddot{\mathbf{u}}_t) \\ c_t^2 \Delta(\nabla \cdot \mathbf{u}_l) + (c_l^2 - c_t^2) \nabla \cdot \nabla (\nabla \cdot \mathbf{u}_l) &= \frac{\partial^2 \nabla \cdot \mathbf{u}_l}{\partial t^2} \\ c_t^2 \Delta(\nabla \cdot \mathbf{u}_l) + (c_l^2 - c_t^2) \Delta(\nabla \cdot \mathbf{u}_l) &= \nabla \cdot \ddot{\mathbf{u}}_l \\ c_l^2 \Delta(\nabla \cdot \mathbf{u}_l) &= \nabla \cdot \ddot{\mathbf{u}}_l \end{aligned}$$

where many terms cancelled out thanks to the relation $\nabla \cdot \mathbf{u}_t = 0$. Finally obtaining

$$\nabla \cdot (c_l^2 \Delta \mathbf{u}_l - \ddot{\mathbf{u}}_l) = 0.$$

The identities used for the previous steps were: $\nabla \cdot \nabla(\mathbf{x}) = \Delta(\mathbf{x})$ (which is the definition of Laplacian) and $\nabla \cdot \Delta(\mathbf{x}) = \nabla \cdot \nabla(\nabla \cdot \mathbf{x}) = \Delta(\nabla \cdot \mathbf{x})$, for any generic vector field \mathbf{x} .

A.4 Diatomic chain

The balance of forces in the elementary unit for a diatomic chain has the form

$$\begin{aligned} M_1 \ddot{u}_{n,1} &= -K[(u_{n,1} - u_{n-1,2}) - (u_{n,2} - u_{n,1})], \\ M_2 \ddot{u}_{n,2} &= -K[(u_{n,2} - u_{n,1}) - (u_{n+1,1} - u_{n,2})]. \end{aligned}$$

For the first mass:

$$\begin{aligned} -M_1 \omega^2 A_1 e^{ikna} &= -K[(A_1 e^{ikna}] - A_2 e^{ik(n+1/2-1)a}) - (A_2 e^{ik(n+1/2)a} - A_1 e^{ikna})], \\ -M_1 \omega^2 A_1 &= -K[(2A_1 - A_2 e^{-ika/2} - A_2 e^{+ika/2})], \end{aligned}$$

and finally

$$(2K - M_1\omega^2)A_1 - (2K \cos ka/2)A_2 = 0.$$

For the second mass instead:

$$\begin{aligned} -M_2\omega^2 A_2 e^{ik(n+1/2)a} &= -K[(A_2 e^{ik(n+1/2)a} - A_1 e^{ikna}) + \\ &\quad - (A_1 e^{ik(n+1)a} - A_2 e^{ik(n+1/2)a})], \\ -M_2\omega^2 A_2 e^{+ika/2} &= -K[(2A_2 e^{+ika/2} - A_1 - A_1 e^{+ika})], \\ -M_2\omega^2 A_2 &= -K[(2A_2 - A_1 e^{-ika/2} - A_1 e^{+ika/2})], \end{aligned}$$

and finally

$$(2K - M_2\omega^2)A_2 - (2K \cos ka/2)A_1 = 0.$$

Bibliography

- [1] L. D. Landau and E. W. Lifshitz. *Theory of Elasticity*. 2nd. Vol. 7. Course of Theoretical Physics. PERGAMON Press, 1970.
- [2] J. D. Achenbach. *Wave Propagation in Elastic Solids*. NORTH HOLLAND Publishing company, 1973.
- [3] W. Ostachowicz et al. *Guided Waves in Structures for SHM: The Time - domain Spectral Element Method*. A John Wiley & Sons, Ltd., publication. Wiley, 2011. ISBN: 9781119965862.
- [4] J.L. Rose. *Ultrasonic Guided Waves in Solid Media*. Cambridge University Press, 2014. ISBN: 9781107048959.
- [5] Filiberto Bilotti and Levent Sevgi. “Metamaterials: Definitions, properties, applications, and FDTD-based modeling and simulation (Invited paper)”. In: *International Journal of RF and Microwave Computer-Aided Engineering* 22.4 (2012), pp. 422–438. DOI: [10.1002/mmce.20634](https://doi.org/10.1002/mmce.20634).
- [6] P.A. Deymier. *Acoustic Metamaterials and Phononic Crystals*. Springer Series in Solid-State Sciences. Springer Berlin Heidelberg, 2013. ISBN: 9783642312328.
- [7] Habib Ammari et al. “Double-negative acoustic metamaterials”. In: *Quarterly of Applied Mathematics* (Sept. 2017). DOI: [10.1090/qam/1543](https://doi.org/10.1090/qam/1543).
- [8] Yiqun Ding, Zhengyou Liu, and Chunyin Qiu. “Metamaterial with Simultaneously Negative Bulk Modulus and Mass Density”. In: *Physical review letters* 99 (Sept. 2007), p. 093904. DOI: [10.1103/PhysRevLett.99.093904](https://doi.org/10.1103/PhysRevLett.99.093904).
- [9] Xiangdong Zhang and Zhengyou Liu. “Negative refraction of acoustic waves in two-dimensional phononic crystals”. In: *Applied Physics Letters* 85.2 (2004), pp. 341–343. DOI: [10.1063/1.1772854](https://doi.org/10.1063/1.1772854).

BIBLIOGRAPHY

- [10] Rui Zhu et al. “Negative refraction of elastic waves at the deep-subwavelength scale in a single-phase metamaterial”. In: *Nat Commun* 5 (Nov. 2014). DOI: [10.1038/ncomms6510](https://doi.org/10.1038/ncomms6510).
- [11] N. Engheta and R.W. Ziolkowski. *Metamaterials: Physics and Engineering Explorations*. Wiley, 2006. ISBN: 9780471784180.
- [12] V.G. Veselago. “Electrodynamics of substances with concurrently negative values of e and m”. In: *Uspekhi Fizicheskikh Nauk = Physics-Uspekhi (Advances in Physical Sciences)* 92 (Jan. 1967), pp. 517–526.
- [13] J.B. Pendry. “Negative Refraction Makes a Perfect Lens”. In: *Physical review letters* 85 (Nov. 2000), pp. 3966–9. DOI: [10.1103/PhysRevLett.85.3966](https://doi.org/10.1103/PhysRevLett.85.3966).
- [14] H. Zhu and F. Semperlotti. “A passively tunable acoustic metamaterial lens for selective ultrasonic excitation”. In: *Journal of Applied Physics* 116.9 (2014), p. 094901. DOI: [10.1063/1.4894279](https://doi.org/10.1063/1.4894279).
- [15] Antonio S. Gliozzi et al. “Metamaterials-based sensor to detect and locate nonlinear elastic sources”. In: *Applied Physics Letters* 107.16 (2015), p. 161902. DOI: [10.1063/1.4934493](https://doi.org/10.1063/1.4934493).
- [16] Marco Miniaci et al. “Proof of Concept for an Ultrasensitive Technique to Detect and Localize Sources of Elastic Nonlinearity Using Phononic Crystals”. In: *Physical Review Letters* 118 (Jan. 2017), p. 214301. DOI: [10.1103/PhysRevLett.118.214301](https://doi.org/10.1103/PhysRevLett.118.214301).
- [17] Paolo Celli and Stefano Gonella. “Manipulating waves with LEGO® bricks: A versatile experimental platform for metamaterial architectures”. In: *Applied Physics Letters* 107.8 (2015), p. 081901.
- [18] Stepan Lomov et al. “Experimental and Theoretical Characterization of the Geometry of Two-Dimensional Braided Fabrics”. In: *Textile Research Journal - TEXT RES J* 72 (Aug. 2002), pp. 706–712. DOI: [10.1177/004051750207200810](https://doi.org/10.1177/004051750207200810).
- [19] J.D. Joannopoulos et al. *Photonic Crystals: Molding the Flow of Light - Second Edition*. Princeton University Press, 2011. ISBN: 9781400828241.
- [20] C J R Sheppard. “Approximate calculation of the reflection coefficient from a stratified medium”. In: *Pure and Applied Optics: Journal of the European Optical Society Part A* 4.5 (Sept. 1995), pp. 665–669. DOI: [10.1088/0963-9659/4/5/018](https://doi.org/10.1088/0963-9659/4/5/018).

BIBLIOGRAPHY

- [21] N.W. Ashcroft and N.D. Mermin. *Solid-state Physics*. Holt-Saunders International Editions: Science : Physics v. 30. Saunders College, 1976. ISBN: 9780126077902.
- [22] Zhengyou Liu et al. “Locally Resonant Sonic Materials”. In: *Science* 289.5485 (2000), pp. 1734–1736. ISSN: 0036-8075. DOI: [10.1126/science.289.5485.1734](https://doi.org/10.1126/science.289.5485.1734).
- [23] Jie Zhu et al. “Acoustic rainbow trapping”. In: *Scientific reports* 3 (Apr. 2013), p. 1728. DOI: [10.1038/srep01728](https://doi.org/10.1038/srep01728).
- [24] Paolo Celli et al. “Bandgap widening by disorder in rainbow metamaterials”. In: *Applied Physics Letters* 114 (Mar. 2019), p. 091903. DOI: [10.1063/1.5081916](https://doi.org/10.1063/1.5081916).
- [25] Sebastian Krödel, N. Thomé, and Chiara Daraio. “Wide band-gap seismic metastructures”. In: *Extreme Mechanics Letters* 4 (June 2015). DOI: [10.1016/j.eml.2015.05.004](https://doi.org/10.1016/j.eml.2015.05.004).
- [26] Andrea Colombi et al. “A seismic metamaterial: The resonant metawedge”. In: *Scientific Reports* 6 (June 2016), p. 27717. DOI: [10.1038/srep27717](https://doi.org/10.1038/srep27717).
- [27] H.H. Huang, C.T. Sun, and G.L. Huang. “On the negative effective mass density in acoustic metamaterials”. In: *International Journal of Engineering Science* 47 (Mar. 2009), pp. 610–617. DOI: [10.1016/j.ijengsci.2008.12.007](https://doi.org/10.1016/j.ijengsci.2008.12.007).
- [28] Y. Pennec et al. “Tunable filtering and demultiplexing in phononic crystals with hollow cylinders”. In: *Phys. Rev. E* 69 (4 Apr. 2004), p. 046608. DOI: [10.1103/PhysRevE.69.046608](https://doi.org/10.1103/PhysRevE.69.046608).
- [29] O. Bou Matar et al. “Band gap tunability of magneto-elastic phononic crystal”. In: *Journal of Applied Physics* 111.5 (2012), p. 054901. DOI: [10.1063/1.3687928](https://doi.org/10.1063/1.3687928).
- [30] J. O. Vasseur et al. “Band structures tunability of bulk 2D phononic crystals made of magneto-elastic materials”. In: *AIP Advances* 1.4 (2011), p. 041904. DOI: [10.1063/1.3676172](https://doi.org/10.1063/1.3676172).
- [31] Alireza Bayat and Faramarz Gordaninejad. “A thermally tunable phononic crystal”. In: *Behavior and Mechanics of Multifunctional Materials and Composites 2016*. Ed. by Nakhiah C. Goulbourne. Vol. 9800. International Society for Optics and Photonics. SPIE, 2016, pp. 190–197. DOI: [10.1117/12.2218692](https://doi.org/10.1117/12.2218692).

BIBLIOGRAPHY

- [32] Baizhan Xia et al. “Temperature-controlled tunable acoustic metamaterial with active band gap and negative bulk modulus”. In: *Applied Acoustics* 112 (2016), pp. 1–9. ISSN: 0003-682X. DOI: <https://doi.org/10.1016/j.apacoust.2016.05.005>.
- [33] Jia-Yi Yeh. “Control analysis of the tunable phononic crystal with electrorheological material”. In: *Physica B: Condensed Matter* 400.1 (2007), pp. 137–144. ISSN: 0921-4526. DOI: <https://doi.org/10.1016/j.physb.2007.06.030>.
- [34] Xiang Yu, Fangsen Cui, and Y.D. Cui. “Tunable acoustic metamaterial with an array of resonators actuated by dielectric elastomer”. In: *Extreme Mechanics Letters* (July 2016). DOI: [10.1016/j.eml.2016.07.003](https://doi.org/10.1016/j.eml.2016.07.003).
- [35] E. Walker, Zhiming Wang, and Arup Neogi. “Radio-frequency actuated polymer-based phononic meta-materials for control of ultrasonic waves”. In: *NPG Asia Materials* 9 (Feb. 2017), e350. DOI: [10.1038/am.2016.209](https://doi.org/10.1038/am.2016.209).
- [36] Weiting Zhang et al. “A disorder-based strategy for tunable, broadband wave attenuation”. In: *Health Monitoring of Structural and Biological Systems 2017*. Ed. by Tribikram Kundu. Vol. 10170. International Society for Optics and Photonics. SPIE, 2017, pp. 97–108. DOI: [10.1117/12.2258605](https://doi.org/10.1117/12.2258605).
- [37] COMSOL Multiphysics®, version 5.2.
- [38] N. Xia et al. “Integrated measurement of ultrasonic parameters for polymeric materials via full spectrum analysis”. In: *Polymer Testing* 70 (2018), pp. 426–433. ISSN: 0142-9418. DOI: <https://doi.org/10.1016/j.polymertesting.2018.08.003>.
- [39] Marco Miniaci. “Behaviour and applications of elastic waves in structures and metamaterials”. PhD thesis. Alma Mater Studiorum, Università di Bologna, 2014.
- [40] Marco Miniaci et al. “Complete band gaps in a polyvinyl chloride (PVC) phononic plate with cross-like holes: numerical design and experimental verification”. In: *Ultrasonics* 56 (2015), pp. 251–259. ISSN: 0041-624X. DOI: <https://doi.org/10.1016/j.ultras.2014.07.016>.
- [41] Smokefoot. *Improved image of polydimethylsiloxane*. Dec. 29, 2012. URL: <https://commons.wikimedia.org/w/index.php?curid=23410088>.

BIBLIOGRAPHY

- [42] Patrick Carlberg, Lars Montelius, and Jonas Tegenfeldt. “Nanoimprint in PDMS on glass with two-level hybrid stamp”. In: *MICROELECTRONIC ENGINEERING* 85 (Jan. 2008), pp. 210–213. DOI: [10.1016/j.mee.2007.05.010](https://doi.org/10.1016/j.mee.2007.05.010).
- [43] Samuel Sia and George Whitesides. “Microfluidic Devices Fabricated in Poly(Dimethylsiloxane) for Biological Studies”. In: *Electrophoresis* 24 (Nov. 2003), pp. 3563–76. DOI: [10.1002/elps.200305584](https://doi.org/10.1002/elps.200305584).
- [44] Angelo Angelini et al. “Reconfigurable elastomeric graded-index optical elements controlled by light”. In: *Light: Science & Applications* 7 (Dec. 2018). DOI: [10.1038/s41377-018-0005-1](https://doi.org/10.1038/s41377-018-0005-1).
- [45] Alberto Puliafito et al. “Driving Cells with Light-Controlled Topographies”. In: *Advanced Science* 6.14 (2019), p. 1801826. DOI: [10.1002/advs.201801826](https://doi.org/10.1002/advs.201801826).
- [46] Emiliano Descrovi et al. “Photo-responsive suspended micro-membranes”. In: *Journal of Materials Chemistry C* 6 (Sept. 2018). DOI: [10.1039/C8TC03877E](https://doi.org/10.1039/C8TC03877E).
- [47] Fiore Nicoletta et al. “Light Responsive Polymer Membranes: A Review”. In: *Membranes* 2 (Dec. 2012), pp. 134–197. DOI: [10.3390/membranes2010134](https://doi.org/10.3390/membranes2010134).
- [48] Christopher Barrett et al. “Photomechanical effects in azobenzene-containing soft materials”. In: *Soft Matter* 3 (Sept. 2007). DOI: [10.1039/b705619b](https://doi.org/10.1039/b705619b).
- [49] Jacques Delaire and Keitaro Nakatani. “Linear and Nonlinear Optical Properties of Photochromic Molecules and Materials”. In: *Chemical reviews* 100 (June 2000), pp. 1817–1846. DOI: [10.1021/cr980078m](https://doi.org/10.1021/cr980078m).
- [50] Maria-Melanie Russew and Stefan Hecht. “Photoswitches: From Molecules to Materials”. In: *Advanced Materials* 22.31 (2010), pp. 3348–3360. DOI: [10.1002/adma.200904102](https://doi.org/10.1002/adma.200904102).
- [51] G. Sudesh Kumar and D. C. Neckers. “Photochemistry of azobenzene-containing polymers”. In: *Chemical Reviews* 89.8 (1989), pp. 1915–1925. DOI: [10.1021/cr00098a012](https://doi.org/10.1021/cr00098a012).
- [52] Federica Pirani. “Bio-oriented Micro- and Nano-Structures Based on stimuli-responsive polymers”. PhD thesis. ScuDo, Politecnico di Torino, 2018.

BIBLIOGRAPHY

- [53] Mariko SHIBAIKE et al. “Synthesis and Physical Properties of Poly (Disperse Red 1 acrylate-co-butyl methacrylate)”. Japanese. In: *Kobunshi Ronbunshu* 63 (Sept. 2006), pp. 621–625. DOI: [10.1295/koron.63.621](https://doi.org/10.1295/koron.63.621).
- [54] Ying-Gang Miao et al. “Effects of strain rate on mechanical properties of nanosilica/epoxy”. In: *Composites Part B: Engineering* 96 (2016), pp. 119–124. ISSN: 1359-8368. DOI: <https://doi.org/10.1016/j.compositesb.2016.04.008>.
- [55] Zhixin Wang and Nathan Gallant. “Crosslinking Effect on Polydimethylsiloxane Elastic Modulus Measured by Custom-Built Compression Instrument”. In: *Journal of Applied Polymer Science* 131 (Nov. 2014). DOI: [10.1002/app.41050](https://doi.org/10.1002/app.41050).
- [56] Zhixin Wang. “Polydimethylsiloxane Mechanical Properties Measured by Macroscopic Compression and Nanoindentation Techniques”. PhD thesis. Scholar Commons, University of South Florida, 2011.
- [57] Himani Jain et al. “PZT–PDMS composite for active damping of vibrations”. In: *Composites Science and Technology* 77 (Jan. 2013), pp. 42–51.
- [58] H.A. Barnes. *A Handbook of Elementary Rheology*. Raymond F. Boyer Library Collection. University of Wales, Institute of Non-Newtonian Fluid Mechanics, 2000. ISBN: 9780953803200.
- [59] Frank Swallow. “Viscosity of polydimethylsiloxane gum: Shear and temperature dependence from dynamic and capillary rheometry”. In: *Journal of Applied Polymer Science* 84 (June 2002), pp. 2533–2540. DOI: [10.1002/app.10563.abs](https://doi.org/10.1002/app.10563.abs).